Ph.D. Dissertation

Magnetic properties of asymmetric layered heavy metal / ferromagnet systems

M.Sc. Sukanta Kumar Jena

Supervisor: Dr. hab. Andrzej Wawro, Prof. IFPAN
Co-supervisor: Dr. Ewelina Milińska, IFPAN

Institute of Physics, Polish Academy of Sciences

A thesis submitted in fulfilment of the requirements for the degree of Doctor of Philosophy

Warsaw
February 2023

ବୋଉ ଆଉ ବାପାଙ୍କୁ ଉତ୍ସର୍ଗୀକୃତ

Dedicated to my Bou and Bapa

Author's Declaration

I, Sukanta Kumar Jena, hereby state that the work presented in this thesis "Magnetic properties of asymmetric layered heavy metal / ferromagnet systems" is original work during my Ph.D. study. No part of this thesis was submitted to any other institute or any other Organization. I hereby declare that this thesis has been prepared for the requirements of the Institute of Physics, Polish Academy of Science (IFPAN) for the fulfilment of Ph.D. degree. It is the original work of candidate. The reference has been specified for the literature review, results, and figures from literatures. This thesis has been prepared by Sukanta Kumar Jena under supervision of Prof. dr. hab. Andrzej Wawro and Dr. Ewelina Miłinska.

Data and Place

Name and signature of candidate

Abstract

Multilayerd thin-film structures are a relatively new group of artificial systems with significantly different properties than those of the component materials in the bulk form. Among them, magnetic materials focus an important attention in basic research and practical applications. Their key feature is dimensional confinement in the direction perpendicular to the layer plane. In such systems, the atoms forming the interface are in a large proportion to the entire layered structure. Their different surroundings cause that they show different properties compared to the atoms with homogeneous coordination inside the layer. Thus, in thin-film structures, interface effects play a clearly noticeable role. In the case of magnetic layers, for example, they significantly modify the perpendicular magnetic anisotropy (PMA) - one of the most important parameters. Another factor modifying the properties is the thickness of the component layers, e.g. the non-magnetic layer separating the magnetic layers. If their thickness is smaller than certain characteristic lengths, such as electron mean free path or spin diffusion length, additional effects of interlayer coupling appear. The selection of appropriate materials for the component layers and their thickness enable intentional modification of the properties of multilayer systems in a wide range.

This doctoral dissertation presents the results of research on asymmetric W/Co/Pt thin-film structures. In addition to the effects mentioned above, the asymmetric surrounding of the ferromagnetic (Co) layer with layers made of heavy metals (W and Pt), which are characterized by a strong spin-orbit coupling, additionally induces the Dzyaloshinskii-Moriya interaction (DMI). This interaction significantly modifies the spin structure of the magnetic layer systems, leading to the occurrence of, for example, spin spirals or skyrmions - topologically protected stable magnetization vortices. The investigated systems were produced using the molecular beam epitaxy technique. It provides a well-defined crystal structure of the component layers and high-quality interfaces that are crucial for the observed phenomena. A more perfect crystal structure enhances the observed effects compared to the similar layers commonly produced by sputtering.

The investigations were carried out in the systems with an increasing degree of complexity: from structures containing a single Co layer (Chapter 4), through structures with two or more (6 or 7) Co layers (Chapter 5), to multilayers with a 20-fold repetition of the basic W/Co/Pt trilayers (Chapter 6). With the increase in the aforementioned complexity, new interactions (magnetic coupling, magnetostatic interaction) appear, which additionally affect the magnetic properties. Such an approach allows for a deeper understanding of the impact of

individual interactions on the resulting properties of the studied systems, which are manifested in their magnetic configurations, magnetization reversal processes, or domain structure. Experimental results were obtained using various experimental techniques, such as: SQUID magnetometry, magnetometry using the polar Kerr effect (PMOKE), magnetic force microscopy (MFM) or inelastic light scattering spectroscopy (BLS). Some of the samples were made in the matrix configuration – the component layers were made in the form of wedges or steps with mutually orthogonal thickness gradients. Such a structure of the multilayers, combined with local sampling of properties, enabled effective determination of their dependence as a function of the thickness of the component layers. Interpretation of experimental results was supported by numerical modelling involving micromagnetic simulations and calculations based on density functional theory (DFT). The described magnetic structures, taking the form of bubble domains (skyrmions) or strip systems, are not only the subject of fundamental research, but also arouse interest in the context of practical applications (e.g. as magnonic crystals or magnetic recording carriers).

In addition to the chapters describing the obtained experimental results, this doctoral dissertation includes a short introduction (Chapter 1), a theoretical approach to the investigated phenomena (Chapter 2) and a brief description of the applied sample production technologies and research techniques (Chapter 3). The dissertation ends with conclusions and a summary of the obtained results.

Streszczenie

Wielokrotne struktury cienkowarstwowe stanowią relatywnie nową grupę sztucznych układów o znacznie odmiennych właściwościach niż te, którymi cechują się składowe materiały w postaci objętościowej. Wśród nich istotną pozycję w badaniach podstawowych i zastosowaniach praktycznych zajmują materiały magnetyczne. Ich kluczową cechą jest ograniczenie rozmiarowości w kierunku prostopadłym do płaszczyzny warstwy. W takich układach atomy tworzące interfejs stanowią duży udział w całej strukturze warstwowej. Ich odmienne otoczenie powoduje, że wykazują one inne właściwości w porównaniu do atomów z wnętrza warstwy o jednorodnej koordynacji. W związku z tym w cienkowarstwowych strukturach efekty interfejsowe grają wyraźnie zauważalną rolę. W przypadku warstw magnetycznych np. istotnie modyfikują prostopadłą anizotropię magnetyczną (PMA) – jeden z ważniejszych parametrów. Innym czynnikiem modyfikującym właściwości jest grubość warstw składowych np. warstwy niemagnetycznej rozdzielającej warstwy magnetyczne. Jeśli ich grubość jest mniejsza od pewnych charakterystycznych długości, takich jak: średnia droga swobodna elektronów, czy długość dyfuzji spinów, pojawiają się dodatkowe efekty sprzężenia międzywarstwowego. Dobór odpowiednich materiałów warstw składowych oraz ich grubości pozwala na intencjonalne modyfikowanie właściwości układów wielowarstwowych w szerokim zakresie.

Niniejsza rozprawa doktorska przedstawia wyniki badań asymetrycznych struktur cienkowarstwowych W/Co/Pt. Oprócz efektów wymienionych powyżej, asymetryczne otocznie warstwy ferromagnetycznej (Co) warstwami wykonanymi z metali ciężkich (W i Pt), które charakteryzują się silnym sprzężeniem spin-orbita, indukuje dodatkowo odziaływanie Dzyaloshinskii-Moriya (DMI). Oddziaływanie to znacząco modyfikuje strukturę spinową magnetycznych układów warstwowych, prowadząc do występowania np. spirali spinowych czy skyrmionów – topologicznie chronionych stabilnych wirów namagnesowania. Badane warstwy zostały wytworzone za pomocą techniki epitaksji z wiązki molekularnej. Zapewnia ona dobrze zdefiniowaną strukturę krystaliczną warstw składowych oraz wysoką jakość interfejsów, które są kluczowe dla obserwowanych zjawisk. Bardziej perfekcyjna struktura krystaliczna wzmacnia obserwowane efekty w porównaniu do badanych warstw powszechnie wytwarzanych metodą sputteringu.

Badania zostały przeprowadzone w układach o rosnącym stopniu złożoności: począwszy od struktur zawierających pojedynczą warstwę Co (Rozdział 4), poprzez struktury z dwoma, lub kilkoma (6 lub 7) warstwami Co (Rozdział 5), aż do wielowarstw z 20-krotnym

powtórzeniem podstawowej trójwarstwy W/Co/Pt (Rozdział 6). Wraz ze wzrostem wspomnianej złożoności pojawiają się nowe oddziaływania (sprzężenie magnetyczne, oddziaływanie magnetostatyczne), które dodatkowo wpływają na właściwości magnetyczne. Takie podejście pozwala na pełniejsze zrozumienie wpływu poszczególnych oddziaływań na wynikowe właściwości badanych układów, objawiających się w ich konfiguracjach magnetycznych, procesach przemagnesowania, czy strukturze domenowej. Wyniki eksperymentalne zostały uzyskane za pomocą zróżnicowanych technik badawczych, takich jak: magnetometria SQUID, magnetometria wykorzystująca polarny efekt Kerra (PMOKE), mikroskopia sił magnetycznych (MFM), czy spektroskopia nieelastycznego rozpraszania światła (BLS). Część próbek została wykonana w wersji matrycowej – warstwy składowe zostały wytworzone w postaci klinów lub schodków o wzajemnie prostopadłych gradientach grubości. Taka struktura warstw wielokrotnych w połączeniu z lokalnym próbkowaniem właściwości umożliwiła efektywne określenie ich zależności w funkcji grubości warstw składowych. Interpretacja wyników eksperymentalnych została wsparta modelowaniem numerycznym obejmującym symulacje mikromagnetyczne i obliczenia oparte na teorii funkcjonałów gęstości (DFT). Opisywane struktury magnetyczne, przyjmujące postać domen bąbelkowych (skyrmiony) czy układów paskowych, są nie tylko przedmiotem badań charakterze fundamentalnym, ale również budzą zainteresowanie w kontekście zastosowań praktycznych (np. jako kryształy magnoniczne lub nośniki zapisu magnetycznego).

Oprócz rozdziałów opisujących uzyskane wyniki doświadczalne niniejsza rozprawa doktorska zawiera krótki wstęp (Rozdział 1), teoretyczne wprowadzenie do badanych zagadnień (Rozdział 2) oraz zwięzły opis zastosowanych technologii wytwarzania próbek i technik badawczych (Rozdział 3). Rozprawę kończą wnioski i podsumowanie uzyskanych wyników.

Frequently used symbols

E_{tot} - total energy in ferromagnets

E_{ex} - Exchange energy

E_{an}- anisotropy Energy

E_Z- Zeeman Energy

E_d - *Demagnetization energy*

E_{DMI} - Dzyaloshinskii-Moriya energy

X - *Susceptibility*

E_0- *Other energy terms*

M - *Magnetization*

Ms - Saturation magnetization

d_0 - Magnetic dead layer

m - Magnetic moment

α - Gilbert damping of the material

γ - Gyromagnetic ratio

J - Coupling energy

H_{IEC} - Coupling field related with the shift of the hysteresis loop

E_a- Anisotropy energy

K_{eff} - Effective anisotropy coefficient.

σ_{DW} - Domain wall energy

A - Exchange stiffness constant

E_{ME} - Magneto elsatic anisotropy

K_U - the uniaxial anisotropy

K_d - shape anisotropy

t_m - thickness of the magnetic layer

ħ- Reduced Planck's constant

q_m-Wave vector

ω_m – Frequency

W - magnetic domain width

K_V - volume anisotropy

K_S - surface anisotropy

H - External magnetic field

V - Volume

E_{zee} - Zeeman energy

H_{ex} - Exchange Hamiltonian

S_i - i_{th} spin operator

J_{ij} - Exchange integral between i_{th} and j_{th} spins

a, b, c, d - lattice constants

λ - Wavelength of X-ray

θ - scattering angle of X-ray

Δf - Difference in frequency of the Stokes and anti-Stokes

k - the wave vector of incident light

d_{Co} -Co thickness

d_w - W thickness

d_{Pt} - Pt thickness

W - Domain width

$\mu_0 H_k$ - Anisotropy field of MH loop

D_{ij} - DMI vector between i_{th} and j_{th} spins

D_{eff} - Effective iDMI constant

D_{thr} - *Threshold iDMI*

D_S - Surface IDMI constant

Δ - *Domain wall width*

Ku - Uniaxial anisotropy

D - DM I strength

t_m - Co layer thickness

t_{stack} -Total thickness of the basic tri-layer stack W/Co/Pt

f - Scaling factor

μm - micrometer

l_{ex} - Exchange length

f_S - Frequency of Stokes signal

f_{aS} - Frequency of anti-Stokes signal

Δf - Frequency difference between Stokes and anti-Stokes peak

List of abbreviations

Perpendicular magnetic anisotropy (PMA)
Dzyaloshinskii-Moriya interaction (DMI) or interfacial DMI (iDMI)
Exchange interlayer coupling (EIC)
Magnetic force microscopy (MFM)
Ruderman Kittel Kasuya Yosida (RKKY)
X-ray diffraction (XRD)
X-ray reflectivity (XRR)
Alternating current (AC)
Aluminium Oxide/Sapphire (Al_2O_3)
Argon (Ar)
Atomic force microscopy (AFM)
Brillouin light scattering (BLS)
Charge coupled device (CCD)
Cobalt (Co)
Co-planar waveguide (CPW)
Direct current (*dc*)
Domain walls (DW)
Electromagnet (EM)
Face centered cubic (*fcc*)
Fast Fourier transform (FFT)
Ferromagnetic (FM)
Ferromagnetic resonance (FMR)
Full width at half maximum (FWHM)
Gigahertz (GHz)
Gold (Au)
Heavy metal (HM)
Hexagonal closed pack (*hcp*)
Iridium (Ir)
Iron (Fe)
Iron Germanium alloy (FeGe)
Landau-Lifshitz-Gilbert (LLG)
Magnesium Oxide (MgO)
Magneto-optical Kerr effect (MOKE)
Magnonic crystal (MC)
Manganese Silicon alloy (MnSi)
Molecular beam epitaxy (MBE)
Molybdenum (Mo)
Monolayer (ML)
Palladium (Pd)
Photo elastic modulator (PEM)
Platinum (Pt)
Polar/longitudinal/transverse MOKE (PMOKE/LMOKE/TMOKE)
Proximity induced effect (PIM)
Radio frequency (*rf*)
Reflection high energy electron diffraction (RHEED)
Low Energy Electron Diffaction(LEED)
Spin orbit coupling (SOC)
Spin reorientation transition (SRT)
Spin wave (SW)
Superconducting quantum interference device (SQUID)
Tandem Fabry-Perot interferometer (TFPI)
Tantalum (Ta)
Tantalum oxide (TaO_x)
Tesla (T)
Tungsten (W)

Acknowledgements

The journey of my Ph.D. was not an ideal case.

Firstly, I would like to give my sincere thanks to Prof. dr. hab. Andrzej Wawro for offering me the opportunity to research under his supervision. It was really a great experience to work with him as he is one of the best teachers and professors I have come across during my academic career. I have learned so many things in the field of magnetism starting from scratch from him.

Secondly, I am deeply thankful to Dr. Ewelina Milinska who provided an opportunity to do research and give me a place in the field of spin-orbitronics as well as be a co-supervisor during my Ph.D. Thesis. She funded my Ph.D. journey from start to finish through her EU-project, allowing me to complete my thesis from scratch

Thirdly, I sincerely thank Dr. Braj Bhushan Singh from the Department of Physics, Harcourt Butler Technical University, who is the first person to show me the path to the spintronics world. I will always be grateful to him.

Institute of Physics, Polish Academy of Sciences

I want to express my appreciation to Marcin Jakubowski for teaching me MOKE, MBE, and MFM, and for his generous help in writing the manuscript. I extend my heartfelt gratitude to Dr. Aleksiej Pietruczik for his invaluable guidance in teaching me about the MBE systems, as well as his unwavering assistance in preparing samples. My sincere appreciation goes to MSc. Eng. Paweł Aleszkiewicz for his assistance in lab view programming, which greatly contributed to the success of my research. I would like to express my thanks to Artem Lynnyk for his meticulous measurements of magnetization for all of my samples. My deepest gratitude goes to Dr. Sabina Lewińska and Dr. hab. Pavlo Aleshkevych for their assistance with VSM and cavity-FMR measurements, respectively. I would like to thank Dr. Tomasz Jaroch for discussing journey of my Ph.D. studies and his inspiring words. I am deeply thankful to Dr. Roman Minikayev for his expertise in XRD and XRR measurements, which greatly contributed to my research. I extend my sincere thanks to Dr. Oleksandr Chumak and Dr. hab. Eng. Adam Nabiałek for their invaluable help with Cavity-based FMR measurements and Mathematica code for FMR analysis. My appreciation goes to Dr. hab. Carmine Autieri, Rajbul Islam, and Amar for their invaluable assistance with DFT calculations. I would like to thank Dr. Maciej Zgirski for his help with VNA-FMR setup, and for teaching me about VAN-FMR set-up and dynamics properties. My heartfelt thanks go to Dr. Marek Foltyn for his inspiring words during my PhD journey. I would like to express my gratitude to Prof. dr hab. Piotr Deuar and Prof. dr hab. Łukasz Kilański for extending my Ph.D. study, which allowed me to further develop my research. My sincere thanks go to Agnieszka Knioła and Agnieszka Jedrzejewska for their assistance during my Ph.D. journey. For NMR measurements, I am very thankful to Prof. Dr. hab. Marek Wójcik and Jaydev Dey. I would like to thank Prof. Dr. hab. Piotr Dłużewski for TEM measurements. I extend my thanks to Anna Senchenko from the Welcome Centre, IFPAN, for her invaluable assistance in applying TRC during my Ph.D. research. I would also like to thank Prof. Daniel for providing the 'Erasmus fund' that allowed me to visit HZDR during my Ph.D. study, which greatly expanded my knowledge and research capabilities.

University of Białystok

My sincere appreciation goes to Prof. dr. hab. Andrzej Maziewski from University of Białystok. Also, I would like to thank Dr. Zbigniew Kurant for MOKE measurement, Dr. Iosif Sveklo for MFM measurements and Wojciech Dobrogowski for technical support. I would like to thank Dr. hab. Ryszard Gieniusz, U. Guzowska, Dr. Anuj Kumar Dhiman for BLS measurments and discussion of BLS results. I would like to thank Dr. Jan Kisielewski for helping in micromagnetic simulation.

I would also like to thank Dr. Piotr Mazalaski for his financial support and giving me the opportunity to work in his Beethoven Project during my 3rd and 4th year of Ph.D. study.

Helmholtz-Zentrum Dresden-Rossendorf

I would like to express my gratitude Dr. Kilian Lenz from HZDR for giving me an opportunity to explore the dynamics measurements for skyrmion resonances in multilayer samples and Dr. Atila Kakay for teaching me micromagnetic simulation for multilayers to create skyrmions. I would like to Thank to Dr. Jürgen Lindner for giving me an opportunity to perform some experiments in his dynamics group. Also, I would like to thank Gaurv Kumar Patel for helping me in VNA-FMR measurements.

I would like to thank the people of my village Bilankauda for their blessings.

My heartfelt thanks goes to my friends in the guest house who always gives inspiration as well as preparing good foods for dinner and lunch, none other than, Ashutosh Wadge, Pradosh Sahoo, Dr. Ishika Palit and Abinash Adhikari.

Also, I would like to thank my friends at IFPAN, Ajeesh, Damian, Archana Didi, Dibyakrupa Bhai, Abdul Bhai, Adili, Kiran. I would like to thank my wife Dipshikha Mangaraj for preparing food for me and supporting me during writing this thesis.

I would like to thank Prof. Dr. Naresh Mishra, Prof. dr. Karmadev Maharana, Prof. dr. Swapna Mahapatra and Dr. Ramakanta Naik from Utkal University for inspirations.

I would like to express my gratitude to several individuals who have inspired and supported me in my academic pursuits. First and foremost, I would like to thank Sangeeta Mohanty for inspiring me to pursue research in Physics. Additionally, I am grateful to Sangeeta, Subrat, and Ratan from ISRO for their guidance and support. I also owe a debt of gratitude to Dr. Sudhansu Das from the University of Tokyo, whose work in the field of spintronics has been a great source of inspiration to me. Finally, I would like to thank Prof. Dr. Debakanta Samal for his unwavering support in helping me to obtain a PhD abroad, as well as Dr. Gopal K. Pradhan for his contributions to my academic journey. I would like to Thank Dr. Niladri Bihari Sahoo for supporting and inspiring me for research.

I would like to thank Dr. Niru Chowdhury from IIT Delhi for her inspiration and also, I have learnt so many things in the field of spintronics. I would like to thank Dr. Thiruvengadam Vijayabaskaran from the Laboratory for Nanomagnetism and Magnetic Materials and people of this lab from National Institute of Science Education and Research. I would like to thank Harihar Sir, Hanan Sir, Dhrubananda Sir and Krushna Sir from SKCG College.

I would like to thank my friends from master degree, Bikash, Jogesh, Pradeep, Jagannath, Sagarika, Biswaranjan, Sanjay, Manash and all other, friends from bachelor Ajit, Amiya, Tanmay, Silu, Dev, Rasmi, Sinu, college friends, Alok, Sinu, Gada and Manoj and my childhood friends Bijay, Parakash. I would like to express my gratitude to my teachers Gada Sir, Rehman Sir, Nimai Sir, Saroj Sir and Chand Sir for their inspiring words from Atibadi Jagannath Das Bidypitha. I would like to thank my teachers Dr. Abatar Mishr, Sukanta Pradhan Sir, Nabaghana Sahu Sir, Sada Sir, Subhajit Nanda Sir, Biswambar Sahoo Sir, Purnachandra Nayak Sir for their inspirations. I would like to thank my uncle Dwarikanath Biswal who always supported me financially and morally from my childhood, I will always be grateful to him.

I would like to Thank to Maa Harachandi, Maa Bhagabati, Maa KanakaDurga, Lord Mahadev, Lord Ram and Krishna, Lord Hanuman and Lord Jagannath for their blessings. I also would like to thank all four fundamental forces and five basic elements for always being with me.

And finally, I am eternally grateful to my family who always supported me and believed in me. Without them, I would not be able to reach this stage of my life. Thank you very much..

Source of Funding

This thesis work is supported by the Foundation for Polish Science (FNP) under the European Regional Development Fund – Program [REINTEGRATION 2017 OPIE 14-20] and by the Polish National Science Centre projects: [2016/23/G/ST3/04196] and [2020/37/B/ST5/02299].

Also, It is supported by IEEE Magnetic Society Student Seed funding 2020-2021 and ERASMUS+ student and staff mobility grant ERASMUS-10 & 11.

Publications, Grants and list of conferences

This thesis is based on the two papers mentioned below.

1. **Sukanta Kumar Jena**, Rajibul Islam, Ewelina Milińska, Marcin M. Jakubowski, RomanMinikayev, Sabina Lewińska, Artem Lynnyk, Aleksiej Pietruczik, Paweł Aleszkiewicz, CarmineAutieri, Andrzej Wawro "Interfacial Dzyaloshinskii-Moriya interaction in epitaxial W/Co/Pt multilayers" Nanoscale 13 (16), 7685-7693, 2021.
   My Contribution:-Sample fabrication, MFM measurements and its analysis, SQUID analysis, K_{eff} method calculation to determine D_{eff}, First draft of manuscript writing, discussion and interpretation of all results.
2. Zbigniew Kurant, **Sukanta Kumar Jena**, Ryszard Gieniusz, U Guzowska, Marek Kisielewski, Piotr Mazalski, Iosif Sveklo, Alex Pietruczik, Artem Lynnyk, Andrzej Wawro, Andrzej Maziewski "**Magnetic ordering in epitaxial ultrathin Pt/W/Co/Pt layers"** Journal of Magnetism and Magnetic Materials 558, 169485, 2022.
   My Contribution:-Investigation

Grants and Fellowship

1. Ph.D. Scholarship by project **Beethoven** which is financed by **Polish National Science Center**: Domain wall dynamics and magnetic texture behavior in magnetic films with Dzyaloshinskii-Moriya interaction,
   At Institute of Physics and Jerzy Haber Institute of Catalysis and Surface Chemistry, Polish Academy of Sciences, August 2020 to June2022.
   1.Preparation and characterization of ultrathin magnetic films using ultra high vacuum techniques
   2.Studies of magnetization dynamics using VNA-FMR setup

2. **IEEE Magnetics Society Educational Seed Funding**
   For small instrument purchasing and grant for IEEE magnetic conference, December 2020 to December 2021.
   To investigate the dynamics of magnetic W/Co/Pt epitaxial multilayers with iDMI by VNA.

Conferences/Presentation

Poster

1. Annual Review IFAPAN 2019, Warsaw, Poland. 14th February
   Magnetization reversal and domain structure of heavy metal/ferromagnetic heterostructures
2. IEEE Magnetic Summer School-2019 Richmond, VA, USA, 2-7th June
   Magnetization reversal and domain structure of heavy metal/ferromagnetic heterostructures
3. JEMS-2019 Uppsala, Sweden. 26-30th August, 2019
   Magnetization reversal, domain structure and ferromagnetic resonance of heavy metal/ferromagnetic heterostructures.
4. European School on Magnetism 2019, Bron, Czech Republic, 2-13th September
   Magnetization reversal, domain structure and ferromagnetic resonance of heavy metal/ferromagnetic heterostructures.
5. Annual Review IFAPAN 2020, Warsaw, Poland. 13th February
   Magnetization reversal, domain structure and ferromagnetic resonance of heavy metal/ferromagnetic heterostructures.

Oral Presentation

1. Ph.D. symposium 2019, IFPAN , Green Park Conference Centre, Serock, Poland, May 28-30th 2019.
   Magnetization reversal, domain structure and ferromagnetic resonance of heavy metal/ferromagnetic heterostructures
2. JEMS-2020 Lisbon, Portugal, 7-11th December, 2020.
   Investigation of interfacial Dzyaloshinskii-Moriya interaction and ferromagnetic resonance of MBE grown W/Co/Pt heterostructures
3. INTERMAG 2021 virtual conference, Leon, France April 26th to 30th 2021.
   Magnetic anisotropy, interlayer coupling and Dzyaloshinskii-Moriya interaction in the epitaxial W/Co/Pt multilayers
4. The European Conference PHYSICS OF MAGNETISM 2021 (PM'21), Poznan, Poland, June 28 - July 2, 202.
   Magnetic domain structure and interfacial Dzyaloshinskii-Moriya interaction in the epitaxial W/Co/Pt multilayers
5. Joint MMM-Intermag 2022, New Orleans, LA, USA, January 10th to 14th 2022.
   Magnetization reversal and domain structure in epitaxial W/Co/Pt multilayers with various basic stack repetition number

Seminar

1. IFPAN, 2018, 11th April
   Study of spin pumping in Co thin film vis-à-vis seed and capping layers using ferromagnetic resonance spectroscopy
2. The University of Białystok, 2018, 8th May
   Study of spin pumping in Co thin film vis-à-vis seed and capping layers using ferromagnetic resonance spectroscopy.

Scientific trips

ESRF, Grenoble, France, 31st Oct to 7th Nov, 2018
Performing XMCD experiments and becoming familiar with synchrotron techniques.

Internship:-

Helmholtz-Zentrum Dresden-Rossendorf (HZDR), Germany. 9.12.2022-21.032023
Magnetization Dynamics:- group of **Dr. Kilian Lenz**
Project: ***Ferromagnetic resonance studies of skyrmion dynamics in epitaxial multilayers***

Table of Contents

Chapter:-1

Introduction

The artificial layered systems offer the possibility to tune their properties in the wide range by playing with their structural parameters such as: thickness of the component layers, their chemical type, sequence in the stack and repetition number of the basic "brick". In this way, it is possible to tune magnetic anisotropy, Dzyaloshinskii-Moriya interaction, interlayer coupling and efficiency of the magnetostatic interactions. Manipulation with these different factors results in numerous magnetic states and different magnetization reversal processes. Consequently various novel domain structures may appear in such systems.

In this thesis, I will explain structural and related magnetic properties of W/Co/Pt thin film layered systems in the presence of interfacial Dzyaloshinskii-Moriya interactions (iDMI)[1]. I selected this type of stack because it is composed of ferromagnetic layers and heavy metals layers with high spin-orbit coupling. Asymmetrical surrounding of the ferromagnetic layer is necessary to emerge DMI being responsible for "exotic" spin structures. In this system it is also possible to induce perpendicular magnetic anisotropy (PMA) and switch between ferromagnetic and antiferromagnetic exchange interlayer coupling (EIC). The investigated layered systems were fabricated by molecular beam epitaxy (MBE) technique, offering much higher crystalline quality of the samples in comparison to commonly used sputtering methods. Particularly, a well-defined structure of the interfaces is very crucial for PMA and DMI, making these properties more effective and distinct.

The aim of my research was to study how such a complex set of various interplaying properties changes with the structural parameters of the stack such as thickness of the component layers. Moreover, by increasing a repetition number of the basic trilayer, other interactions such as: interlayer coupling and magnetostatic interaction were gradually introduced, resulting in evolving magnetic states, magnetization reversal mechanism and domain structure. For this reason, I study systematically complicated fabricated structure of the investigated stacks, starting from the single Co layer (PMA and DMI), via double and moderate repletion number of the Co layers (IEC) up to high repetition number reaching 20 (increasing role of magnetostatic interactions).

A part of the results presented in this thesis has been already reported in two papers with my authorship. These works were published in *Nanoscale* and *Journal of Magnetism and Magnetic Materials*. Remaining results from my thesis are the subject of further articles that

are currently in preparation. Many of these data were also presented personally by me at numerous conferences.

The investigated structures were designed by myself. I also assisted in the sample fabrication process and in-situ structural characterisation. I investigated magnetic anisotropy in various configurations of W/Co/Pt stack with the single Co layer in comparison with Mo/Co/Au system. In the Pt/W(d_W)/Co(d_{Co})/Pt stack, I took part in initial investigations of magnetic states and hysteresis loop shapes in a function of (d_W, d_{Co}).

Also I contributed to investigations of interlayer coupling in the systems containing two Co layers. Based on the shape of the hysteresis loop, I estimated the interlayer coupling strength.

In the multilayers with medium repetition numbers, I performed magnetic domain investigations using magnetic force microscopy (MFM).

In a multilayered system, I performed MFM measurements as well and modified the magnetic domain structure from labyrinth- to stripe-like alignment. Based on the domain width, I calculated the strength of iDMI using the effective magnetic medium model under approach of effective coefficient of magnetic anisotropy (K_{eff}). I prepared an initial version of the manuscript and took part in the further (re)submission procedure finished by a successful publication in the *Nanoscale* journal (as the first author).

A short introduction to the content of my thesis is presented below.

From last decades, many research groups[1] have been investigating the chiral nature of numerous spin structures. The chiral magnetism firstly was observed in the FeGe bulk material which shows magnetic skyrmions due to presence of iDMI with high spin orbit coupling strength and intrinsic broken symmetry inversion. However, in thin film magnetic heterostructures composed of heavy metal and magnetic layer, the inversion symmetry breaking can be induced at the interface of ferromagnetic and the non-magnetic heavy metal. The heavy metal should exhibit high spin orbit coupling strength as a basic factor for iDMI occurrence. The engineering of such heterostructures gives the degrees of freedom to tune the iDMI strength as well as induce the topological particles, called skyrmions which can be used for future spintronics. Here, I will describe the epitaxial; W/Co/Pt system which is a potential candidate to possesses the one of the highest iDMI strength due to additive nature of the iDMI at the two different interfaces formed by the magnetic layer with W and Pt, due to high crystal quality and sharp chemical interface profile.

The growth of Co on W(110) depends upon the thickness of the Co. Initially, the Co grows in pseudomorphic mode and then, it forms closed packed structure with further increase in thickness. In the samples described in this thesis, the W layer is deposited on Pt(111) fcc

buffer layer. The W layer grows W(111) in pseudomorphic mode up to 5Å which was confirmed by RHEED images and further with increasing in the thickness, it starts to grow as the W(110) bcc structure. The RHEED images show the superposition of two patterns of W layer on Pt which is due to the random orientation of the crystallite domains rotated by 30° or 90° in three different directions with respect to Pt(111) layer. The presence of symmetry misfit between W(110) bcc and close packed structure of the Co layer can be a reason of a local in-plane anisotropy. However, mentioned mutual misorientation of W crystallites results in the global isotropic behavior of the magnetic layer.

A single crystal structure of the W(110) bcc layer is responsible for the anisotropic behavior in iDMI strength along the different crystallographic directions, which further can give the stabilization of the antiskyrmions. Camosi *et al.* shows that the iDMI strength is 2-3 times higher along the axis bcc(-110) than the axis bcc(001) in W/Co/Au system[2]. The presence of this anisotropic behavior results in elliptical skyrmion[3] in a particular orientation of crystallographic directions. Most of the Pt/Co/W systems have been deposited by sputtering technique. They exhibit the higher interface roughness and worse defined crystalline structure. So, the deposition of W results in the rougher interface and intermixing at the Co/W interface, which affects the behavior of the magnetic layer. With the increasing the thickness of W layer, the roughness increases. As a result, a part of magnetic layer close to Co/W interface behaves as nonmagnetic material due to intermixing and it is called as a dead layer[4,5]. The presence of dead layer in sputtered Pt/Co/W systems mainly affects the magnetic properties at lower repetition numbers due to higher roughness of Co/W interface[6]. Another aspect of W/Co/Pt is the spin reorientation transition in the Co layer with increasing the Co film thickness. In Pt/Co/W stacks, the SRT is observed for the Co layer thickness of 15Å and is weakly dependent on the Pt and W layer thickness. However, for Pt/W/Co/Pt system the SRT thickness of Co markedly depends upon the buffer layer of W which deposited on Pt fcc(111). The SRT thickness of Co increases with increasing W thickness and it starts from 9Å to 30Å for W thickness ranging from 3Å to 100Å. In this specific system the magnetic properties depend upon the both thickness of the W and Co. For various stack structural combinations nonmagnetic and numerous magnetic states can be observed. The details will be discussed in chapter 4.

The other properties of the W/Co/Pt system with two Co layers separated by a spacer to tune the interlayer magnetic coupling in the presence of iDMI which has been investigated in this thesis. Generally, the interlayer coupling depends upon the thickness of the spacer between two magnetic layers and shows oscillatory behavior with increasing the spacer thickness,

associated with the parallel or antiparallel configuration of magnetization of individual layers. The interlayer coupling can be described as ferromagnetic or antiparallel antiferromagnetic coupling of magnetization in terms of RKKY (Ruderman–Kittel–Kasuya–Yosida) interaction. The antiferromagnetic coupling only exists if the Co layers are separated by the double layer spacer Pt/W. Otherwise, it shows the ferromagnetic coupling for the same thickness of single layer spacer W or Pt. Therefore, the effective interlayer coupling may not depend merely on pure RKKY interaction but also on the iDMI strength of the system. However, one should be aware that in the final magnetic states of the layered system also PMA plays an important role. The RKKY strength has been estimated to be in the range from -0.01 mJ/m^2 to -0.08 mJ/m^2 for the thickness of the spacer Pt(12Å)/W(12Å) to Pt(7Å)/W(7Å), the strength is comparable to the system Co/Pt/Ru/Pt/CoFeB[7]. Recently, Szulc *et al.* reported that two Co layers with different thicknesses separated by W show the two different resonances by BLS in Pt/Co/W/Co/Pt system[8]. The origin of the two resonances may be different anisotropy of the top and bottom Co layer depending upon the different growth of Co layer on W and Pt, and the different thickness of Co film. Also, it has been reported that the nonreciprocity of frequency due to interlayer DMI increases when the both layers top and bottom have the same heavy metal neighbours with the opposite sign of iDMI at the top and bottom layer in antiparallel configuration in Pt/Co/Cu/Co/Pt system[9]. However, the nonreciprocity of the frequency decreases due to different signs of iDMI at the interface in Pt/Co/Pt and gives the zero value in change in frequency. The details about interlayer coupling in W/Co/Pt/W/Co/Pt system will be discussed in chapter 5.

First Jiang *et al.*[10] and Lin *et al.*[11] reported the existence of iDMI Pt/Co/W multilayer thin films with formation of skyrmion without and in the presence of the external magnetic field. However, the multilayers were deposited by sputtering, thus they showed the lower surface iDMI constant with respect to the epitaxial sample grown by molecular beam epitaxy (MBE)[12]. The surface iDMI constant started from 0.3 pJ/m to 1.5pJ/m for various thickness of Co in Pt/Co/W systems. The calculation of iDMI strength was performed by considering the skyrmion radius and asymmetric domain wall propagation using Kerr microscopy[10, 11]. However, for the epitaxial multilayered sample $(W/Co/Pt)_N$ (N =20), we calculated the DMI strength by two different methods i.e. by K_{eff} method and by first principle calculation. Further, both results were also confirmed by micromagnetic simulations. The surface iDMI constant for epitaxial thin films $(W/Co/Pt)_{20}$ is equal to 1.83pJ/m which is discussed in chapter-6.

Apart from the double layer of Co separated by Pt/W, we also study the interlayer coupling in multilayers with moderate repetition number (n = 6 or 7) which showed the purely

antiferromagnetic coupling and the layer by layer reversal with the applied field. For an even number of Co layers, it shows zero magnetization at zero field due to fully antiferromagnetic compensation. However, for odd layer numbers, the magnetization is different from zero when the magnetic field is zero. We study the stacks with different spacer thicknesses W(5Å)/Pt(5Å) and W(10Å)/Pt(10Å) for multilayer 6 and 7 repetition systems and thickness of the Co layer d_{Co} = 10Å. The magnetization curve, for the spacer layer with W(5Å)/Pt(5Å) between two Co layers shows only antiferromagnetic coupling where the RKKY coupling strength is dominating over dipolar coupling strength and behavior of the system can be explained by macrospin model[13]. The samples with the spacer thickness W(10Å)/Pt(10Å) between Co layers show the ferromagnetic coupling due to domination of dipolar coupling and negligible antiferromagnetic coupling strength. The details of RKKY interaction in W/Co/Pt multilayers are discussed in chapter-5.

Further, to study the magnetic domain evolution by magnetization reversal in the presence of external magnetic field in the W/Co/Pt multilayers, we have performed the magnetic force microscopy with magnetic field perpendicular to the sample plane. The lattice bubble skyrmions structure was observed with diameter of the individual objects equal to 75 nm. The detailed study of domain evolution in $[W(10Å)/Co(6Å)/Pt(10Å)]_{20}$ will be discussed in chapter-6.

1.1:-References

1. Tokura, Y. & Kanazawa, N. Magnetic Skyrmion Materials. *Chemical Reviews* **121**, 2857–2897 (2021).
2. Camosi, L. *et al.* Anisotropic Dzyaloshinskii-Moriya interaction in ultrathin epitaxial Au/Co/W(110). *Physical Review B* **95**, 1–6 (2017).
3. Camosi, L. *et al.* Self-organised stripe domains and elliptical skyrmion bubbles in ultra-thin epitaxial Au0.67Pt0.33/Co/W(110) films. *New Journal of Physics* **23**, 0–10 (2021).
4. Fritzsche, H., Kohlhepp, J. & Gradmann, U. Epitaxial strain and magnetic anisotropy in ultrathin Co films on W(110). *Physical Review B* **51**, 15933–15941 (1995).
5. Wulfhekel, W., Gutjahr-Löser, T., Zavaliche, F., Sander, D. & Kirschner, J. Relation between structure, stress, and magnetism in Co/W(001). *Physical Review B - Condensed Matter and Materials Physics* **64**, 1–8 (2001).
6. Benguettat-El Mokhtari, I. *et al.* Interfacial Dzyaloshinskii-Moriya interaction, interface-induced damping and perpendicular magnetic anisotropy in Pt/Co/W based

multilayers. *Journal of Applied Physics* **126**, (2019).

7. Fernández-Pacheco, A. *et al.* Symmetry-breaking interlayer Dzyaloshinskii–Moriya interactions in synthetic antiferromagnets. *Nature Materials* **18**, 679–684 (2019).
8. Szulc, K. *et al.* Nonreciprocal spin-wave dynamics in Pt/Co/W/Co/Pt multilayers. *Physical Review B* **103**, 134404 (2021).
9. Franco, A. F. & Landeros, P. Enhancement of the spin-wave nonreciprocity in antiferromagnetically coupled multilayers with dipolar and interfacial Dzyaloshinskii-Moriya interactions. *Physical Review B* **102**, 184424 (2020).
10. Jiang, W. *et al.* Quantifying chiral exchange interaction for Néel-type skyrmions via Lorentz transmission electron microscopy. *Physical Review B* **99**, 104402 (2019).
11. Lin, T. *et al.* Observation of room-temperature magnetic skyrmions in Pt/Co/W structures with a large spin-orbit coupling. *Physical Review B* **98**, 174425 (2018).
12. Jena, S. K. *et al.* Interfacial Dzyaloshinskii-Moriya interaction in the epitaxial W/Co/Pt multilayers. *Nanoscale* **13**, 7685–7693 (2021).
13. Hellwig, O., Kirk, T. L., Kortright, J. B., Berger, A. & Fullerton, E. E. A new phase diagram for layered antiferromagnetic films. *Nature Materials* **2**, 112–116 (2003).

Chapter:-2

Theoretical review

Magnetism is one of the fundamental properties of matter manifesting in the macro- as well as microscale. It originates from the attributes of matter at the atomic level: magnetic moment induced by orbiting electrons in atoms and intrinsic quantum property of electron – spin. From the ancient age to the modern, magnetic materials have fund numerous practical application and last decades have been used for data-storage technology. It is believed that the magnetic material was used in 800-700 BC in ancient Bharat for medical purposes by Sushruta who describes in his book "*Sushruta Samhita*". In ancient Greece, Aristotle describes the magnetism to the philosopher Thales of Miletus around 625 BC to about 545 BC. In the 19th century, Hans Christian Ørsted observed the behavior of magnetic compass near the current-carrying conductor and Michael Faraday showed that alternating magnetic field induces electric current. James Clark Maxwell wrote the equation for magnetism. This was the beginning of electromagnetism. The first theory for a permanent magnet was proposed by Pierre Weiss in 1906. Many years later, Heisenberg wrote the Hamiltonian for exchange interactions of neighboring spins, which describes magnetism at the atomic scale. This is a very short history of magnetism and its development in the modern age.

In this chapter, some of the theoretical concepts of magnetism will be explained, which are the backbone of the experimental observations described in this thesis. Firstly, the basic idea of dia-, para-, and ferromagnetism and then its origin will be discussed. Then, different kinds of interactions and components of the total energy of magnetic material will be presented, i.e. and asymmetric exchange interactions (i.e. Interfacial Dzyaloshinskii-Moriya interaction, iDMI), magnetic anisotropy, Zeeman energy, etc. I will discuss how to induce the DM interaction in the thin-film system with the broken inversion symmetry at the interface of ferromagnet and 5-d metals. Further, the different types of magnetic domains stabilized in such thin film systems will be considered.

Table of Contents

2.1:- Types of Magnetic materials

Three basic kinds of magnetic materials are distinguished by the arrangement of the magnetic moments at atomic level: diamagnets, paramagnets, and ferromagnets. Figure 2.1 schematically presents the types of alignment of magnetic moments in those different systems [1].

In paramagnets, the atoms carry permanent magnetic moments. They do not interact with one another and in the ground state they are disoriented mainly by the thermal fluctuation giving a net moment equal to zero. However, external magnetic field forces their alignments towards parallel ordering. In diamagnets, the atoms do not exhibit magnetic moments. Diamagnetism is a quantum mechanical effect. In the presence of external magnetic field, low magnetic moments are induced and oriented in antiparallel direction to the field. This property of all materials, however due to weak strength is often covered by other much stronger features.

The material that shows, due to exchange interaction, an ordered parallel arrangement of spins in the ground state expanding in a long range is called ferromagnet. It exhibits a permanent magnetic moment much higher than mentioned paramagnet. In the antiferromagnetic systems the identical moments are ordered antiparallel giving the net moment equal to zero. Usually, this phenomena is explained as the antiparallel coupling of two sublattices with ferromagnetic ordering each. If, in such an ordering, two sublattices have different moments, the material exhibits a net moment and is called a ferrimagnet.

Mentioned above long range orderings are temperature dependent and appear below a certain characteristic temperature called as Curie temperature in the case of ferromagnets and ferrimagnets and as Néel temperature for antiferromagnets. Ferrimagnets may display moreover a compensation point below Curie temperature in which net magnetization is equal to zero because of mutual cancelation of contributions from individual sublattices. Above critical temperatures magnetic materials lost their long range orderings and can be considered as paramagnets.

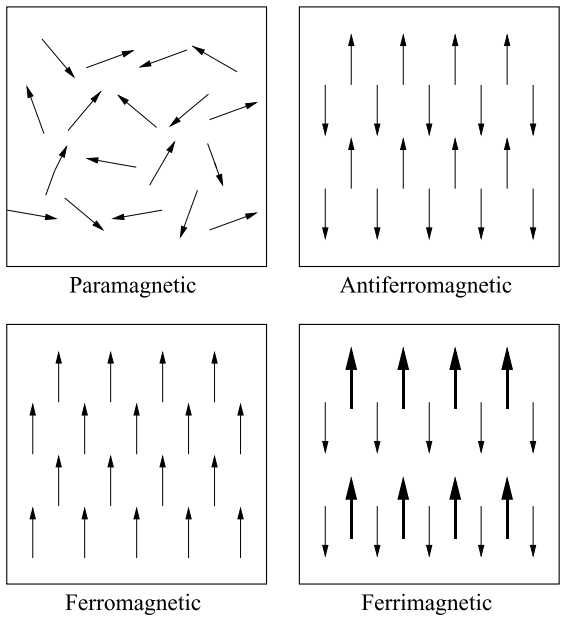

Figure 2.1 Schematic presentation of different types of magnetization alignment. The image is adopted from [1].

Magnetic susceptibility describes a response of magnetization on magnetic field and is defined as $\chi = M/H$, where M- magnetization and H – magnetic field. The susceptibility of diamagnets is low and negative and weakly depends on temperature, whereas it is positive in paramagnets. In ferromagnetic material this parameter takes a positive, much higher values with respect to paramagnetic material. The temperature dependence of the inverse susceptibility of various types of magnetic materials is shown in figure 2.2.

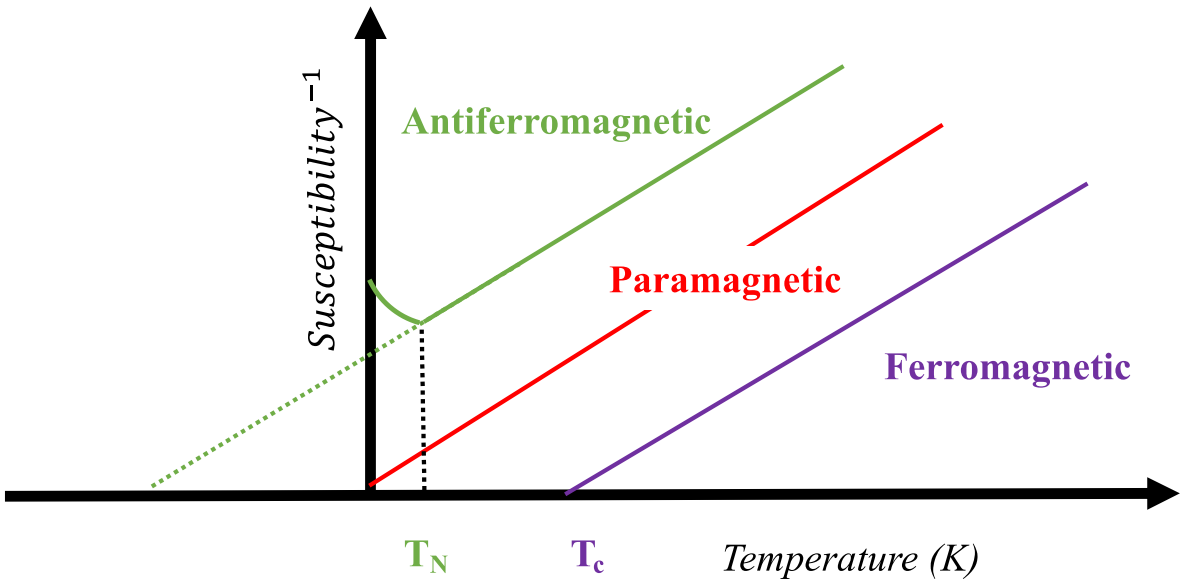

Figure 2.2 represents the schematic of 1/χ (T) dependence for Ferro, Para and antiferromagnetic material.

2.2:- Energy of ferromagnet

The appearance of a specific magnetic alignment is related to the presence of numerous interactions. A balance of energy components at the total energy minimum determines a magnetic ground state. The total energy in ferromagnetic material in the presence of applied magnetic field is a sum of different components:

$$E_{tot} = E_{ex} + E_{an} + E_Z + E_d + E_{DMI} + E_0 \quad (2.1)$$

where E_{ex} - exchange; E_{an}-anisotropy; E_z- Zeeman; E_d- demagnetization; E_{DMI}- Dzialoshinskii-Moriya interaction and E_0 - other contributions.

2.3:- Direct Heisenberg exchange interaction

The exchange interactions are responsible for the long range magnetic order. If the electrons of neighboring magnetic atoms can interact through exchange interaction without any mediating atom, such behavior is called direct exchange interaction. In 3d transition metal (Fe, Co, Ni) d-electrons, responsible for magnetic properties, are valence ones and they are engaged effectively in the direct exchange interaction.

The Heisenberg interaction describes the exchange interaction between two atoms with spins S_i and S_j. According to the Pauli exclusion principle, two electrons with the same quantum number cannot occupy the same energy level. The electrons, called fermions, obey the Fermi-Dirac statistics and these particles are indistinguishable. Therefore, the wave function of two electrons must be antisymmetric. Heisenberg formulated the Hamiltonian for a set of spins in crystalline lattices [2].

$$H = -J_{ij}S_iS_j \quad (2.2)$$

where S_i is the spin of the i-th atom and S_j is the spin of the j-th atom. J_{ij} is the exchange constant that determines magnetic alignment. If the J is negative, the system accommodates the antiparallel configuration of spins and if J is positive the magnetic moments are parallel to each other and collinear which forms the ferromagnetic system.

Due to various factors (e.g. thermal excitation) the magnetization state of the sample may be modified. Spin waves are one among excitations described by low energy. They can be described as processing magnetic moments exhibiting phase shift along propagation direction. The spin waves are described by the frequency ω and wave vector q. As their usual wavelength is of the order of 1000 Å, a continuum medium approach is used for their description. The

fundamental formula describing the propagation of spin waves is the Landau-Lifshitz- Gilbert [3, 4] torque equation of motion:

$$\frac{d}{dt}M = -\gamma\mu_0(M \times H) + \frac{\alpha}{M}(M \times \frac{d}{dt}M) \quad (2.3)$$

where M - the total magnetic moment, γ-the gyromagnetic ratio, α-Gilbert damping of the material.

2.4:- Indirect exchange interaction

In the case of e.g. 4f rare earth metals, the orbitals of 4f electrons carrying magnetism are shielded by outer electrons and overlapping is rarely possible Therefore, the direct exchange interaction is not very effective. Thus the magnetic properties of 4f rare earth metals cannot be described in terms of only direct exchange interaction. So, some magnetic materials, e.g. Gd, can be described by an indirect exchange interaction. In the indirect exchange the interaction may be mediated by the conduction electrons of metal (so called s-d model). The conduction electrons of metal get polarized by the magnetic atom electrons and interact with other magnetic atoms. One of the examples is RKKY (Ruderman, Kittel, Kasuya, and Yosida) [5, 6, 7, 8] interaction.

In the case of thin film structures, where two magnetic layers are separated by a non-magnetic metal layer, the RKKY interaction depends on the type and thickness of the spacer between the two magnetic layers. It can form ferromagnetic or antiferromagnetic magnetization alignment. The coupling energy can be expresses by the following formula:

$$J = \mu_0 M_S H_{IEC} d \quad (2.4)$$

where H_{IEC} is the coupling field related with the shift of the hysteresis loop or its components. The oscillatory character of the coupling can be observed with increasing thickness of the non-magnetic spacer. Figure 2.3 shows the exemplary oscillatory behavior of two NiCo layers separated by nonmagnetic Ru spacer with different thicknesses [9].

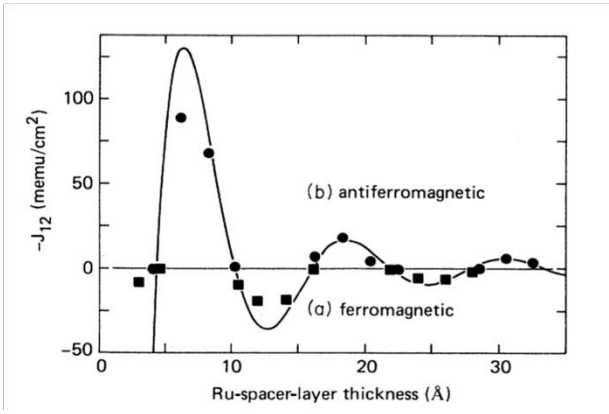

Figure 2.3. The oscillatory nature of two magnetic layers separated by Ru spacer due to RKKY interaction. The figure is adopted from [9].

2.5:- Magnetic Anisotropy

Isotropy term refers to the material properties which are the same in any direction. In contrast, anisotropy means that different properties are observed in the various directions of the material. The main reasons for anisotropy are: internal (e.g. crystalline or composite) structure of matter and/or the sample shape. When magnetic anisotropy occurs, magnetic moments in the absence of external magnetic fields tend to align along a specific direction called the easy axis.

In the case of magnetic thin film layered structures, magnetic anisotropy has a complex character. Such a system is characterized by: reduced dimensionality along its thickness and high contribution of atoms with broken environment symmetry that form interfaces. Four basic components of anisotropy can be clearly distinguished there: magnetocrystalline (related to the crystalline structure of the magnetic layer), interface (resulting from the broken symmetry and electron hybridization between the atoms forming interfaces), magnetoelastic (being a result of lattice deformation due to strains induced by the lattice mismatch at the interfaces) and dipolar (or shape, that results in creation of demagnetizing field in the system with reduced dimensionality which interacts with magnetization). The three first components may align magnetization along perpendicular or in-plane direction whereas the dipolar one always orients magnetization in the sample plane.

Magnetocrystalline anisotropy is a consequence of crystalline structure of magnetic material and spin-orbit coupling. The crystalline field modifies the shapes of the electron orbitals according to the symmetry of the lattice. Due to the spin-orbit coupling, the magnetic moments are aligned in a particular direction which reflects again the crystal symmetry. Such a single-ion contribution mechanism satisfactorily explains the properties of ferromagnetic elements like: Fe (body cubic centred, bcc), Ni (face cubic centred, fcc) and Co (hexagonal, hcp). Dipolar interactions between ions that stabilise their orbitals can be another source of magnetocrystalline anisotropy, called two-ion anisotropy. The efficiency of this mechanism depends on the crystal lattice symmetry. It vanishes in the cubic lattices, whereas in noncubic structures, it can give a substantial contribution to the overall anisotropy.

The energy expressions for magnetocrystalline anisotropy for different symmetries: hexagonal and cubic are given by equations 2.5 and 2.6, respectively [10].

$$E_a = K_1 sin^2\theta + K_2 sin^4\theta + K_3 sin^6\theta + K_3' sin^6\theta sin6\phi \quad (2.5)$$

$$E_a = K_{1c}(\alpha_1^2\alpha_2^2 + \alpha_2^2\alpha_3^2 + \alpha_3^2\alpha_1^2) + K_{2c}(\alpha_1^2\alpha_2^2\alpha_3^2) \quad (2.6)$$

where θ is the angle between magnetization and anisotropy axis. K with different under-scripts refers to the different orders of anisotropy constants.

For Fe the easy axis is (100) and the hard axes are (110) and (111), whereas for Ni, the easy axis is (111) and the hard axes are (110) and (100). The anisotropy in Fe and Ni called cubic. For Co, which has hexagonal closed packed structure, the easy axis is (0001) and hard axis is (10-10) as shown in the figure-2.4(a) [11]. The 3D distribution of magnetocrystalline energy for Fe[100], Co(0001) and Ni[111] is shown in the figure 2.4(b) [10].

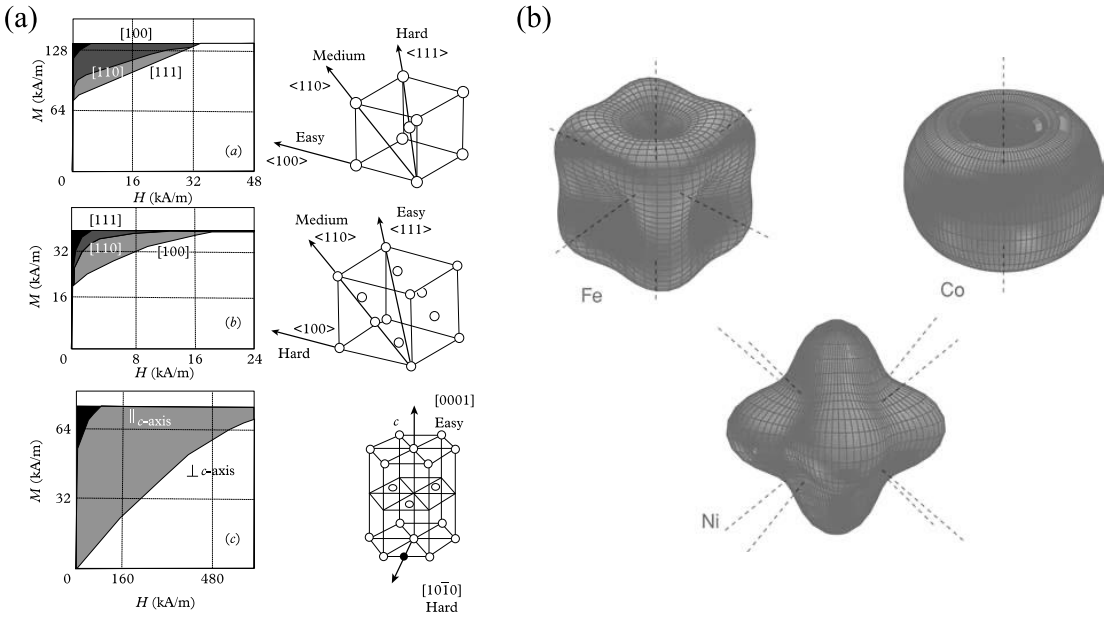

Figure 2.4. (a) Magnetization curves in the magnetic field applied along various directions for different crystalline structures of ferromagnets [11]*. (b) the 3D representation of magnetocrystalline energy for Fe, Co and Ni, adopted from* [10].

Magnetoelastic anisotropy is related to the lattice deformation of the ferromagnetic material. Lattice deformation introduces modifications of the orbital shapes and through the spin-orbit coupling changes orientation of the spins. This component of anisotropy is often met in thin film structures. In epitaxial thin films, the magnetic material grows by homoepitaxy or heteroepitaxy depending upon the buffer layer or substrate. If there is a lattice or structural mismatch describing the crystals of the deposited magnetic material and the substrate or the bottom layer, there is a possibility of stress occurrence.

The energy of magnetoelastic anisotropy for uniaxial system is the product of the stress and the magnetostriction constant, and can be written as [12]:

$$E_{ME} = -\frac{3\sigma\lambda cos^2\theta}{2} \quad (2.7)$$

where θ is the angle between saturation magnetization and the stress σ. If the value of $\sigma\lambda > 0$, then it favours the perpendicular magnetization for a compressive stress.

Surface or interface anisotropy is associated with the systems exhibiting lowered dimensionality. Surface atoms have an asymmetric environment and different shape of the electron orbitals in comparison to the atoms building bulk due to unsaturated bonding or appearing reconstruction (so called Néel anisotropy). The atoms forming interfaces interact with the neighbours of other types and exchange the electrons in the hybridization process. This phenomenon may result in modifications of the magnetic moment and preferred direction of magnetization. Nonmagnetic atoms can gain a magnetic moment (e.g. Pt), whereas the moment of the atoms forming the magnetic material may be lowered. It should be emphasized that the quality of interface described by sharp chemical profile, alloying or roughness substantially affects the strength of the interface anisotropy.

Interface anisotropy becomes effective particularly in ultrathin film structures. For example in the magnetic film five atomic layers thick, 40% of atoms form the interface and suffer influence of the neighbours.

Shape anisotropy plays an important role in the magnetic structures with reduced dimensionality. In thin films, the magnetic moment oriented along the perpendicular direction to the sample plane induces a strong stray field outside the sample. The increasing of the energy of the system is due to the appearance of demagnetization field (due to strong stray field) in the sample that interacts with magnetization. The demagnetization field is described by the following tensor:

$$\boldsymbol{N} = \begin{pmatrix} N_x & 0 & 0 \\ 0 & N_y & 0 \\ 0 & 0 & N_z \end{pmatrix}$$

which satisfies $Tr\boldsymbol{N} = N_x + N_y + N_z = 1$.

The demagnetising field for thin films with perpendicular anisotropy is given by

$$H_d = -\boldsymbol{NM} \quad (2.8)$$

where N is the demagnetization tensor.

For thin films with perpendicular anisotropy $N_x = 0 = N_y$ and $N_z = 1$.

Thus for the sample in the shape of ultrathin infinite plane exhibiting uniform (monodomain) magnetization, the specific demagnetizing energy is given by $E_d = (1/2)\mu_0 M^2 cos^2\theta$, where θ is an angle between magnetization vector M and normal to the film plane. Demagnetising field and related energy play the crucial role in the formation of magnetic domains which will be discussed in the magnetic domain section. It should be emphasized that the shape anisotropy forces magnetization to align in the sample plane, whereas other contributions may orient magnetization both in the sample plane and in perpendicular direction.

2.6:- Phenomenological approach

2.6.1:- Volume anisotropy and surface anisotropy

Because of symmetry breaking at the interface in magnetic thin film systems, the anisotropy energy is different from the bulk crystalline structure. Due to presence of broken symmetry, electron hybridization with bottom and top neighbours and presence of spin orbit coupling under the lattice deformation, the surface anisotropy is induced. The surface anisotropy contribution increases with decreasing the film thickness and vice versa.

Due to the magnetic anisotropy, the ultrathin Co layers sandwiched between non-magnetic layers may be magnetized perpendicularly to the plane in a certain range of thickness. At a critical thickness, a spin reorientation transition (SRT) from perpendicular direction to the film plane alignment (perpendicular magnetic anisotropy, PMA) is observed. In general, the SRT depends upon the thickness of ferromagnetic layer as well as on the type of adjacent layer of nonmagnetic material. Total effective anisotropy in thin Co magnetic film can be described by an uniaxial effective anisotropy model characterized by the K_{eff} coefficient. In this model, the effective anisotropy is considered as the total contribution from all anisotropy components discussed above:

$$K_{eff} = K_U - K_d \qquad (2.8)$$

where K_U is the uniaxial anisotropy related to the sample structural properties and K_d – shape anisotropy origination from the sample shape. In the case of thin films exhibiting a monodomain state, the second term can be expressed as $K_d = 1/2\mu_0 M_S^2$. When the sample is not in a monodomain state, the shape anisotropy should be calculated individually for the real domain structure. However, when $t_m << W$ (t_m is the thickness of the magnetic layer and W is the magnetic domain width), the method for K_d estimation, as applied for monodomain state, provides satisfactory approximation.

In the phenomenological approach it can be written as following:

$$K_{eff} = K_V + 2K_S/t_m \qquad (2.9)$$

where K_V is the volume anisotropy including demagnetization and K_S is the surface anisotropy, t_m is the thickness of the magnetic material. The factor equal to 2 indicates that surface contribution comes from the two interfaces [12]. In such a convention K_{eff} is positive, when magnetization is perpendicular to the film plane and negative for magnetization aligned in the sample plane. The SRT is observed when K_{eff} changes its sign.

The K_{eff} depends on the thickness of the ferromagnetic material t_m. By plotting $K_{eff}t_m$ vs t_m, the values of K_V and $2K_S$ can be determined. The exemplary plot for $K_{eff}t_m$ vs t_m for Co/Pd multilayers with different Co thickness is shown in figure 2.5. It should be noted that K_V contains the demagnetization component. Subtracting it, allows us to obtain a pure volume material parameter related merely to the crystalline structure of the magnetic component layer.

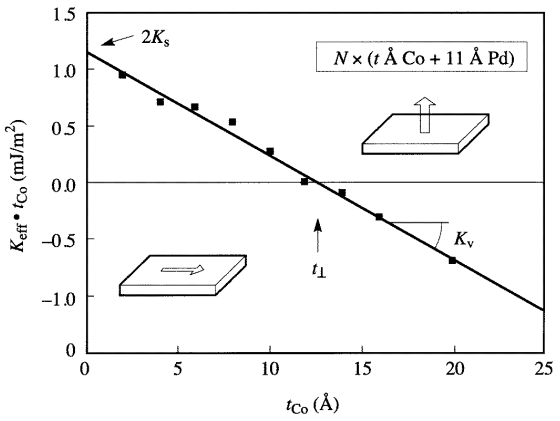

Figure 2.5 The dependence of effective anisotropy coefficient on magnetic layer thickness and corresponding magnetization alignment. [12,13].

One can define, then, a quality factor $Q = 2K_u/\mu_0 M_s^2$. $Q < 1$ corresponds to in-plane magnetization alignment whereas for $Q > 1$ the perpendicular anisotropy is observed.

The influence of discussed above anisotropy components of $K_V$and K_S depend on the crystalline quality of heterostructures. Magnetocrystalline anisotropy is associated with K_V term whereas interfacial anisotropy with K_S one. If the strains induced due to the interface lattice mismatch spread across the whole magnetic film volume and deforms its lattice, then magnetocrystalline anisotropy modifies additionally K_V. However, when these strains are relaxed by a dislocation network formed in the vicinity of interfaces, then the magnetoelastic component contributes to K_S.

2.7:- Dzyaloshinskii-Moriya Interaction (DMI)

Before 1958, the alignment of magnetic moments observed in ferromagnetic and antiferromagnetic materials was considered in terms of symmetric direct or indirect (s-d model) exchange. To describe the weak ferromagnetism in antiferromagnetic material, Dzyaloshinskii [14] introduced the antisymmetric term:

$$E_{DMI} = D_{ij} \cdot (S_i \times S_j) \qquad (2.10)$$

where D_{ij} is the vector of DMI strength and S_i and S_j are two neighbouring magnetic spins of magnetic material.

It is also called antisymmetric exchange interaction which arises due to the high spin-orbit coupling (SOC) in the presence of broken inversion symmetry in the crystal lattice.

Later Moriya proposed that the antisymmetric interaction arises due to the presence of high spin-orbit coupling in considering superexchange interaction [15].

In the bulk non-centrosymmetric crystal B20 type, due to the presence of broken inversion symmetry DMI occurs as the intrinsic property. Levy and Fert [16] investigated the DMI in CuMn system by dusting the heavy metals (HM) with high SOC elements i.e. Pt or Au. They concluded that the existence of DMI arises due to the spin-orbit scattering of conduction 5d electrons in the atoms of added nonmagnetic heavy metal (Figure 2.6(a)).

Moreover, it is also possible to induce the interfacial DMI (iDMI) in the layered structures at the interface between ferromagnetic and heavy metal components with high SOC in the presence of lack of mirror symmetry. In these structures the exchange interaction between interfacial atoms of the ferromagnetic layer is mediated by the atoms of heavy metal (Figure 2.6(b)). The interfacial DMI energy in the layered system can be written as [17].

$$E = D[m_z \frac{\partial m_x}{\partial x} - m_x \frac{\partial m_x}{\partial x}] + D[m_z \frac{\partial m_y}{\partial y} - m_y \frac{\partial m_z}{\partial y}] \qquad (2.11)$$

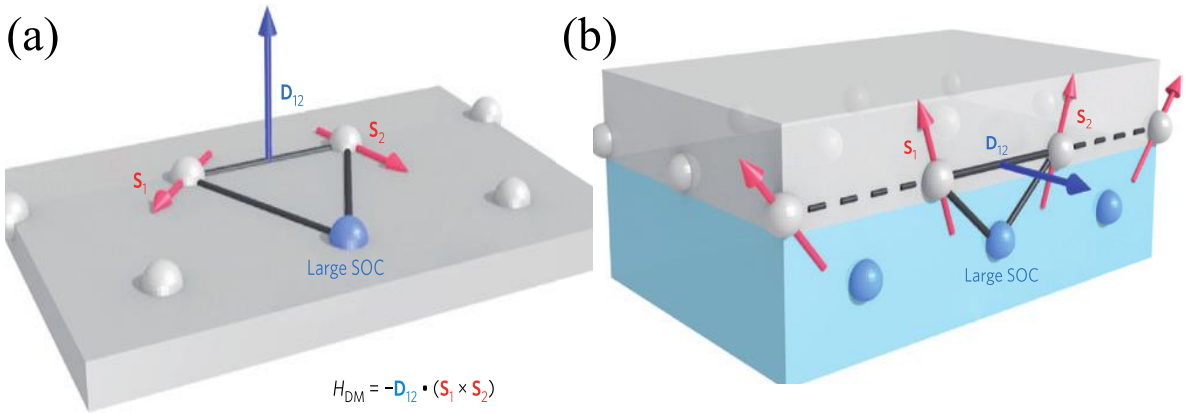

Figure 2.6. Schematic configuration of spins and D vector describing DMI occurring in (a) bulk materials and (b) layered structures [18].

Due to the presence of interfacial DMI, thin film systems may exhibit more complex magnetic non-collinear alignments such as: spin springs, chiral magnetic domain walls and skyrmions [18, 19, 20], which are topologically protected magnetic vortices. Besides the basic research, such structures are also very promising for their application in new methods of magnetic recording and in spintronics.

2.8:- Domains and domain wall

Interaction of the stray fields with the sample magnetization results in demagnetization energy (and related anisotropy). In order to reduce its total energy, magnetic ordering adopts a shape of magnetic domains, a concept proposed by Weiss [21, 22]. The domains are local volumes with well- defined magnetic ordering (e.g. ferromagnetic). They are usually differently oriented in space and are separated by the domain walls.

However, in many cases thin film magnetic structures are better ordered and freedom of magnetic domain directions is limited and structure of the domain walls better defined. Figure 2.7 shows creation of domains in thin film with perpendicular magnetization starting from a monodomain state (Figure 2.7(a)). By dividing into two domains with opposite magnetization directions (Figure 2.7(b)), the dipolar energy is reduced. Further, reduction of dipolar energy may take place by formation of the more complex multidomain state (Figure 2.7(c)).

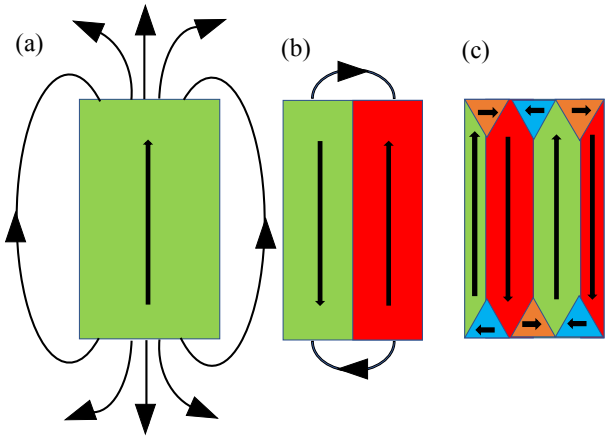

Figure 2.7 Various domain structures: (a) single domain, (b) double domain and (c) complex structure with closing domains in thin magnetic film.

Appearance of the domain structure involves creation of the domain walls. Across the domain wall the magnetization continuously changes its orientation. It gains domain wall

energy by increasing in exchange and anisotropy contributions. The domain wall energy per unit area can be defined as $\sigma_{DW} = \pi\sqrt{(AK_{eff})}$ [1 17], where A is exchange stiffness constant and K_{eff} – effective anisotropy coefficient. Therefore, the resultant domain structure is a balance of demagnetization energy and the domain wall energy.

Depending on the spin spatial configuration the domain wall can be either Néel type or Bloch type as schematically shown in figure 2.8. In the Néel type domain wall, the magnetic moment rotates along the line perpendicular to the domain wall, and in the domain wall plane when the wall is of Bloch type. The domain wall width can be written as [17] $\delta = \pi\sqrt{A/K_{eff}}$.

Appearance of the interfacial DMI(iDMI) in the layered structures may substantially affect the domain properties. The domain wall energy is lowered and expressed as $\sigma = \sqrt{A}K_{eff} - \pi|D|$. Moreover the domain wall in multilayers can be a combination of Néel and Bloch wall, called hybrid domain wall [23]. However, in a presence of strong iDMI, above the certain strength threshold, the pure Néel domain wall is observed. Lowering in the domain wall energy may result in decrease in the domain width.

In the multilayer case with the presence of iDMI, the value of domain width and domain wall energy can be calculated by considering an approach of the effective medium which is discussed in chapter 6.

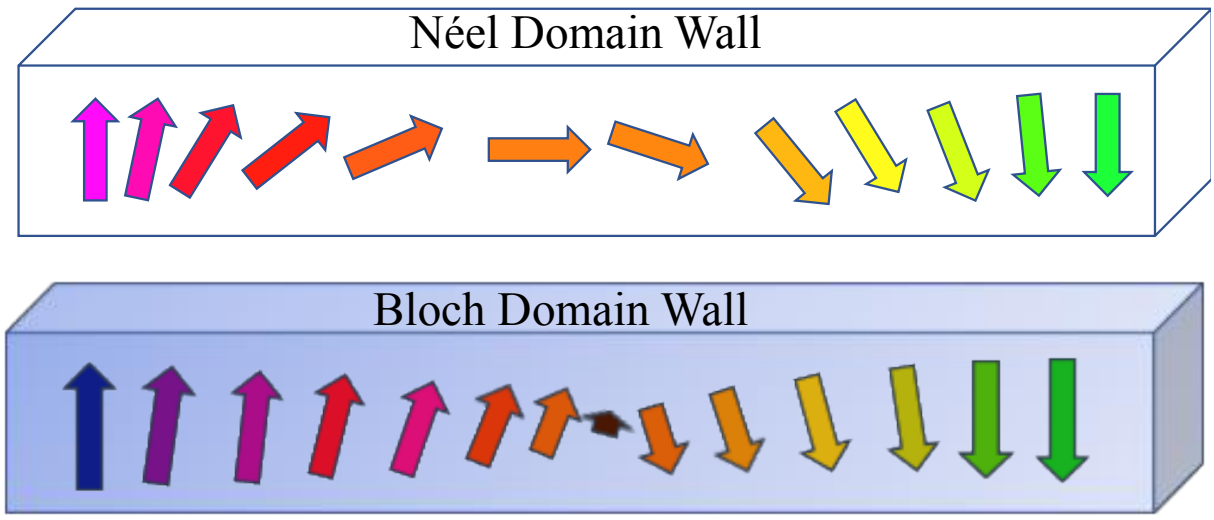

Figure 2.8 Schematic representation of the Néel and Bloch type of domain wall in ferromagnetic material.

Apart from the pure or mixed Néel and Bloch domain walls, other complex spin structures can be observed[24]. They result from interplay between iDMI and PMA. Weak and strong PMA without the presence of DMI favours uniform magnetization in the sample plane or perpendicular to in at the large distances. Gradual increase in iDMI triggers evolution of spin

structures towards chiral one. In the case of very strong DMI pure spin spirals may appear. Their periodicity decreases with decrease in the PMA strength. By controlling the dipolar interaction, anisotropy and interfacial DMI, the skyrmions can be induced which are the topologically protected spin whirls. By engineering the DMI vector direction and sign, it is possible to induce the skyrmions, anti-skyrmions, meron and antimeron, etc. in magnetic bulk materials as well as in thin films [20].

2.9:- Interaction of light with spin waves

Brillouin light scattering is the interaction between the light illuminating a magnetic sample surface with photon energy $\hbar\omega_s$ and momentum $\hbar q_s$ and spin waves characterized by frequency ω_m and wave vector q_m. Interaction of the light with quanta of spin waves, magnon [25, 26], satisfies conditions of energy and momentum conservation. Two processes may occur with comparable probability: magnon annihilation and creation (figure 2.9). The resulting loss or gain in the scattered phonon energy is visible in the form of Stokes and anti-Stokes peaks in the BLS spectrogram. In classical approach the BLS effect can be understood as an interaction of the light with atoms engaged in spin wave propagation, exhibiting spin-orbit coupling and Doppler shift resulting from the spin wave frequency.

The presence of DMI causes an asymmetric modification of the spin-wave dispersion relation. If the spin-wave spatial chirality is favoured by the DMI, the spin-wave frequency is reduced. Conversely, it is increased for the opposite chirality. The dispersion characteristics of spin waves in thin magnetic films can be measured with BLS. DMI presence manifests itself as a shift of Stokes and anti-Stokes peaks in the magnetic fields applied in the opposite directions which is a direct measure of iDMI strength D (further information are presented in the chapter Experimental techniques).

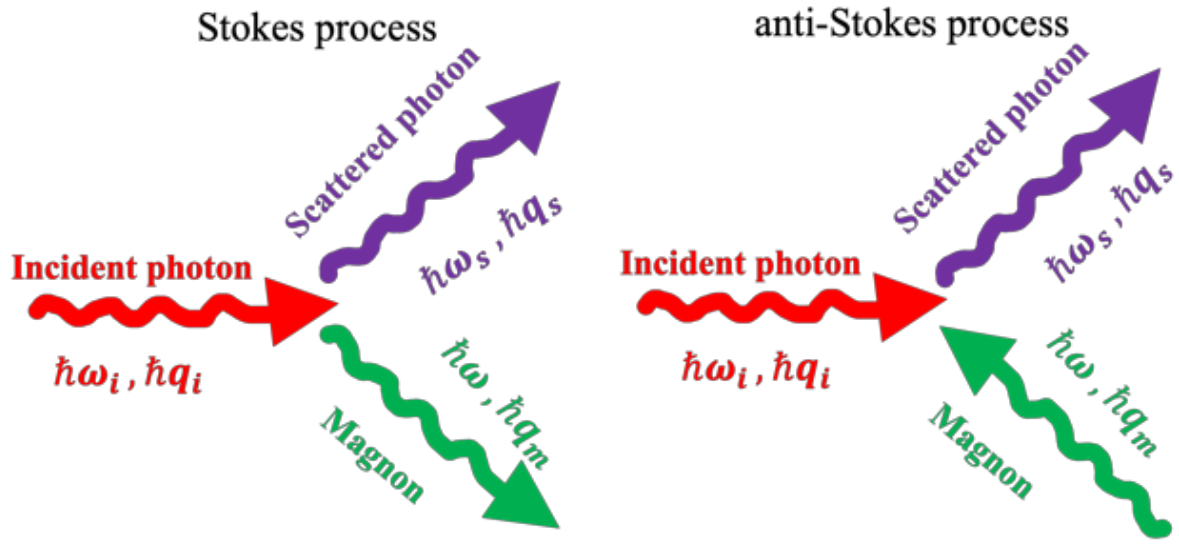

Figure 2.9:- Schematic representation of the creation and annihilation of magnon during Stokes and anti-Stokes process, respectively.

2.10:- References

1. Spaldin, N. A. *Magnetic Materials*. (Cambridge University Press, 2010). doi:10.1017/CBO9780511781599
2. Blundell, S. *Magnetism in Condensed Matter: Paperback: Stephen Blundell - Oxford University Press*. (2001).
3. LANDAU, L. & LIFSHITZ, E. On the theory of the dispersion of magnetic permeability in ferromagnetic bodies. *Phys. Zeitsch. der Sow.* **153**, 153–169 (1935).
4. Gilbert, T. L. A phenomenological theory of damping in ferromagnetic materials. *IEEE Transactions on Magnetics* **40**, 3443–3449 (2004).
5. Yafet, Y. Ruderman-Kittel-Kasuya-Yosida range function of a one-dimensional free-electron gas. *Physical Review B* **36**, 3948–3949 (1987).
6. Ruderman, M. A. & Kittel, C. Indirect Exchange Coupling of Nuclear Magnetic Moments by Conduction Electrons. *Physical Review* **96**, 99–102 (1954).
7. Kasuya, T. A Theory of Metallic Ferro- and Antiferromagnetism on Zener's Model. *Progress of Theoretical Physics* **16**, 45–57 (1956).
8. Yosida, K. Magnetic Properties of Cu-Mn Alloys. *Physical Review* **106**, 893–898 (1957).
9. Parkin, S. S. P. & Mauri, D. Spin engineering: Direct determination of the Ruderman-Kittel-Kasuya-Yosida far-field range function in ruthenium. *Physical Review B* **44**, 7131–7134 (1991).

10. Coey, J. M. D. *Magnetism and Magnetic Materials*. *Physics Today* **12**, (Cambridge University Press, 2001).
11. Krishnan, K. M. *Fundamentals and Applications of Magnetic Materials*. *Fundamentals and Applications of Magnetic Materials* (Oxford University Press, 2016). doi:10.1093/acprof:oso/9780199570447.001.0001
12. Johnson, M. T., Bloemen, P. J. H., Broeder, F. J. A. den & Vries, J. J. de. Magnetic anisotropy in metallic multilayers. *Reports on Progress in Physics* **59**, 1409–1458 (1996).
13. Draaisma, H. J. G., de Jonge, W. J. M. & den Broeder, F. J. A. Magnetic interface anisotropy in Pd/Co and Pd/Fe multilayers. *Journal of Magnetism and Magnetic Materials* **66**, 351–355 (1987).
14. Dzyaloshinsky, I. A thermodynamic theory of "weak" ferromagnetism of antiferromagnetics. *Journal of Physics and Chemistry of Solids* **4**, 241–255 (1958).
15. Moriya, T. Anisotropic Superexchange Interaction and Weak Ferromagnetism. *Physical Review* **120**, 91–98 (1960).
16. Fert, A. & Levy, P. M. Role of Anisotropic Exchange Interactions in Determining the Properties of Spin-Glasses. *Physical Review Letters* **44**, 1538–1541 (1980).
17. Thiaville, A., Rohart, S., Jué, É., Cros, V. & Fert, A. Dynamics of Dzyaloshinskii domain walls in ultrathin magnetic films. *EPL (Europhysics Letters)* **100**, 57002 (2012).
18. Fert, A., Reyren, N. & Cros, V. Magnetic skyrmions: advances in physics and potential applications. *Nature Reviews Materials* **2**, 17031 (2017).
19. Fert, A., Cros, V. & Sampaio, J. Skyrmions on the track. *Nature Nanotechnology* **8**, 152–156 (2013).
20. Tokura, Y. & Kanazawa, N. Magnetic Skyrmion Materials. *Chemical Reviews* **121**, 2857–2897 (2021).
21. Weiss, P. L'hypothèse du champ moléculaire et la propriété ferromagnétique. *Journal de Physique Théorique et Appliquée* **6**, 661–690 (1907).
22. Kittel, C. Physical Theory of Ferromagnetic Domains. *Reviews of Modern Physics* **21**, 541–583 (1949).
23. Legrand, W. *et al.* Hybrid chiral domain walls and skyrmions in magnetic multilayers. *Science Advances* **4**, eaat0415 (2018).
24. Kisielewski, J., Kisielewski, M., Zablotskii, V., Dejneka, A. & Maziewski, A. Mapping magnetization states in ultrathin films with Dzyaloshinskii-Moriya interaction. *New*

Journal of Physics **21**, (2019).

25. Chumak, A. V., Serga, A. A. & Hillebrands, B. Magnonic crystals for data processing. *Journal of Physics D: Applied Physics* **50**, 244001 (2017).
26. Kruglyak, V. V., Demokritov, S. O. & Grundler, D. Magnonics. *Journal of Physics D: Applied Physics* **43**, 264001 (2010).

Chapter:-3

Experimental techniques

In this chapter, the experimental techniques are described that were applied for epitaxial sample fabrication and characterisation of the samples.

Table of Contents

3.1:- Molecular Beam Epitaxy technique

All fabricated samples described in this thesis have been deposited by molecular beam epitaxy (MBE). This deposition technique provides a possibility to grow a well-defined epitaxial structure on a monocrystalline substrate at very high vacuum and very low growth rate with one atomic monolayer precision. Due to low kinetic energy of depositing atoms, their stable flux and elevated temperature of the substrate, the surface diffusion is enhanced and ensures almost equilibrium material growth resulting in a high crystalline quality of the fabricated layers and their epitaxial nature. Moreover, in the case of artificial layered heterostructures the interfaces are chemically sharp and their crystallinity is also well defined. The ultra-high vacuum in the growth chamber enables also application of numerous characterisation methods monitoring structural and chemical sample quality such as: reflective high energy electron diffraction (RHEED), low energy electron diffraction (LEED) and Auger electron spectroscopy (AES). Moreover, such vacuum deposition conditions protect highly reactive deposited materials (e. g. rear earths) from oxidation. The MBE technique is very

useful for growing numerous material types: semiconductors, topological insulators, 2D materials and the purely metallic structures which are an object of our studies.

3.2:- Description on MBE

Our MBE (Prevac) growth chamber contains eight effusion cells (EF) and two e-beam evaporators (Telemark). Each e-beam evaporator has 6 crucibles, thus up to 20 various metals can be loaded in the chamber. However, due to the planned samples to be grown some materials are duplicated. The loaded materials are schematically shown in figure 3.1.

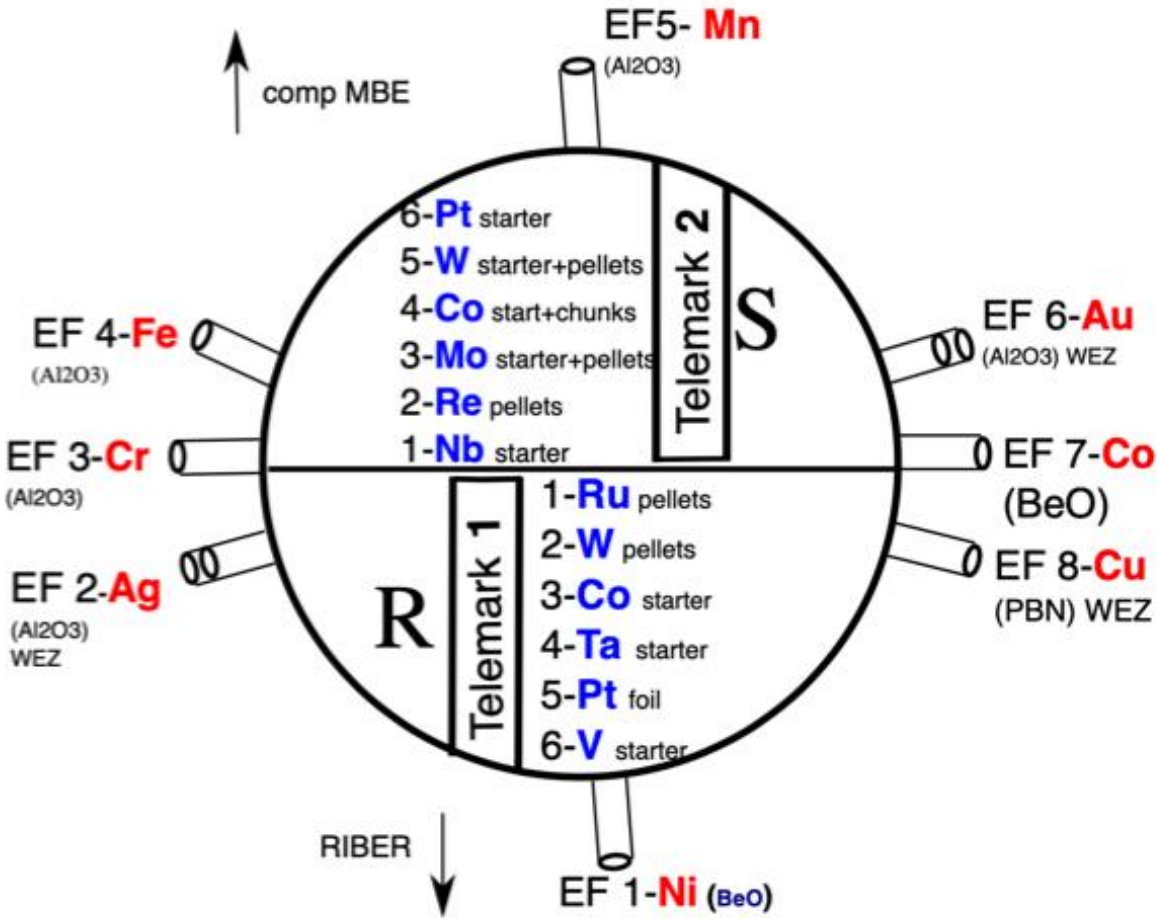

Figure 3.1The arrangements of the source materials inside the MBE chamber (Telemark – electron gun, EF – effusion cell).

Other chambers of the system are connected via a transfer chamber called UFO through which the samples can be delivered to any place in the setup. The scheme of the MBE system and photos of individual parts are shown in figure 3.2.

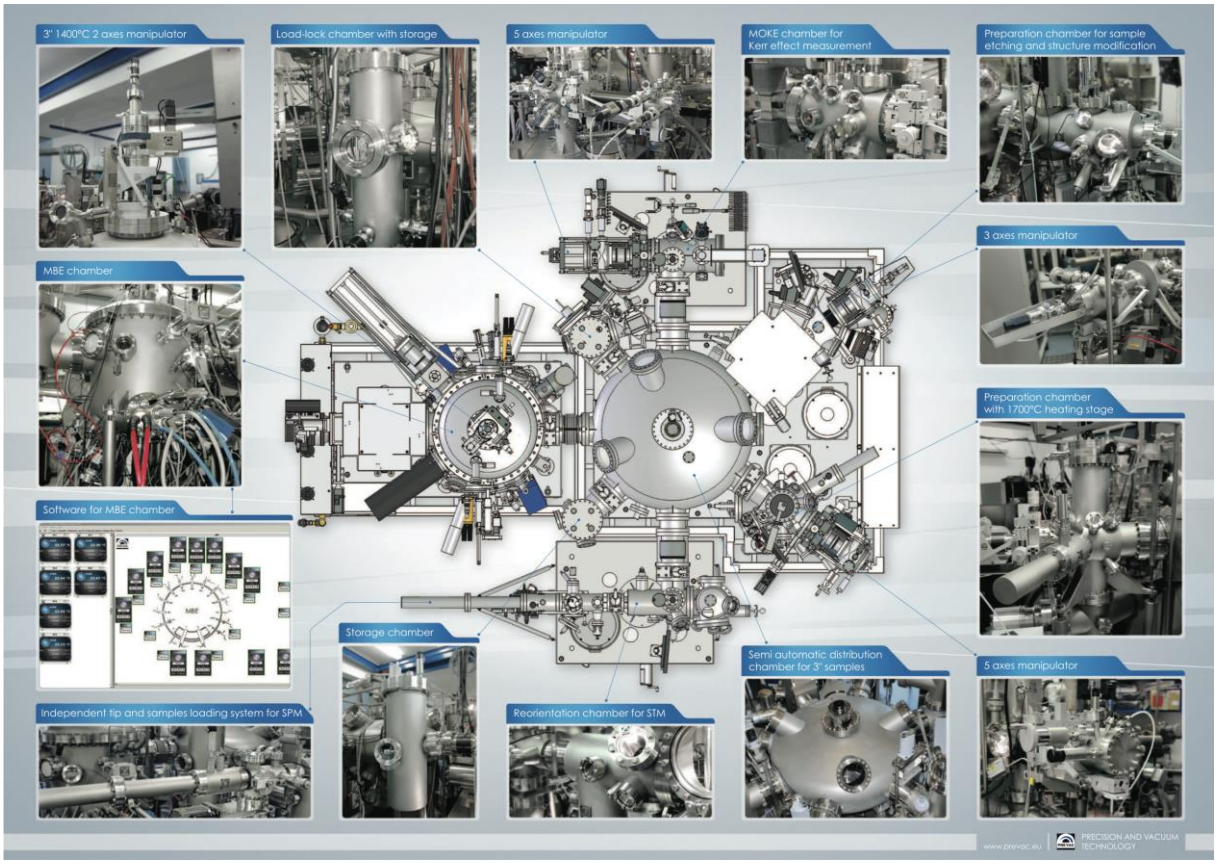

Figure 3.2 The schematic representation of the MBE chamber and its associated components which are connected to the MBE chamber. The image has been taken from https://www.prevac.eu.

Installed ion pumps and turbo molecular pumps connected to MBE chambers enable to achieve the ultra-high vacuum of 1*10e-10 mbar. The RHEED is situated inside the growth chamber to monitor the sample structure during the deposition process. The RHEED technique, described slightly wider in the further part of this chapter, is surface sensitive and gives the information on the crystalline structure as well as the roughness of the thin films. Also, it is possible to determine the crystallographic directions of deposited thins films with respect to the substrate crystallographic orientations and deduce the structure type and possible strains. Two mass spectrometers are situated inside the growth chamber to control the flux rate of the material and stabilize it. In the case of alloy layer fabrication by coevaporation of materials from different sources the controlled flux ratio enables to obtain a desired stoichiometry of the film. Moreover, the thickness is also monitored by a quartz crystal monitor. The samples are mounted on 3-inch in diameter molyblocks. The sample holder enables rotation of the molyblock ensuring layer thickness uniformity and growth of the more complex structures, described shortly below. Every evaporation source is equipped with its own shutter. Moreover,

the chamber is equipped with the main shutter, that covers the sample from the flux, and the linear shutter. The second one enables the fabrication of the deposited layers in the shape of wedges or steps. Desired film thickness gradient and thickness range can be obtained by appropriate combination of linear shutter speed and evaporation rate. Exemplary sample configurations (in our investigations we also used other configurations) are shown in figure 3.3. The double wedge samples can be deposited with help of linear shutter and 90° sample rotation before depositing the second wedge layer. Every sample point in such system corresponds to different sample structure. In this way, we are able to fabricate 2D matrix samples with the structure and properties depending on (d1, d2), where d1 and d2 are the thicknesses of the component wedge-like layers. In this case, it is also possible to study locally the magnetic properties in different areas of the sample by e.g. MOKE and magnetic force microscopy. For example, the investigation of the inter-layer coupling between Co layers across the double layer nonmagnetic spacer are available for the sample shown in figure 3.3b. If the Co layer is wedge-shaped and the buffer and capping layer is Pt, it is easy to estimate the spin reorientation transition (SRT) of Co by visual magneto-optic Kerr effect microscopy. Such an approach enables to obtain 2D maps of investigated properties. So, one sample on one substrate can give the different areas to study the different magnetic behaviour and may substitute a set several samples to investigate e.g. SRT or the interlayer coupling.

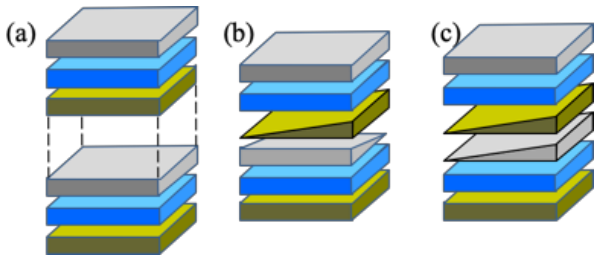

Figure 3.3 The exemplary schemes of various heterostructures: (a) multilayers, and wedge-shaped structures with (b) orthogonal and (c) parallel orientation of the wedge-like component layers. . Colour code for the layers: Co – blue, W (Re) – olive, Pt – gray.

3.3:- Epitaxial Growth

In molecular beam epitaxy, the molecules or atoms deposit on a single crystal substrate usually kept at temperature which creates favorable conditions for equilibrium high quality crystalline growth or to reproduce the lattice of the bottom layer or substrate. There are various types of the ordered growth [1] (i) commensurate, (ii) incommensurate or relaxed and (iii) pseudomorphic with uniaxial dilation growth as shown in the figure 3.4.

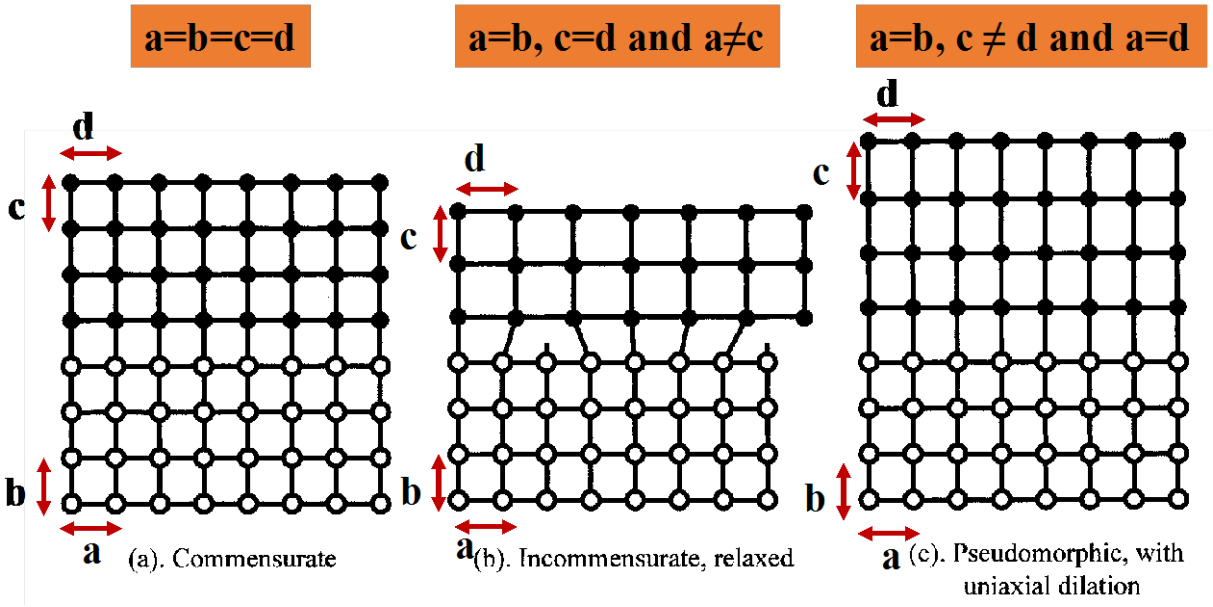

Figure 3.4. Different kinds of epitaxial growth. The images are from [1].

In the case of commensurate growth, the depositing material follows the exact structure of the substrate without any relaxation or any modification. The lattice mismatch between substrate and desired material is negligible and the lattice constant is the same as the bottom material a=b=c=d. For incommensurate growth, the lattice of depositing material is not same as the substrate and its lattice is relaxed after deposition by the lattice of dislocations, as shown in the figure 3.4(b). The third type of growth is pseudomorphic in which the strain expands across the grown layer (Fig. 3.4(c)). So, the best way to grow the epitaxial material is to choose the proper substrate or the buffer layer to reduce the lattice mismatch in the grown films. It is also possible to change the pseudomorphic growth to a relaxed one e.g. by changing the concentration of the alloy and also the thickness of the deposited material as described in the literature [1].

3.4:- Reflection High Energy Electron Diffraction (RHEED)

The RHEED is the commonly applied technique in MBE systems to monitor the epitaxy of the deposited material and to check the thickness (by counting streak intensity oscillations) of the material during the deposition process. The RHEED setup operates at high energy ranging from 10-40 keV. The angle of the electron incident beam relative to the sample plane is very low of (1-3°) as shown in figure 3.5. Due to such low angle incidence, only a few layers of the atomic layer interact with the incident electron beam i.e. the diffracted electrons come from only one or two monolayers. The thickness of 1 atomic layer or even 0.5 layer of the

deposited material can be probed. After diffraction from the 2D lattice of the atomic surface plane, the beam takes the shape of vertical stripes on the fluorescent screen. From the streak pattern (shape of the streaks and the distance between them) and its angular appearance one can determine the crystalline structure of the grown film, possible lattice strains and estimate the surface roughness [2, 3].

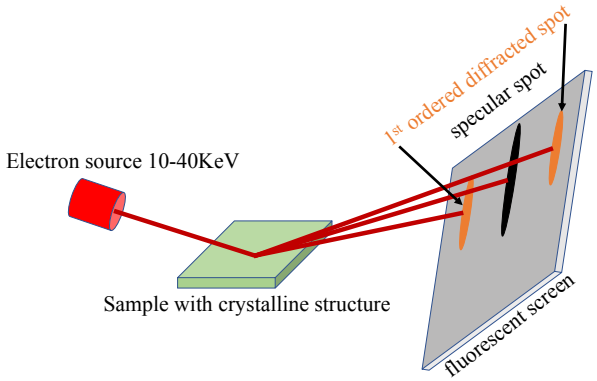

Figure 3.5. The schematic diagram of RHEED setup with diffraction pattern on the fluorescent screen.

3.5:- X-Ray Diffraction (XRD) and X-Ray Reflectivity (XRR)

The structural characterisation (lattice constant and thickness of multilayers) was done by XRD to determine the epitaxy and crystal structure of the investigated thin films. The incident monochromatic X-ray beam with wavelength of 1.54 Å (Cu Kα with energy of 8 keV) was applied. The wavelength of x-ray is comparable to the distance between the atoms. In crystalline materials, the incident X-ray is elastically scattered and diffracted from the set of lattice planes and detected by the detector located in the configuration $\theta - 2\theta$, where θ is the angle of incident X-ray. The X-ray beam after diffraction from the atoms interferes and forms spatial intensity distribution which depends upon the arrangement of atoms inside the material. The diffraction wave bundle with the same phase is constructive and gives the maximum sharp intensity (Bragg peaks) which corresponds to the particular plane of the crystalline structure. The position of the Bragg peaks can be described by Bragg's law [4].

$$2dsin\theta = n\lambda \qquad (3.1)$$

where d is the distance between atomic planes, θ is the scattering angle, λ is the wavelength of X-ray and n indicates the order of diffraction peak. In the case of multilayered structures, an additional satellites related with their periodicity may appear. Then, it is possible

to estimate the thickness of the basic tri-layers in $[W/Co/Pt]_N$ multilayers from such supper lattice peaks position using the following formula [5] [6].

$$(2\ sin\ sin\ \theta_{n} - 2\ sin\ sin\ \theta_{SL}) / \lambda = \pm n / \Lambda \quad (3.2)$$

Where Λ is the thickness of superlattice period, λ – X-ray wavelength, θ_n is the n th-order peak, θ_{SL} is the zero-order peak. The thickness of trilayer has been calculated by using software X'pert Epitaxy and smooth fit v-4.0.

To estimate the thickness, roughness, interface quality and intermixing at the interface, the X-ray reflectivity (XRR) measurements were applied. This technique is applicable for both crystalline as well as amorphous layered materials. The in depth electronic density of the thin films is probed by grazing incidence X-ray beams being deflected at low angle from the sample plane. The total reflection takes place when the incident beam angle is below a critical value related to the density material. Above the critical angle, the penetration depth of X-ray increases rapidly. Due to the change of the electron density in multilayered samples, the reflected beam exhibits intensity oscillations with an angle θ. The standard reflection curve exhibits Bragg peaks and Kiessig fringes[7, 8]. The Bragg peak position allows us to determine the periodicity. The Kiessig fringes originate from the presence of two bottom and top interfaces. The period of the observed Kiessig fringes is inversely related to the total thickness of the film. The fall in intensity gives information about the surface roughness.

3.6:- Magneto Optic Kerr Effect (MOKE)

The interaction of light and matter is the basic principle of the magneto-optic Kerr Effect discovered in 1877 [9]. When a linearly polarized light is reflected from the magnetic surface, it converts into elliptically polarized beam rotated by an angle θ. This phenomenon can be explained in terms of the balance between two circularly polarized beams in opposite directions that interact with magnetic material exhibiting different dichroism and absorbance depending on circularity. The interaction between electromagnetic field and atoms in the magnetic material by spin-orbit coupling[10] is the main microscopic origin of the magneto optic Kerr effect. The different transition intensity from d-orbital to p-orbital is responsible for elliptical nature of the polarized light after interaction with the surface of magnetic film. In MOKE, the change in polarization direction of the linearly polarized incident light and reflected from the surface of magnetic sample (which behaves as an effective medium) described by rotating angle depends on the magnetization of the magnetic film and its direction. However, the absolute value of magnetization cannot be determined by MOKE. The MOKE is only sensitive to the surface, not the volume of the sample and the information can be extracted from the penetration depth

of light, which reaches a few tens of nanometers. Since it is a non-destructive method and a local method, it is very useful for quick measurement of magnetic hysteresis loops of magnetic thin films even with spatially changing thickness. There are three types of MOKE measurements: longitudinal MOKE (LMOKE), transverse MOKE (TMOKE) and polar MOKE (PMOKE) depending on the mutual configuration of magnetic field and the plane of laser beam incidence as shown in the figure 3.6. In longitudinal configuration (LMOKE) the applied field is parallel to the sample plane and is aligned in the plane of incidence. In transverse mode (TMOKE) the applied filed is parallel to the sample plane and perpendicular to the plane of incidence. For polar alignment: the applied field is perpendicular to the plane of magnetic thin films. The schematic diagrams of LMOKE, TMOKE and PMOKE configurations are shown in the figure 3.6.

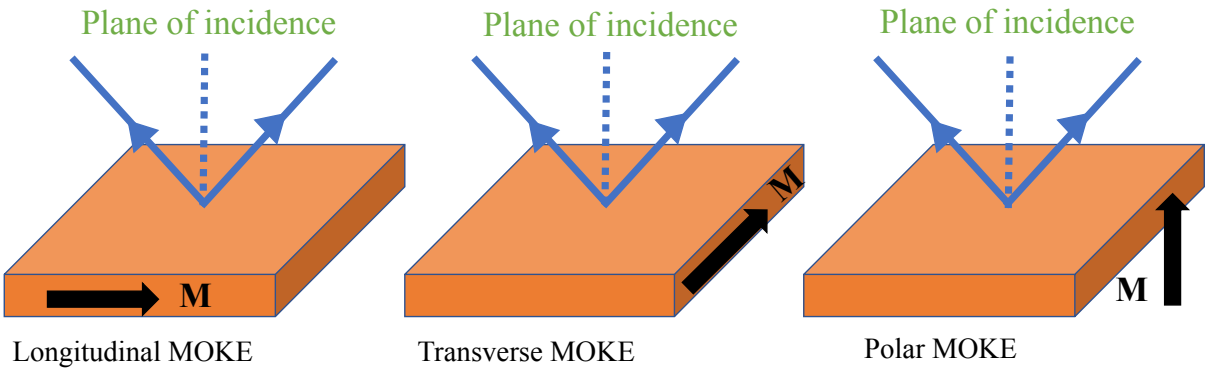

Figure 3.6 Schematic diagrams of different configurations of the MOKE.

The schematic diagram of the PMOKE setup used for our measurements is shown in figure 3.7. A laser incident beam of 6400 Å wavelength passes on the sample surface through the polarizer which is kept at 0° with respect to its principle axis and photo elastic modulator. The reflected light which passes through the analyzer is detected by the photodetector. The analyzer is fixed at nearly equal to 90° with respect to the polarizer, thus the light from the polarizer cannot pass through it without rotation. A reference signal 50 kHz is given to a photo-elastic modulator (PEM) from a lock-in amplifier. The voltage from diode is detected by lock-in which is directly proportional to the Kerr rotation and change in ellipticity of the reflected wave from the surface of magnetic thin film. An electromagnet generates the external magnetic field up-to 0.5T. The changing of magnetic field affects magnetic moment direction as well as its component value. Consequently, this magnetic moment changes the ellipticity and rotation of the electromagnetic wave of incident light. The maximum rotation occurs when the film is saturated. As results of the field sweep from negative saturation to positive saturation field and

back, the Kerr rotation changes are observed as the hysteresis loop. The sample is fixed to the sample manipulator which helps to localize precisely the laser beam on its surface and measure the properties at the desired point of the sample. The laser spot is less than 500 micron. So, for the dimension of 10mm*10mm sample, a matrix of 100 or more spots can be reliably measured and provide 2D map of magnetic properties.

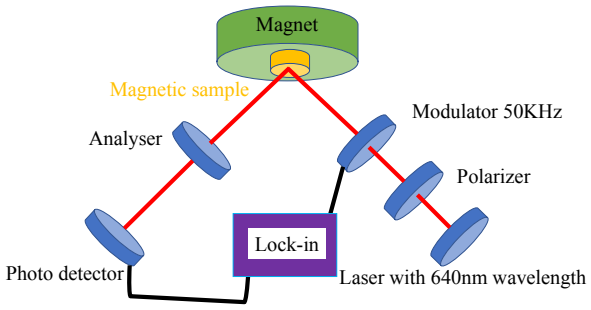

Figure 3.7 Schematic diagram of PMOKE set-up in our lab.

3.7:- Atomic Force Microscopy and Magnetic Force Microscopy

The surface morphology and the surface roughness has been studied by atomic force microscopy (AFM) and the magnetic domain configuration has been studied by the magnetic force microscopy (MFM). The AFM was invented by Binnig, Quate and Gerber [11] to study the surface of an insulator. The AFM is the developed version of the scanning tunnelling microscope which is very useful for investigation of conducting materials. The basic principle of AFM operation is the measure of cantilever deflection, amplitude, phase or frequency affected by the interaction of the probe with the sample surface. These parameters are taken into account depending on the operation mode of the microscope discussed slightly wider below. Resulting cantilever reaction is registered e.g. by the reflected laser beam illuminating multi-segment photodetector. The signal from the photodiode detector with help of the software is used to create the image of the surface. The schematic diagram is shown in the figure 3.8.

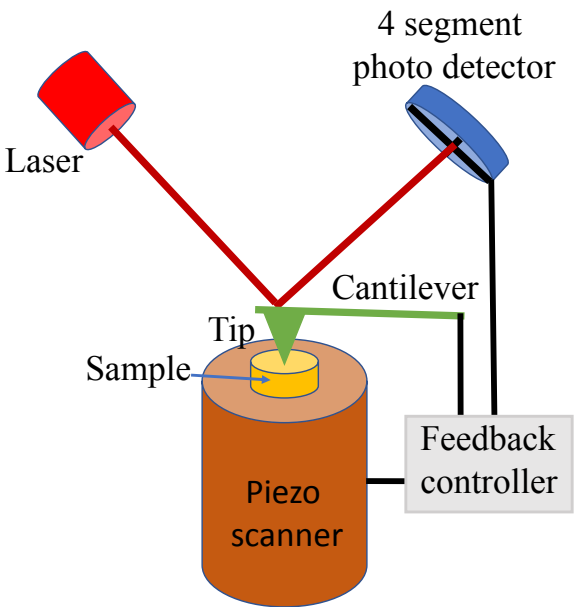

Figure 3.8:- The set-up of atomic force microscope. The feedback controller keeps constant the set parameter. The correction signal from the piezo-element is used to create sample property map.

The sample is placed on the piezoelectric scanner which allows to move the sample along x, y and z axes. The laser beam is incident on the cantilever and reflected to the four segment photodiode. The silicon tip with radius 50-100 Å is located at the end to the cantilever. In basic operating mode the strength of interaction (being measured by the cantilever deflection) between the tip and the surface is stabilized. Any deviation from the set value, originating from the sample topography features, is corrected via feedback. The voltage change applied to the piezoscanner is “translated” by the microscope software into the topography map. There are three types of operating modes of AFM: contact mode, non-contact mode and tapping mode depending on the tip-sample interaction type and the related distance (Figure 3.9).

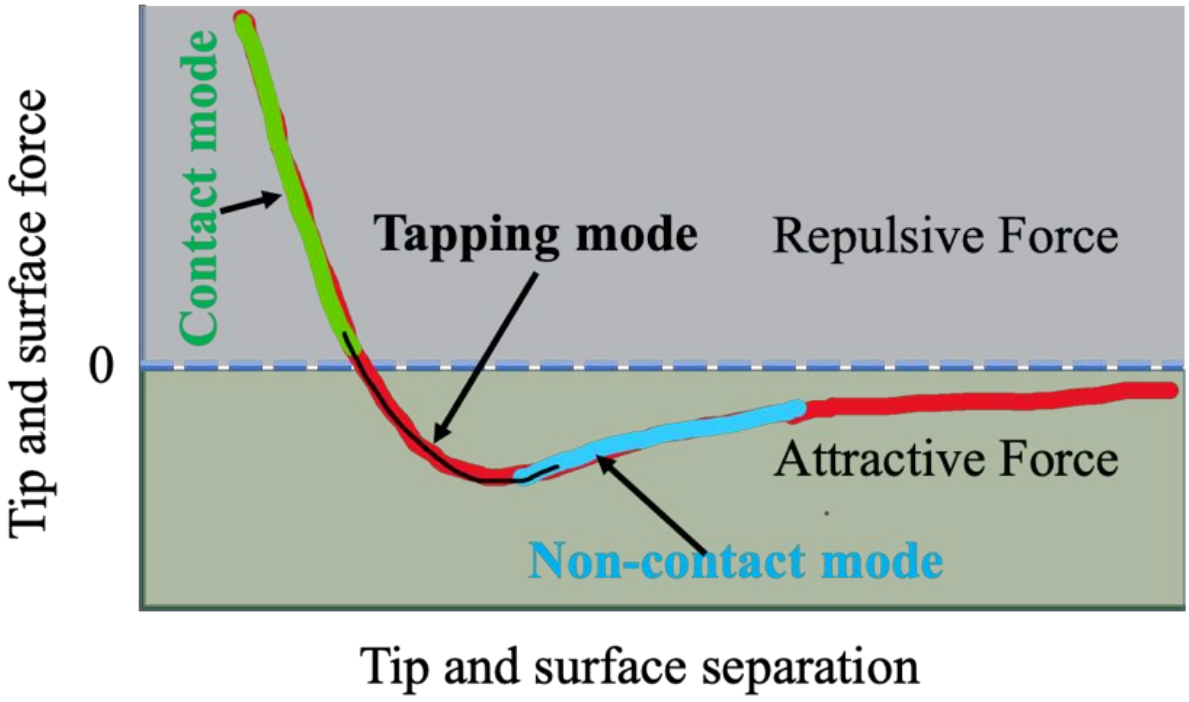

Figure 3.9 Tip-sample interaction as a function on separation distance in AFM operation.

In the contact mode, the tip touches the surface during the scanning of the interested area. The interaction has a nature of the repulsive electrostatic forces as shown in figure 3.9. In this mode, the cantilever deflection is registered. Destruction possibility of the soft and weakly adhesive surface is a disadvantage of this mode. The long range van der Waals attractive interaction between the tip and the surface is exploited in the non-contact mode with the distance kept in the range of 10 Å to 200 Å. In this mode both the deflection or resonance condition (phase or frequency) are registered. Weak interaction with possible high noise-to-signal ratio and lower resolution are the main disadvantages of this method. In many cases the tapping mode offers optimum measuring conditions of the topography features. It is "located" in between the contact and non-contact modes. The tip operating at a resonance frequency knocks the sample surface. This method provides satisfactory resolution and allows to avoid possible surface destruction, unlike in the contact mode.

Apart from the AFM surface characterisation, the magnetic force microscopy (MFM) measurements were performed to investigate domain structure of magnetic samples. In general, the principles of MFM operation are similar to AFM. However, the used tip should be magnetic (coated e.g. with CoCr alloy). During the surface imaging MFM operates in double pass mode In the first pass, it works as AFM in the tapping mode and registers the sample topography. In

the second pass 200-1000 Å above the surface the magnetic tip probes the stray magnetic field emitting by the magnetic sample. This interaction appears as the changes of resonant frequency or phase of the cantilever. The tip follows the profile registered in the first pass to minimize the influence of tip – sample distance changes on magnetic interactions. Because the stray field distribution is directly related to sample magnetic domain structure, it can be easily measured in this mode. The typical topography and phase images of the same region of Au/Co/Pt layered system are shown in the figure 3.10.

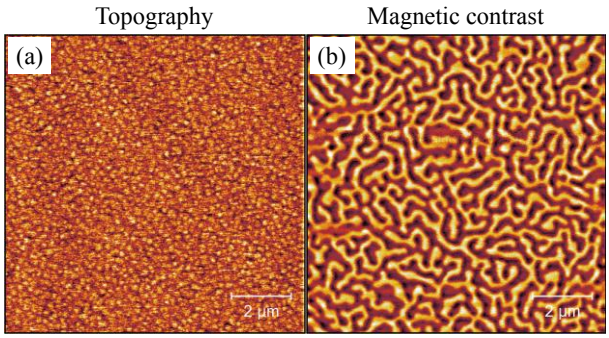

Figure 3.10. The topography and image of the magnetic domain structure for the same area of the Au/Co/Pt sample.

3.8:- Superconducting Quantum Interference Device (SQUID)

The magnetization of all investigated samples was measured by SQUID magnetometry at room and low temperatures. The SQUID operation principle is based on the Josephson effect[12, 13]. Magnetic sample itself is a source of spatially distributed magnetic flux which surrounds it. During the measurements, the sample oscillates in the vicinity of coils which pick-up the signal resulting from the oscillating magnetic flux. The method is extremely sensitive as it can detect a flux quantum by the Josephson tunnelling junction, being a component of the coil. The flux changes detected by these coils are ascribed to the magnetic moment of the sample oriented in the desired direction. The magnetization and the hysteresis loops were measured in both in-plane and out of plane direction of the sweeping field.

3.9:- Hysteresis Loop

Figure 3.11 shows the hysteresis loops typical of easy (red) and hard (blue) axis directions for monodomain state of magnetic sample. The hysteresis loops illustrate the magnetization reversal of the sample in the presence of sweeping magnetic field. A linear dependence (blue M-H line) is typical of reversible behaviour of the sample, usually in the field applied along the hard axis. The rectangular shape of the loop is registered when the field is

applied along an easy axis. Several parameters of the magnetic material can be determined from the hysteresis loop. The anisotropy H_a field equal to the saturation field, when the field is applied along the hard axis is related to the sample magnetic anisotropy (see, explanation below). The M_S is a magnetization saturation, reached at maximum applied field, where all magnetic moments are aligned in the same direction along the field. M_r is the sample magnetization at remanence that remains at zero field after initial saturation. The width of the hysteresis loop is described by the coercive field H_C. In this field, the net magnetization of the sample changes its sign (orientation). For the monodomain state, the coercivity field H_C has non zero value. However, for multidomain state in W/Co/Pt, which will be discussed in the next chapters, the value of H_C is equal to zero. Therefore, the H_C value depends upon the specific systems.

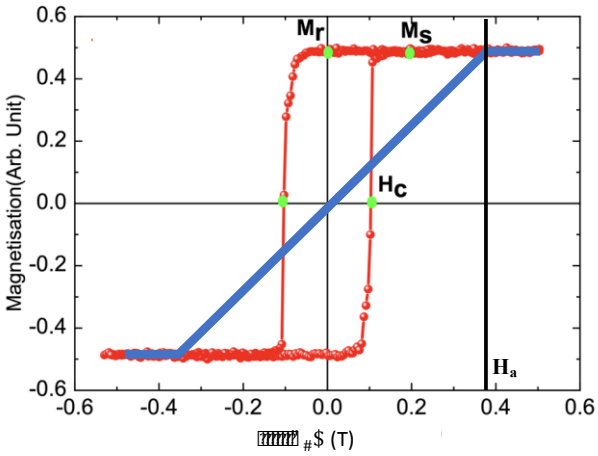

Figure 3.11 Typical magnetic hysteresis loops for the easy (red) and hard (blue) sample axes with marked parameters.

When the magnetic field is applied along hard axis, the sample saturates above H_a. This field is called anisotropy field as it is necessary to overcome magnetic anisotropy of the sample in order to saturate. It allows to determine the effective magnetic anisotropy K_{eff} from the relation: $H_a = 2K_{eff}/M_S$, where M_S is magnetization saturation of the sample. However, this simple approach can be applied merely to the samples in the monodomain state. In more general case the K_{eff} value should be estimated from the field confined between the M-H curves registered for the perpendicular and parallel to the sample plane magnetic field (figure 3.12). In our convention the effective anisotropy value is positive and negative for the easy axis and the easy plane, respectively.

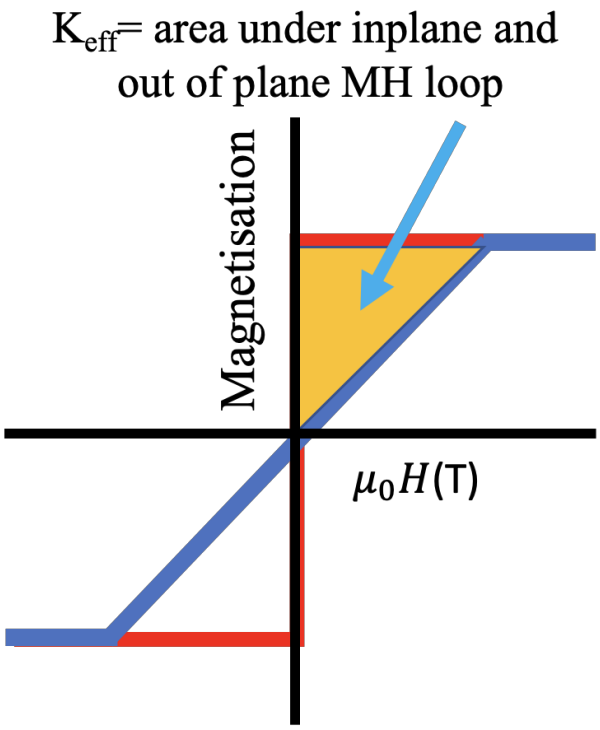

Figure 3.12 The diagram of the effective anisotropy calculation from the area of in-plane and out of plane hysteresis loops.

3.10:- Brillouin light scattering spectroscopy

The strength of iDMI and the magnetization dynamics was studied for Co single layer and multilayered samples with neighbouring asymmetrical heavy metals covers by using the Brillouin light scattering (BLS) spectroscopy in Damon-Eshbach geometry. The basic configurational set is shown in the figure 3.13.

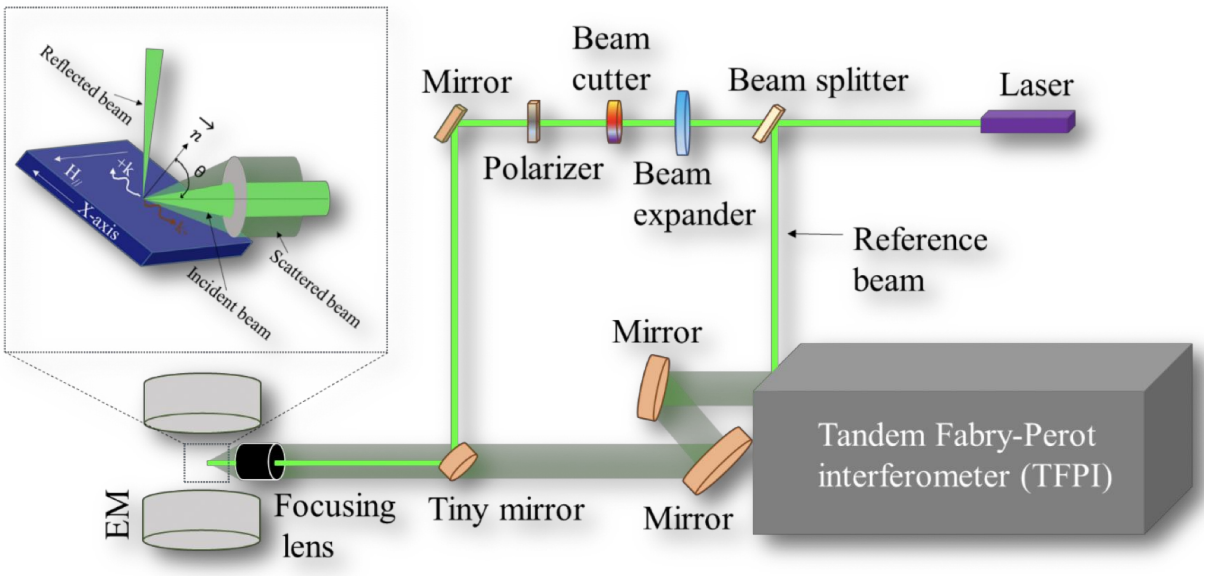

Figure 3.13 The scheme of a BLS setup. The inset shows the sample configuration against the laser beam. This image has been taken from the doctoral thesis:-Magnetization statics and dynamics in selected ultrathin films and multilayers with Dzyaloshinskii-Moriya interaction by Anuj Kumar Dhiman, University of Bialystok 2022.

The fundamental principle of a Brilloiun light scattering is interaction of the laser light with the spin waves propagating in the magnetic materials. The results are obtained from the reflected light inelastically scattered at the sample surface.

The light of a stabilized frequency is emitted by the laser and after passing devices forming the beam is focused on the sample surface. The reflected light contains both the elastic (non-interacting) and inelastic (interacting with spin waves) contributions. The spectrum of the reflected light is analyzed by the Fabry-Perot interferometer playing a role of the monochromator. The tandem configuration usually contains two sets of etalons that transmit the light with precisely selected wavelengths that can be chosen. The light leaving interferometer is analyzed by a photomultiplier and converted to the light spectrum containing Stokes and anti-Stokes peaks whose positions are related to the spin wave energy. Setting the angle of incident light on the sample surface enables to carry out the measurements in a function of wave vector k. In this way, determination of the spin wave dispersion relation is available. In the mentioned Damon-Eshbach geometry the surface spin wave modes are detected. In this configuration the wave vector k and applied magnetic field are aligned in the sample plane, however mutually perpendicularly oriented.

In the standard approach to determine the coefficient of interfacial Dzyaloshinskii-Moriya interaction (iDMI), D_{eff}, the BLS spectrum is registered for one direction of the applied magnetic field. Then the mirror image is superimposed and from the shift between the corresponding peaks and the DMI strength can be determined. This approach is illustrated in figure 3.14. The dotted spectra is experimental data which is fitted by the Lorentzian distribution marked as the red line. The blue spectra shows the mirror-reflected Stokes line.

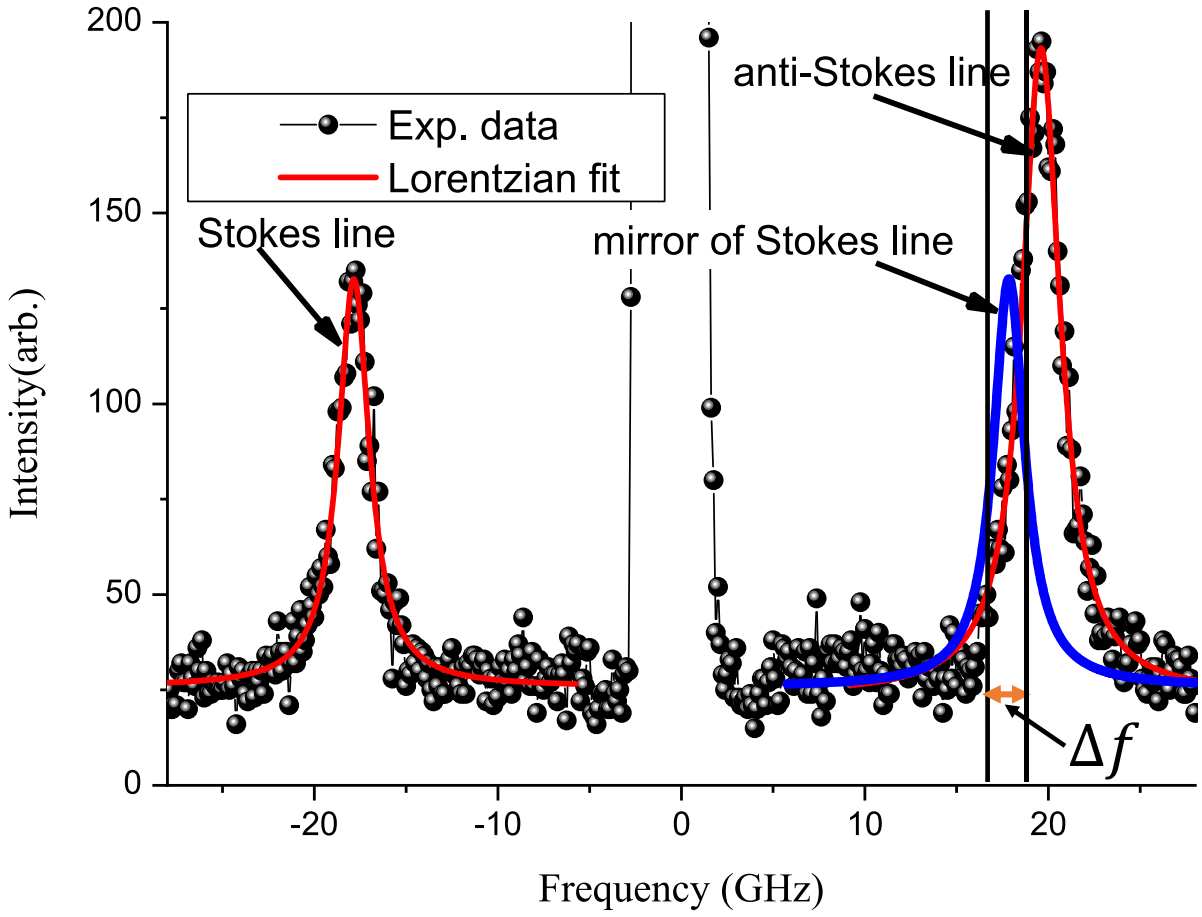

Figure 3.14 The Stokes and anti-Stokes lines reflecting the interaction of the laser beam with magnons for a particular wave vector of incident light in a presence of magnetic in-plane field applied to the sample. The black dots and red line are the experimental points and fitting, respectively. The asymmetrical shift Δf of Stokes and anti-Stokes lines is due to presence of iDMI at the interface between heavy metal and magnetic material.

From the difference in frequency of the Stokes and anti-Stokes lines, one can determine the iDMI strength described by following equation [14].

$$\Delta f = \frac{2\gamma}{\pi M_S} D_{eff} k$$

Where Δf is the difference in frequency of the Stokes and anti-Stokes lines. γ is the gyromagnetic ratio for magnetic materials, M_S is the saturation magnetization of Co thin films, D_{eff} is the effective iDMI strength and k is the wave vector of incident light.

3.11:- References

1. Arthur, J. R. Molecular beam epitaxy of compound semiconductors. *Surface Science* **299–300**, 818–823 (1994).

2. Braun, W. *Applied RHEED*. *Applied RHEED* **154**, (Springer Berlin Heidelberg, 1999).
3. Ichimiya, A. & Cohen, P. I. *Reflection High-Energy Electron Diffraction*. *Characterization of Materials* (Cambridge University Press, 2004). doi:10.1017/CBO9780511735097
4. Bragg, P. W. H. & Bragg, W. L. The reflection of X-rays by crystals. *Proceedings of the Royal Society of London. Series A, Containing Papers of a Mathematical and Physical Character* **88**, 428–438 (1913).
5. Kim, K.-W., Ghosh, S., Buvaev, S., Hebard, A. F. & Norton, D. P. Superlattice periodicity and magnetic properties of Ba 2 FeMoO 6 /Ba 0.5 Sr 0.5 TiO 3 system. *Journal of Applied Physics* **119**, 215303 (2016).
6. Liu, E. & Wu, X. X-Ray Diffraction Analysis of III-V Superlattices : Characterization , Simulation and Fitting. 1–15 (2013). doi:https://www.semanticscholar.org/paper/X-Ray-Diffraction-Analysis-of-III-V-Superlattices-%3A-Liu-Wu/1403a4cf7aeb2b9d44c13e7c49b224f85fb21255#references
7. Kiessig, H. Untersuchungen zur Totalreflexion von Röntgenstrahlen. *Annalen der Physik* **402**, 715–768 (1931).
8. Stoev, K. N. & Sakurai, K. Review on grazing incidence X-ray spectrometry and reflectometry. *Spectrochimica Acta Part B: Atomic Spectroscopy* **54**, 41–82 (1999).
9. Kerr, J. XLIII. On rotation of the plane of polarization by reflection from the pole of a magnet. *The London, Edinburgh, and Dublin Philosophical Magazine and Journal of Science* **3**, 321–343 (1877).
10. Argyres, P. N. Theory of the Faraday and Kerr Effects in Ferromagnetics. *Physical Review* **97**, 334–345 (1955).
11. Binnig, G., Quate, C. F. & Gerber, C. Atomic Force Microscope. *Physical Review Letters* **56**, 930–933 (1986).
12. Josephson, B. D. The discovery of tunnelling supercurrents. *Reviews of Modern Physics* **46**, 251–254 (1974).
13. Josephson, B. D. Possible new effects in superconductive tunnelling. *Physics Letters* **1**, 251–253 (1962).
14. Dhiman, A. K. *et al.* Magnetization statics and dynamics in (Ir/Co/Pt) 6 multilayers with Dzyaloshinskii–Moriya interaction. *AIP Advances* **12**, 045007 (2022).

Chpater:- 4

Structural and magnetic properties of single and multilayers W/Co/Pt heterostructures

Table of Contents

In this chapter, I discuss how the magnetic state and related phenomena such as perpendicular magnetic anisotropy (PMA), domain structure (DS) formation, and interfacial Dzialoshinskii- Moriya interaction (iDMI) can be modified in a controlled way by structural engineering of the system containing single Co layer. The main research is focused on asymmetrical W/Co/Pt system in which ferromagnetic layer is sandwiched between two different heavy metal forming HM1/FM/HM2 stack

4.1:- Introduction: Magnetic properties of single Co layer in selected various types of heterostructures

It is well known that Co has uniaxial anisotropy in the c-axis direction because of the hexagonal closed packed structure. It grows epitaxially with hcp structure on Pt(111) face centred cubic (fcc) surface. Thin Co layer structures with adjacent capping and buffer layers exhibit a sequence of magnetic configurations with increasing thickness. The magnetic material shows superparamagnetic behaviour in the lower thickness range. Further, with increasing thickness, the layer becomes ferromagnetic with an easy axis of magnetization perpendicular

to the sample plane. Above a critical thickness magnetization reverses from out of plane to in-plane orientation, which is called easy plane. This crossover of magnetization is called as a spin reorientation transition (SRT).

Initial investigations of magnetic states as a function of Co layer thickness and type of sandwiching noble metal covers (Ag and Au) were reported in literature [1] In the epitaxial Au/Co/Au heterostructures the SRT occurs at dCo = 18Å. Very similar behaviour was observed for Pt/Co/Pt layers with slightly higher dCo=22 Å at which SRT occurs [2]. These symmetrical stacks with well-recognized anisotropy served in the further investigations of asymmetric systems as the reference structures.

If Au capping layer is replaced by Mo, the Co thickness of SRT decreases down to 15 Å (figure 4.1). It turns out that SRT is very sensitive not only to d_{Co}, but also to the layer sequence. For Mo/Co/Au stack, the Co thickness for SRT is equal to 10 Å and for Mo/Co/Mo, there is no perpendicular magnetic anisotropy region and only an easy plane zone exists [3].

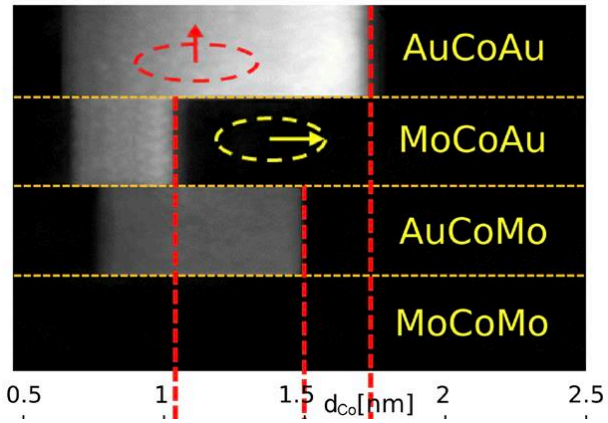

Figure 4.1 P-MOKE map of the four-zone sample containing the single Co magnetic layer sandwiched between Mo and/or Au layers in all possible configurations. The bright colour corresponds to PMA whereas dark to superparamagnetic (left) and in-plane ferromagnetic state (right), respectively [3].

Both the structure and lattice parameters of Mo and W as well Au and Pt are very similar, respectively. Au and Pt are 5d fcc noble metals and are the neighbours in the table of elements. A similar situation is with Mo and W. These metals have the same bcc structure and almost identical lattice parameters (3.14 and 3.17 Å, respectively). Therefore one may expect that Mo/Co/Au and W/Co/Pt systems should display very similar behaviour. However, the experimental comparison of their PMA shows that substantial differences are observed. The

difference in electronic structure: various filling of 5d orbital in Au and Pt as well as 4d and 5d element types of Mo and W are the most probable factors responsible for these findings. This difference is clearly illustrated by four-zones samples shown in Figs. 4.1 and 4.2(A).

4.2:- Influence arranging surroundings W and Pt layers on Co magnetic properties

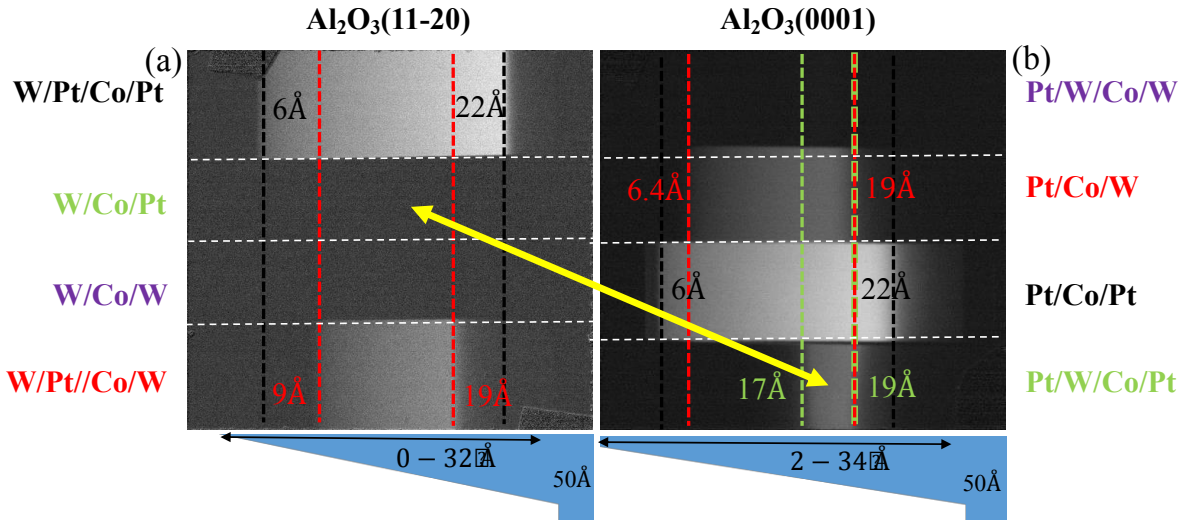

Figure 4.2: The SRT of the thin wedge shaped Co on W and Pt with capping layers Pt and W in different sequential configurations. The different colour dotted lines indicates the PMA area for Co with different adjacent capping and buffer layers. The dark and the bright areas on both figures represent the PMA and in-plane anisotropy region at remanence observed by visual Kerr microscopy. The yellow arrow indicates the different behaviour of the W/Co/Pt stack induced by the buffer layer structure.

To investigate the W/Co/Pt type system, we prepared in the first step the sample (figure 4.2(a)), containing 4 zones, similarly as we did for Mo/Co/Au stack, shown in figure 4.1. The thickness of the bottom buffer layers of W (common for all 4 zones) and Pt (2 zones) before Co wedge shaped deposition was the same and equal to 100Å , whereas the capping layers Pt and W thicknesses were equal to 30 Å each. In this sample, the Al_2O_3 substrate (11-20) orientated was used routinely for bcc high melted metal evaporation, on which W layer was deposited and next, two-zone Pt bottom layer was prepared. Further the wedge-shaped Co layer was grown and partially capped with W and Pt layer. In consequence the four-zone sample

containing all possible component layer sequences: W/Co/Pt, W/Pt/Co/Pt, W/Co/W and W/Pt/Co/W was fabricated.

The figure 4.2 (a) presents the remanence image, obtained by polar Kerr magnetometry. As previously, bright colour indicates the range of the Co thickness with the perpendicular component of anisotropy, whereas the dark areas represent the in-plane anisotropy. When the Co layer is deposited on the bottom Pt layer the properties are similar to the Mo/Co/Au system – the Co layer exhibits perpendicular magnetic anisotropy (PMA) in the wider d_{Co} range up to 22 Å for Pt capping and narrower (up to 15 Å) – for W capping. However, when the Co layer is deposited on the W buffer, it does not display PMA regardless the overlayer type. It is a different behaviour from Mo/Co/Au system.

To explore deeper, this difference a slightly other in the structure sample was prepared. We started with the bottom Pt buffer 100 Å thick. This sample was deposited on the sapphire (0001) substrate to get optimal growth condition for fcc-type buffer. The W layer 100 Å thick was deposited partially on the Pt buffer. The Co wedged layer was grown on the whole sample surface. The capping layer (Pt or W) was evaporated selectively to provide again 4 zone sample with the following sequences of the component layers: Pt/Co/Pt, Pt/Co/W, Pt/W/Co/Pt and Pt/W/Co/W. The PMOKE map illustrating magnetization orientation in this sample is shown in figure 4.2(b). Lack of PMA in the W/Co/W part as well as the wider and narrower d_{Co} range with PMA for Pt/Co/Pt (up to 22 Å) and Pt/Co/W (up to 15 Å) stacks, respectively, is a common feature of the sample previously discussed with the inverted bottom layer sequence and Mo/Co/Au system. However, the most intriguing properties are observed for the Pt/W/Co/Pt stack. Contrary, to the W/Co/Pt stack (figure 4.2(a)) in the Pt/W/Co/Pt sample (figure 4.2(b)) a region with PMA is well resolved. However, it appears in the much thicker d_{Co} range (13-16 Å) than the analogous zone in Mo/Co/Au system (8-11 Å). This difference is marked with the yellow arrow in figure 4.2.

Therefore, we have concluded that apparently similar systems of Mo/Co/Au and W/Co/Pt types are markedly different and moreover – the structure of the buffer layer is of great importance in the sandwiches of the latter type. Recently, it has been reported that in the Co layers directly deposited on W(110) buffer by pulsed laser deposition technique and with capping layer Au or Pt layers, the PMA can be induced in W/Co/Pt or W/Co/Au systems [4], what is in a contrast to our results. It confirms that also preparing method of the buffer layer might be crucial for magnetic properties.

These findings inspired to investigate the epitaxial Pt/W/Co/Pt structure in much more detailed way. The obtained results are described in the next chapter of my thesis.

4.2:- Structural and magnetic properties of single Co layer structures in W/Co/Pt systems

4.2.1:- Structural properties of W, Co and Pt analysed by RHEED images

Detailed structural and morphological studies the Pt/W/Co/Pt system, deposited in sapphire (0001) substrate were carried out by means of RHEED, TEM and AFM techniques. Particularly, RHEED enabled monitoring of structural evolution at various stages of the sample growth after fully deposited Pt layer, and after reaching 5, 10, 20, 40 and 70Å of W thicknesses, and 5, 10 and 20Å of Co thickness respectively (figure 4.3). First, the buffer Pt layer 400 Å thick grows in the pure fcc(111) structure confirmed by RHEED (figure 4.3(a)) and LEED [5]. The W layer grows on Pt buffer layer pseudomorphically up-to 5 Å as fcc-like structure. This is confirmed by still clear RHEED streaks (figure 4.1b). With further increase in W thickness, the RHEED pattern evolution becomes visible. The single RHEED strikes from W(5Å) split into two different and spotty distinct RHEED streaks, being more pronounced when the thickness of W increases from 5Å to 20Å as shown in figure 4.3(b-d). With further increasing the W thickness on Pt(111), the streaks become brighter (figure 4.3(d-f)). Considering angular dependence of the evolving RHEED pattern and the evaluated distance between atoms, forming atomic surface plane, one can deduce crystalline ordering of the growing W layer. The schematic presentation of the W crystallites on Pt(111) is shown in figure 4.4. W crystallites grow in three different orientations marked as A1, B1 and C1 with respect to Pt(111) preferred directions with six-fold symmetry. Another possible orientation is marked as A2, B2 and C2, obtained after 90° rotation of W crystallites. However, after analysis of epitaxial relations at the Pt/W interface (angular dependence and the estimated interatomic distance, see yellow vertical lines), the second possibility was excluded. Deposition of the Co layer on such buffer results in gradual improvement of the streaky RHEED pattern. Six-fold symmetry of Co atomic plane correlates well with all three orientations of the W structural grains. In consequence the crystalline quality of the Co layer becomes better and its surface smoother, which is reflected in the evolution toward continuous streaks with increasing thickness (Figure 4.3(g-i)).

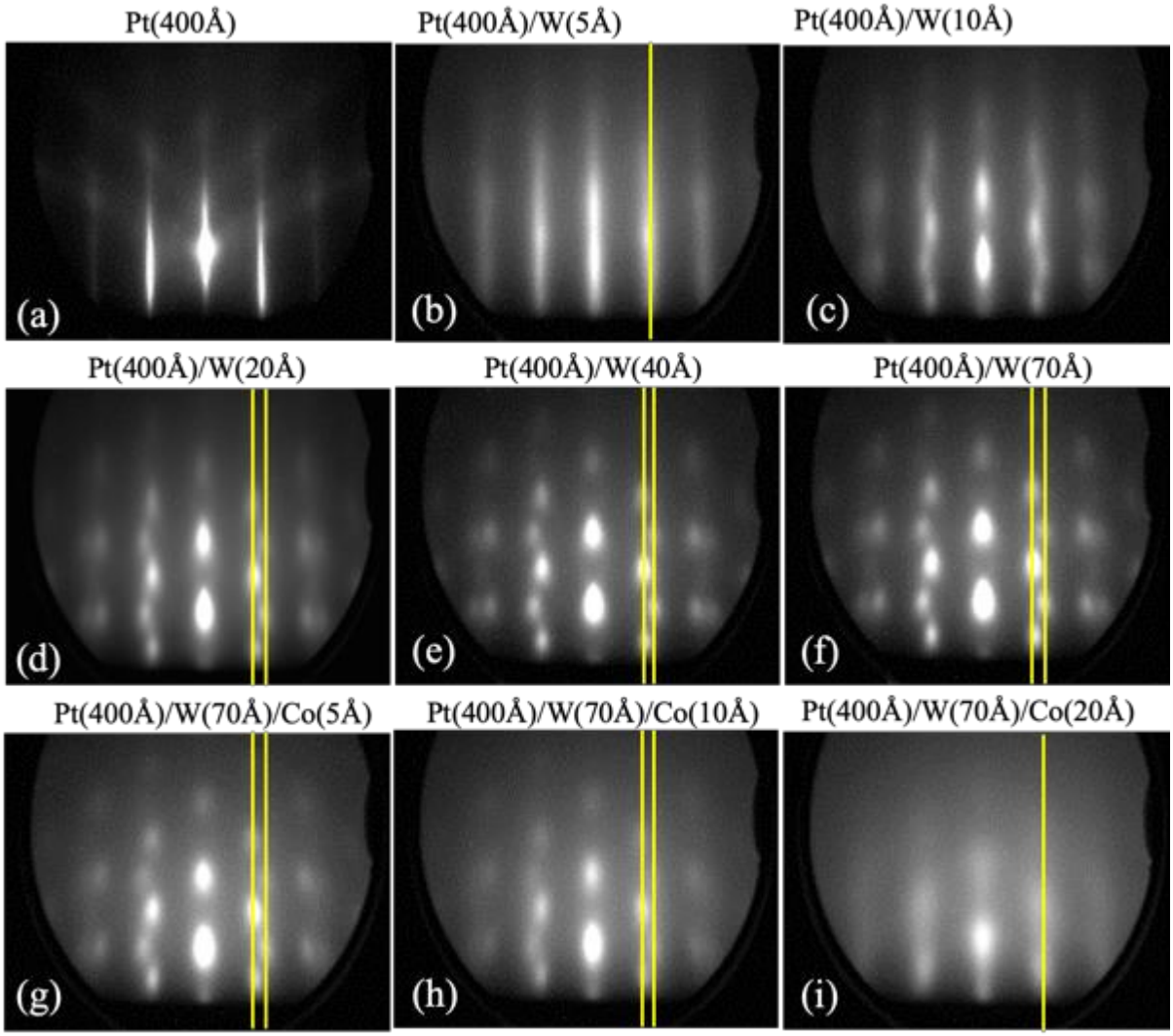

Figure 4.3. The evolution of RHEED patterns observed during deposition of Pt (a), W(b-f) and Co layers (g-h). Yellow lines indicate dotty streaks and are used to estimate a distance between atomic rows along the electron beam. Deatiled structural description of the Pt/W/Co stack deduced from these RHEED patterns is given in the text.

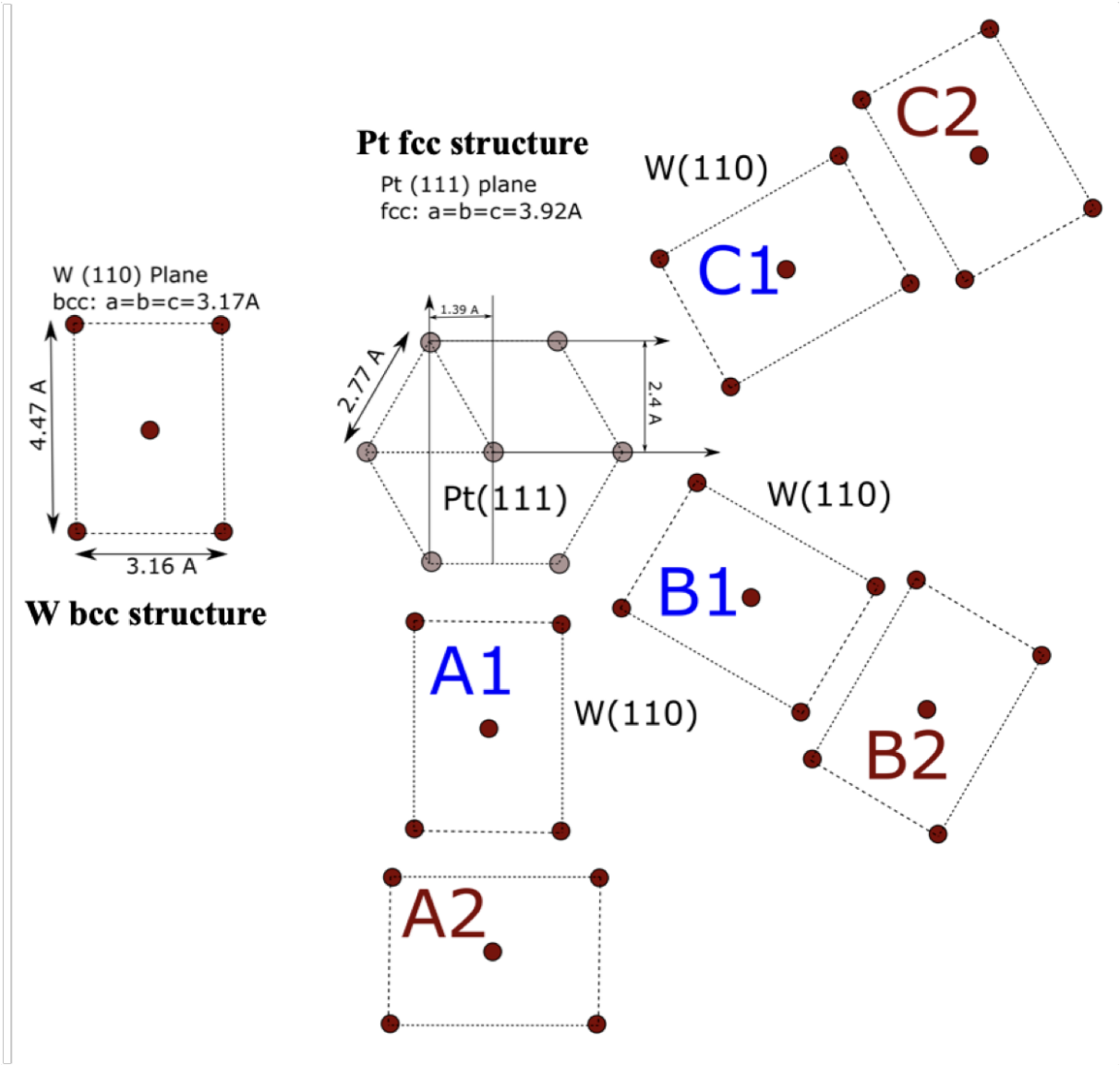

Figure 4.4 The two possible orientations of W crystallites growth on Pt(111). The (A1, B1, C1) and (A2, , B2, C2)represent the two different possible growth modes of W crystallites after rotation by 90° with respect to Pt(111) atom configurations.

Dotty character of the RHEED pattern suggests roughness of the studied surface. To estimate the roughness of W which grows on Pt(111), the topography has been studied by ex-situ atomic force microscopy (AFM). For this purpose, the sample of *of W(80Å) deposited on Pt(100Å)* was prepared by MBE. The surface rms roughness was estimated to be equal to 2 Å as shown in figure 4.5(a).

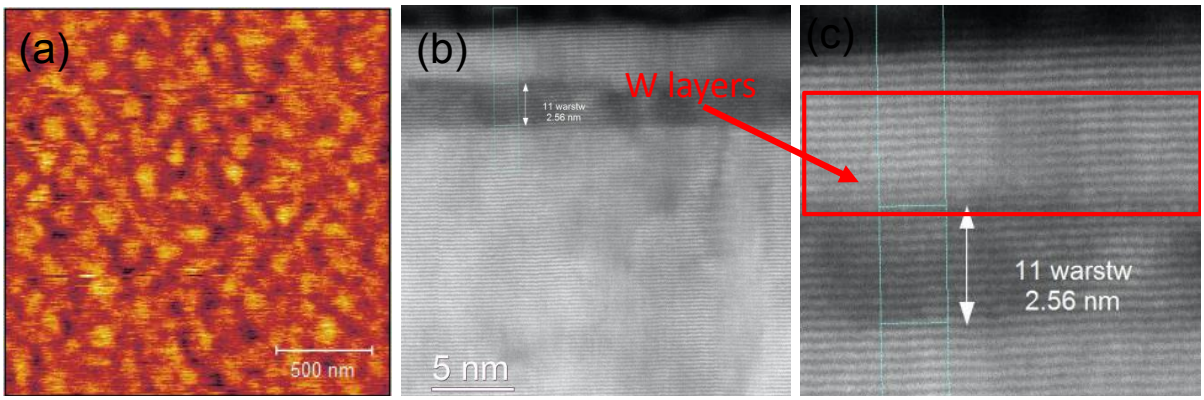

Figure 4.5(a) The topography image of W(80Å) deposited on Pt(100Å). (b) TEM cross sectional image of the Pt/W(24 Å)/Co(8Å)/Pt(30 Å). The black contrast shows the W layer. (c) the zoomed image of (b) for the W layer. It shows every atomic layers and confirms a good crystalline quality of the studied stack.

To confirm the epitaxial nature of the W, the cross sectional transmission electron microscopy study has been performed. The W film grown on Pt is epitaxial with clearly distinguished individual atomic layers (Figure 4.5(b) and (c)). Every distinct parallel line inside the red rectangular box in figure 4.5(c) represents the atomic layer of W. Although, the W grows on Pt in three different directions after rotation of crystallites, still the growth of W on Pt is epitaxial in nature as revealed by different techniques i.e. cross sectional TEM and in-situ RHEED. The suspected roughness of W surface is low as confirmed by TEM and topography studies.

4.3:- Influence of thickness of the W buffer on Co magnetic behaviour W/Co/Pt system

Inspired by the unexpected properties of the Pt/W/Co/Pt stack shown in figure 4.2(b), we started study to determine the influence of the W buffer thickness on magnetic anisotropy in this system. For this purpose, we have prepared the samples in which both W and Co layers were grown as step-shaped with mutually orthogonal directions along which the component layer thickness increased.

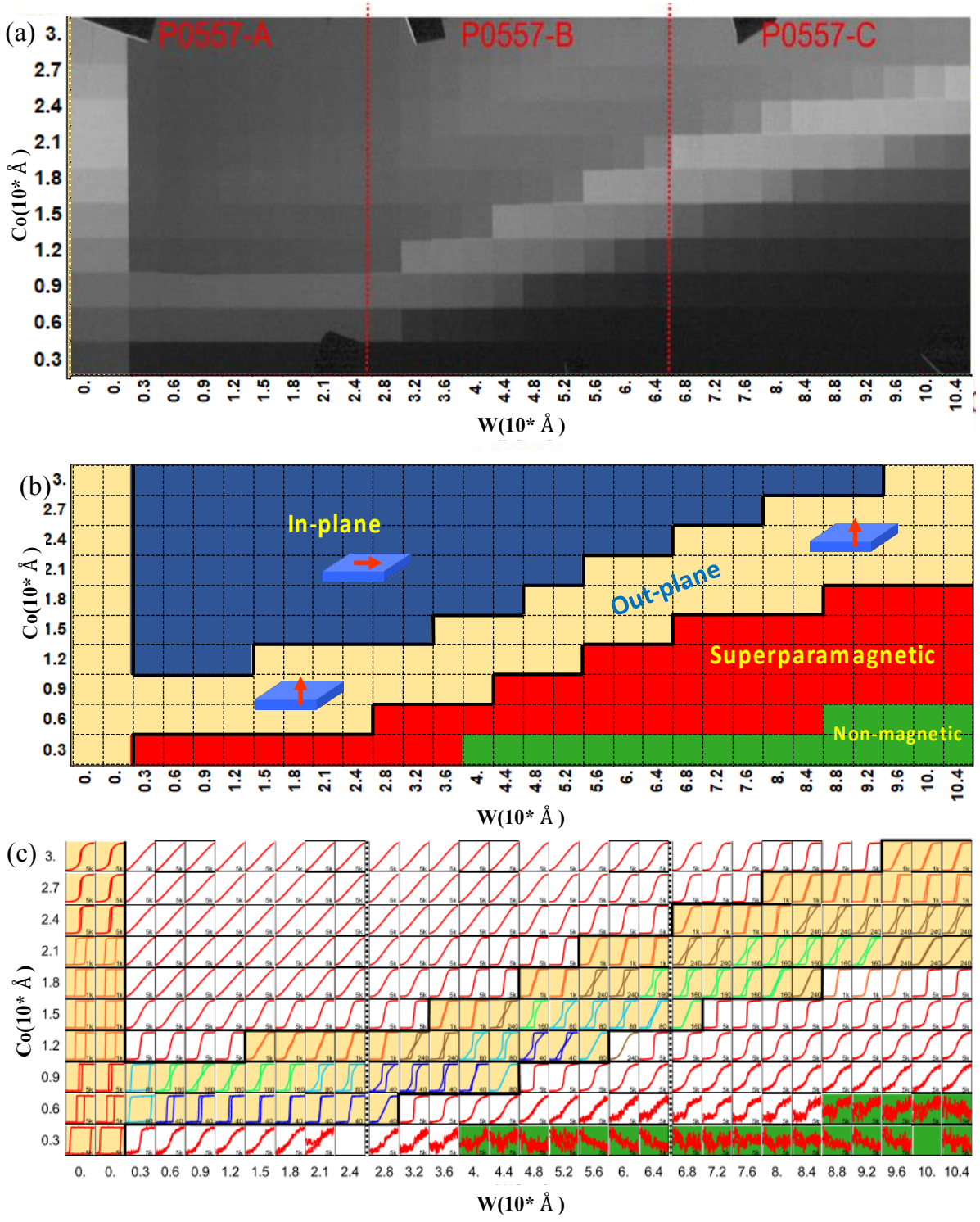

Figure 4.6 Magnetization states in the Pt/W(d_W)/Co(0-30 Å)/Pt(40 Å) stack (a) The remanence image of the sample registered by visual PMOKE. The dark areas represent the nonmagnetic or superparamagnetic state in the lower d_{Co} range or in-plane magnetization orientation for the bigger d_{Co}. The bright area corresponds to out-of plane magnetization component (PMA) at remanence state. (b) schematic map of various magnetic states observed in the sample: non-magnetic (green area), superparamagnetic (red), ferromagnetic with PMA

(yellow) and ferromagnetic with in-plane magnetization (blue). (c) a map of hysteresis loops measured locally by PMOKE in individual cells of the matrix sample.

To obtain satisfactory spatial resolution of the magnetic properties, the investigated sample was deposited on 3 sapphire (0001) substrates. Pt buffer 400 Å thick was deposited uniformly at 750 °C. By using the linear shutter, W was deposited as step starting from 3Å with increasing of 3Å for each 1mm distance. Further, Co layer was deposited in the same manner starting with the Co (3Å) thickness with increasing the step 3Å in the orthogonal direction with respect to grown W layer by 90° rotation the of moliblock. Finally, the capping Pt layer (30Å) was deposited. Prepared sample in the matrix form with different thickness of W and Co in the every square cell allows to investigate effectively the thickness influence of these layers on magnetic anisotropy in Pt/W(d_W)/Co(d_{Co})/Pt system.

The figure 4.6(a) presents the remanence images, obtained by visual Kerr microscopy in polar configuration. It is clearly seen that the area with the perpendicular magnetic anisotropy components (bright area) changes both with the Co and W layer thickness. For bigger thickness of the W bottom layer, the range of the Co layer thickness in which the PMA is induced shifts towards higher values. Because the MOKE technique offers possibility to probe magnetic locally, in every cell of the matrix, the hysteresis loops were measured (figure 4.6(c)), and the general magnetic characteristics were deduced on the base of them (figure 4.5(b)). It is easy to recognize four different types of the hysteresis loops ascribed to the various magnetic states of the sample: non-magnetic, superparamagnetic, ferromagnetic with perpendicular magnetization and ferromagnetic with in-plane magnetization. The non-magnetic state was observed for big W layer thicknesses and small Co layer thicknesses. The corresponding magnetic signal is represented by flat noisy line (green area). Another superparamagnetic state is observed in the lower range of the d_{Co} (red area) and expands toward larger d_{Co} with d_W increase. Typical loops are closed suggesting reversible character of magnetization reversal process and their shapes are well-described by Langevin equation. With further increase in the Co layer thickness, the PMA state can be found (yellow zone). It is illustrated by the open hysteresis loops with characteristic necking in the central part. Such shape suggest formation of the domain structure with perpendicular magnetization which is discussed in the further part of this thesis. The d_{Co} range with PMA is nearly constant and shifts to the higher values with d_W increase. For the biggest d_{Co} values the in-plane magnetization is observed (blue area). This magnetic state corresponds to closed hysteresis loops with nearly linear inclined shape between saturations points. This hysteresis shape suggests reversible magnetization rotation from in-plane

alignment toward perpendicular direction with increasing magnetic field applied along normal to the sample plane.

From the magnetization maps shown in figure 4.6, it is clearly visible that the d_{Co} range with PMA has rather constant width and shifts towards higher values with d_W increase. Also for bigger d_W, the non-magnetic region appears and superparamagnetic phase expands over larger d_{Co} range. It suggest that thicker W layer affect more effectively on magnetic properties of the Co layer. It seems that the thickness of magnetically dead Co layer increases with d_W, maintaining the constant d_{Co} range in which PMA occurs. Such observation is repeatedly observed in a big series of fabricated and investigated samples. This behaviour is not fully understood so far. One explanation is that with the increasing W thickness, the roughness at the W/Co or interfacial mixing becomes larger as is discussed in paragraph 4.4.1. Due to higher coordination of Co atoms by W atoms part of the Co layer behaves as a nonmagnetic at the interface of W/Co. This further gives the dead layer of Co i.e. Co loses his magnetic moment and becomes nonmagnetic [6, 7]. Another possibility is the strain evolution affecting magnetic properties of the Co layer with d_W increase. When the in-plane lattice constant of the Co film decreases magnetoelastic effects lower PMA whereas its expansion strengthen this property. Consequently, characteristic d_{Co} for which spin reorientation transition (SRT) occurs with d_W increase. By increasing the Co layer thickness, it is possible to induce transition from the nonmagnetic state to out-of-plane orientation of magnetization via superparamagnetic state However, the specific shape of PMA region in (d_W, d_{Co}) space causes that SRT can be induced not only by d_{Co} increase. Also, this magnetic phase transition is expected for fixed d_{Co} while d_W is getting smaller.

4.3:- Magnetic properties in epitaxial ultrathin Pt/W/Co/Pt layers

4.3.1:- Magnetic anisotropy in Pt/W/Co/Pt

To investigate in more details the effect of influence of the W buffer layer thickness on magnetic properties of Co, we selected from the matrix of the Pt/W/Co/Pt system (figure 4.6), the particular cells with particular thicknesses of the W and Co layers and prepared flat samples with those parameters for further investigations. The results were recently published in the paper [8].

We considered four different regions from figure 4.6, to study four different magnetic states i.e. the nonmagnetic, superparamagnetic, soft magnetic, and normal ferromagnetic states with PMA based on the magnetization curves. The magnetization reversal was studied for the

samples Pt/W(68Å)/Co(d_{Co})/Pt with different Co layer thicknesses 3 Å, 9 Å and 18Å, and Pt/W(24 Å)/Co(6 Å)/Pt by perpendicular magneto optic Kerr effect (PMOKE) instruments at room temperature. Obtained results are shown in figure 4.7.

For three samples with the same buffer thickness (W=68Å), different thicknesses of the Co layer: 3, 9 and 18Å, the measured hysteresis loops are presented in figure 4.7(a-c) respectively. In case of the thinnest Co layer (figure 4.7(a)), the measured signal from PMOKE shows the nonmagnetic nature. Increasing the magnetic field in the whole range of applied values (+/- 1T) results with zero Kerr rotation angle. Further, for the bigger thickness of the Co layer (d_{Co} = 9 Å) with the same thickness of the W, the measured hysteresis loop shows characteristic shape for the superparamagnetic state of the sample, with coercivity field and remanence equal to zero. By fitting the Langevin function to the hysteresis loop, (as shown by the red dashed lines in figure 4.7(b)) as described by literature [9], the size of the Co nanoparticles equal to 40Å in diameter was estimated. Next, by increasing the magnetic layer thickness (d_{Co} = 18 Å), the magnetic state is changed to ferromagnetic with PMA. The PMOKE hysteresis loop shows typical shape for the perpendicular component of magnetization, with coercivity field 1 mT as shown in figure 4.7(c). Characteristic necking in the central part of the loop may suggest a tendency to formation of the domain structure with preserved perpendicular orientation in the remnent state.

The results of magnetization reversal studies performed by PMOKE in the Pt/W (24 Å)/Co(6 Å)/Pt sample is presented in figure 4.7(d). For a first sight deduction of the magnetic state is not straightforward. However, based on the domain structure investigations, discussed in the further part of this thesis, this sample can be considered as ultra-soft magnet perpendicular orientation of the magnetic moments with coercivity equal to 0.02 mT. The d_{Co} = 6Å deposited on W(d_W = 24Å) is the transition thickness between superparamagnetic to ferromagnetic state. Investigated by visual PMOKE analysis, the domains are of labyrinth type at remanence with equal area of up and down oriented magnetic domains (figure 4.11(f)).

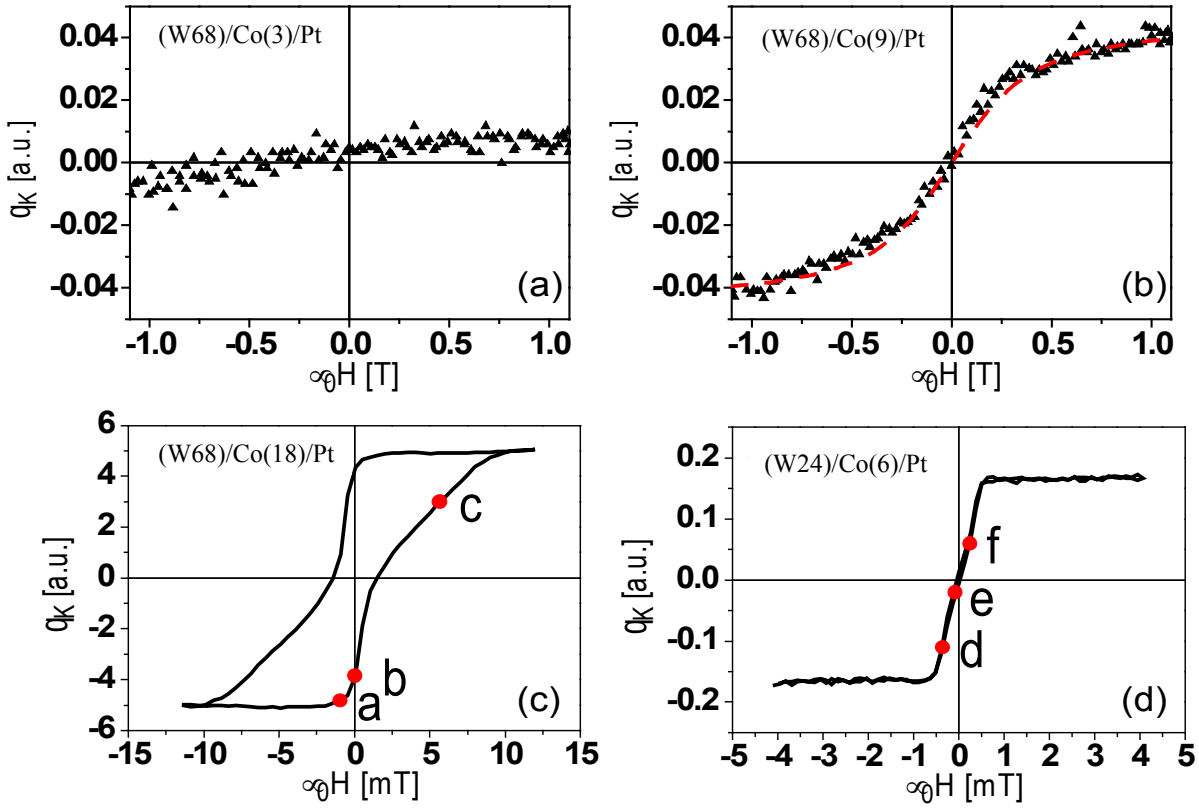

Figure 4.7:- The hysteresis loops measured by PMOKE for different thickness of Co and W in Pt/W(d_W)/Co(d_{Co})/Pt heterostructures. (a), (b) and (c): shows the magnetic hysteresis loops from Pt/W(68 Å)/Co(d_{Co})/Pt, where Co layer thicknesses is equal to 3, 9 and 18Å, respectively. The red dashed line in (b) represents fitting by Langevin function to calculate the size of nanoparticles which further confirms the superparamagnetic nature of the Co layer with dCo = 9Å. (d) : the hysteresis loop for Pt/W (24 Å)/Co(6 Å)/Pt which shows the behaviour of ultra-soft magnet with coercivity of 0.02mT. All indicated thickness in this figure are in Å. The red dots marked in the hysteresis loops ((c) and (d)) correspond to conditions in which the domain structure was registered, as shown infigure 4.10[8].

From the measured hysteresis loops it is possible to extract the values of the effective anisotropy field. It is equal to the field necessary to saturate the sample in perpendicular direction while it exhibits in-plane magnetization at remanence. The obtained anisotropy fields in a function of d_{Co} are presented for the sample with d_W = 68 Å in figure 4.8(a). It clearly shows that the anisotropy field decreases with increasing Co layer thickness, and its value goes from positive to negative value for d_{Co}=24Å (figure 4.8(a)), which corresponds to SRT from out of plane to in-plane magnetization alignment., It should be also noted that anisotropy field $\mu_0 H_{A1}$ = 360 mT can be also determined for Pt/W(68 Å)/Co(9 Å)/Pt stack which shows the

superpara-magnetism behaviour. It suggests that mentioned earlier Co discs also favours perpendicular orientation of their magnetic moment.

Further to observe how the anisotropy field behaves with changing buffer W thickness, at constant Co thickness the layer Pt/W(d_W)/Co(18 Å)/Pt, was studied. The dependence of anisotropy field for different thicknesses of W bottom layer is shown in figure 4.8(b). Surprisingly, there are two SRT points observed at two different W thicknesses. In the absence of W, Pt/Co/Pt stack exhibits perpendicular anisotropy with positive anisotropy field. With increasing the thickness of W(d_W = 3 Å), the sharp drop from positive to negative value of anisotropy field is observed with the appearance of the first SRT1. Thus, a monolayer of W is sufficient to change anisotropy from out of plane to in-plane. With further increasing the W layer thickness, the in-plane anisotropy decreases and the second SRT2 point with transition from in-plane to out-of-plane magnetization is found at d_W = 50 Å. The out of plane anisotropy further increases with the W layer thickness and takes a constant value for d_W > 80 Å.

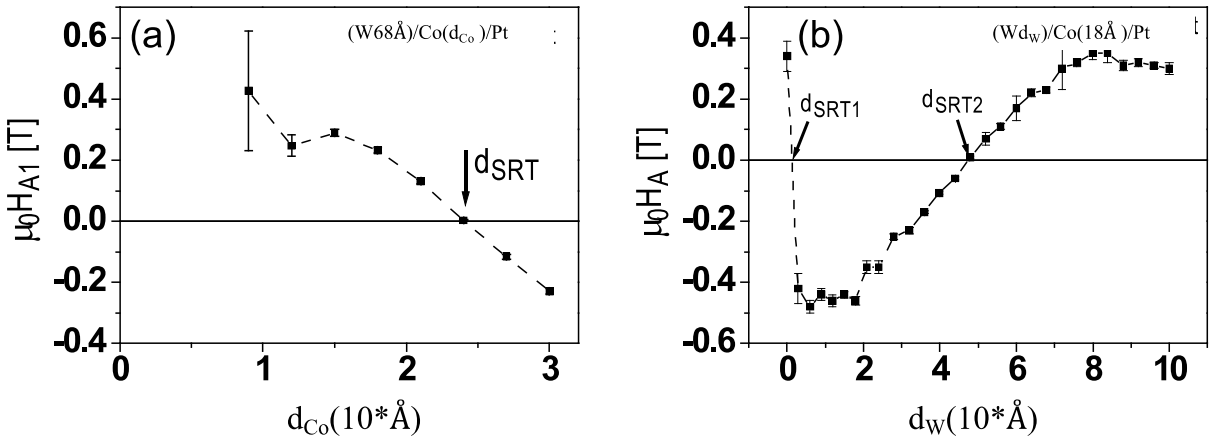

Figure 4.8 the anisotropy field as a function of: (a) Co layer thickness deposited on W bottom (d_W = 68 Å) with indicated SRT (b) W layer thickness in the stack Pt/W(d_W)/Co(18 Å)/Pt; two SRT points are marked with the arrows [8].

In the well-defined Pt/Co/Pt system, at the interfaces Pt/Co and Co/Pt, neighbouring atomic layers of Pt gain magnetic moment from Co. It gives the additional magnetization value in the Pt/Co heterostructures, and is called as magnetic proximity effect [10, 11]. Magnetization proximity effect at the Pt/Co interface can be estimated from maximum Kerr rotation signal measured by PMOKE. In the absence of proximity effect the maximum Kerr rotation is directly proportional to the thickness of the magnetic layer and extrapolated dependence crosses θ_{max} (d_{Co} = 0) = 0 point. Any proximity effect perturbs this dependence, particularly in the range of

small d_{Co}. It deviates it up in the case of gained moment or down when gained moment is oriented antiparallel or dead magnetic layer occurs. In consequence the extrapolated fitting line crosses the x-axis in the $\theta_{max}(d)$ plot in negative or positive range values, respectively, ascribed to d_0 offset.

By fitting the straight line to the experimental points in the maximum Kerr rotation vs Co layer thickness dependence, one can estimate the magnetic resultant proximity effect in Pt/W/Co/Pt system originating cooperatively from the two interfaces. By plotting maximum Kerr rotation vs Co thickness, the dead layer thickness of the Co film can be determined. This dependence for the sample with 68Å thick bottom W layer is shown in figure 4.9(a). The estimated dead layer thickness reaches 7 Å (here, d_0 = 7 Å) which is comparable with three atomic layers. The magnetic dead layer is formed at the interface W/Co among others due to the roughness which increases with W layer thickening. For the reference Pt/Co/Pt heterostructures, the extrapolated straight-line crosses d_{Co} axis at the negative value, which suggest occurrence of magnetic moment polarisation due magnetic proximity effect at the Pt/Co and Co/Pt interfaces [10, 11].

As mentioned earlier, the resultant gain or loss of magnetic moment is a cooperative effect originating from the two interfaces. Variation of d_0 offset with d_W illustrate changing contribution of oppositely acting proximity effects at two different interfaces. Such dependence is shown in figure 4.9(b). Below d_W = 18 Å, d_0 parameter is negative suggesting effective domination of Co/Pt interface over W/Co one. Above this value, d_0 becomes positive and further increases with d_W up to 8 Å in the investigated range. It means that dead layer effect from the W/Co interface overcomes polarisation enhancement at Co/Pt interface. Increasing influence of dead layer might result from the increasing roughness at the W/Co interface and raising coordination of Co atoms with W atoms. Under such circumstances the suppression of the magnetic moment at Co atoms is expected. The same effect may also origin from the induced moment at W atoms, which is oriented antiparallel to that at Co atoms. Unfortunately, these two possible effect that may occur at the W/Co interface cannot be easily separated and individually recognized. Similar dead layer of magnetic material has been studied on W single crystal in this literature [7, 6].

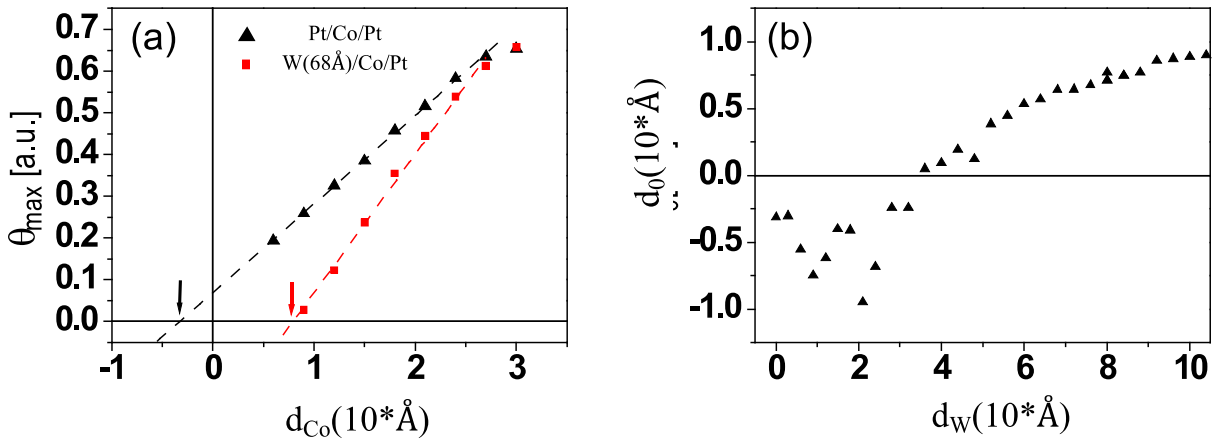

Figure 4.9. (a): Dependence of maximum Kerr rotation vs cobalt layer thickness for the reference Pt/Co/Pt stack (black symbols) and Pt/W(68 Å)/Co(d_{Co})/Pt structure (red symbols). The arrows indicate d_0 parameter illustrating the proximity effect occurring at the interfaces. (b): Change of d_0 parameter for different thicknesses of the W bottom layer in Pt/W(d_W)/Co(18 Å)/Pt stack[8].

4.3.2:- Domain structures of the W/Co/Pt system

From the shapes of hysteresis loops shown in figure 4.7 existence of the domain structure at remanence was deduced. Formation of the domain structure is a result of the competition between demagnetization energy and domain wall energy dependent on magnetic anisotropy and magnetic stiffness. In the chapter, we discuss the evolution of the domain structure with applied field in perpendicular directions observed by means of PMOKE microscopy. The two sample configurations were selected for considerations – the same as illustrated by the hysteresis loops shown in figure 4.7 exhibiting: typical ferromagnetic behaviour with PMA (Pt/W(68Å)/Co(18Å)/Pt) and the ultra-soft magnetic properties in the sample Pt/W(24Å)/Co(6Å)/Pt located close to the transition between superparamagnetic and ferromagnetic with PMA states. PMOKE images are presented in figure 4.10. Magnetic states illustrated by the domain structure images are indicated in the corresponding hysteresis loops by the red dots. For more detail understanding the domain evolution process in the sample Pt/W(24Å)/Co(6Å)/Pt, the complementary images are shown in figure 4.11.

Figure 4.10 (a, b and c) illustrate the domain structure evolution during the magnetization reversal from negative to positive saturation in the (Pt/W(68Å)/Co(18Å)/Pt) stack. At the negative magnetic field below saturation, the dendrite domains are formed. White dendrite domains start to nucleate with the decreasing in strength magnetic field below -0.96 mT and further expand covering the whole investigated sample area while the field decreases

down to zero (figure 4.10(b)). The area covered by black and white domains seems to be equal. In the positive field, the white domains expand and black irregular domains with decreasing areal coverage between them start to disappear. Similar domain observation has been studied in CoFeB systems by Anuj et al [13].

In the ultra-soft Pt/W(24Å)/Co(6Å)/Pt system, the evolution of magnetic domains structure has been studied by same procedure between the negative saturation positive saturation fields. Qualitatively, the magnetic domain evolution takes place in the similar manner, however in some details differ, particularly in bubble domain formation. In the negative field of -0.36mT, the bubble structure with individual object diameter around 1.5 μm and the spacing around 3 μm between them is observed (figure 4.10(d)). With further decrease in the field amplitude in the negative range, the increasing density of bubbles leads to coalescence and short, elongated white domains are formed (figure 4.10(e)). At a remanence state the labyrinth configuration with nearly equal amount of up and down magnetically oriented domains are present because both net magnetization in this state and the coercivity in this sample are very low (figure 4.7(d)). When magnetic field is switched to the opposite direction and its amplitude is increased, the white labyrinth domains become dominating in the image (figure 4.10(f)). Just below the saturation again the bubble lattice is formed (figure 4.11(h)). Similar behaviour of the domain structure was observed in Pt/Co/Os/Pt systems, however the domains were significantly larger [14]. It should be noted that the size of the domain structure images shown in figure 4.10 is the same. Therefore it is clearly visible that the domain structure in the soft magnetic cell ((d)-(f)) is coarser that in the sample with bigger d_{Co} (a)-(c)).

As it was mentioned earlier, the domain size may depend upon the magnetostatic energy and the domain wall energy. Additionally, in asymmetric systems like W/Co/Pt, where magnetic material Co is surrounded by two different materials, the additional exchange energy component from the iDMI may be significant. In the presence of iDMI the domain size can be reduced. Also, reduction of domain size is observed when the magnetic layer thickness approaches to the SRT critical point. Apart from single thin films of Co, it is also possible to observe the reduction in the domain size in higher thickness of Co films and in the multilayer heterostructures. [15] [16] [17] [18].

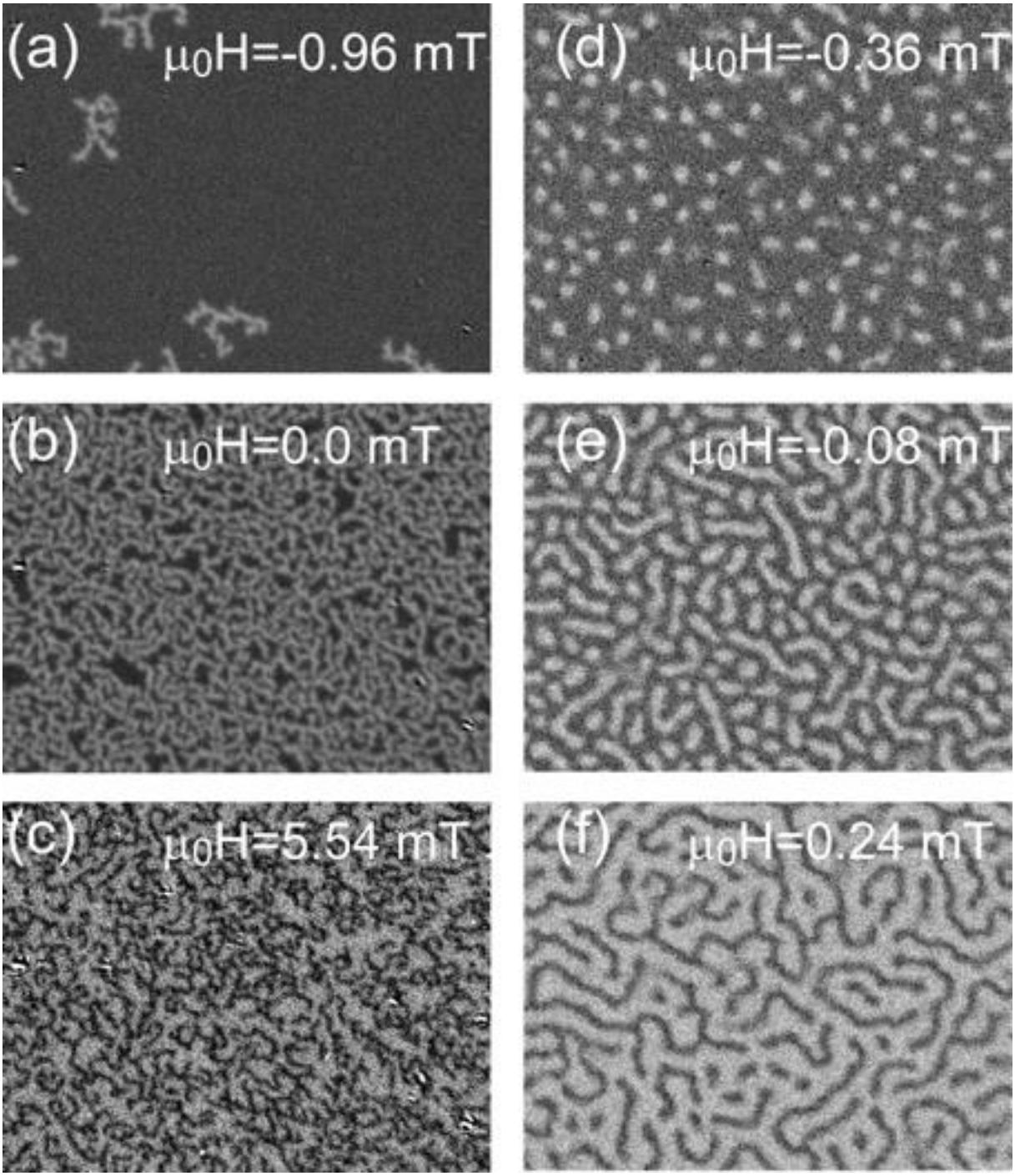

Figure 4.10 : Evolution of magnetic domain structure in the Pt/W/Co/Pt stacks during magnetization reversal registered by PMOKE microscopy. (a)-(c): ferromagnetic with PMA Pt/W(68Å)/Co(18Å)/Pt stack, (d)-(f): magnetically soft Pt/W(24Å)/Co(6Å)/Pt sandwich. Each image has the same size 45x34 μm^2. Presented here magnetic states are marked by the red dots at the corresponding hysteresis loops shown in figure 4.7 (c,d)[8].

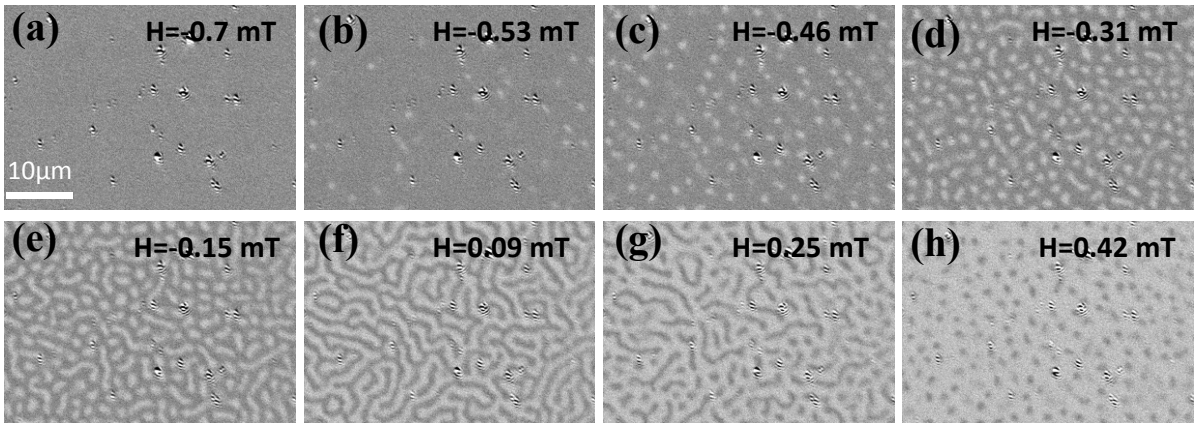

Figure 4.11: Complementary (in respect to figures. 4.10(d-f) images showing the domain structure evolution in the Pt/W(24Å)/Co(6Å)/Pt sandwich.

Described above properties of the Pt/W/Co/Pt stack are substantially different from those observed in the mentioned earlier Mo/Co/Au system. In the current one the hysteresis loops for ferromagnetic state with PMA exhibit characteristic necking in their central part. This feature is related to the domain structure formation at the remnant state. As it was mentioned earlier iDMI occurrence might be a factor responsible for the observed differences.

To investigate in more details this aspect the cell with d_W = 24Å and dCo 6Å, in which the bubble domain formation is evident, the BLS measurement for estimation of iDMI were performed. The DMI strength may answer the question whether the trivial bubble domains or topologically protected ones due to the existence of iDMI (called magnetic skyrmion bubbles) are observed. Obtained BLS spectra is shown in figure 4.12(a). The resonance Stokes and anti-Stokes lines are asymmetric. The difference in frequency between Stokes and anti-Stokes line, related to the iDMI strength D_{eff} was estimated by considering saturation magnetization Ms = 1370 kA/m, estimated from the SQUID measurement, and γ = 178 GHz/T for Co. The frequency difference has been measured at different wave vectors as shown in figure 4.11(b). Evaluated on this basis iDMI strength was equal to D_{eff} -1.12 mJ/m^2.

The observed iDMI value is substantially higher than that reported for in the sputter-deposited polycrystalline Pt/Co/W systems where was equal to 0.2 mJ/m^2 [19] and 0.3 mJ/m^2 [20] for different studied Pt/Co/W samples, respectively [21]. We are convinced that the well-defined epitaxial structure with sharp interface might be responsible for the higher iDMI amplitude observed in this discussed W/Co/Pt epitaxial systems than polycrystalline systems.

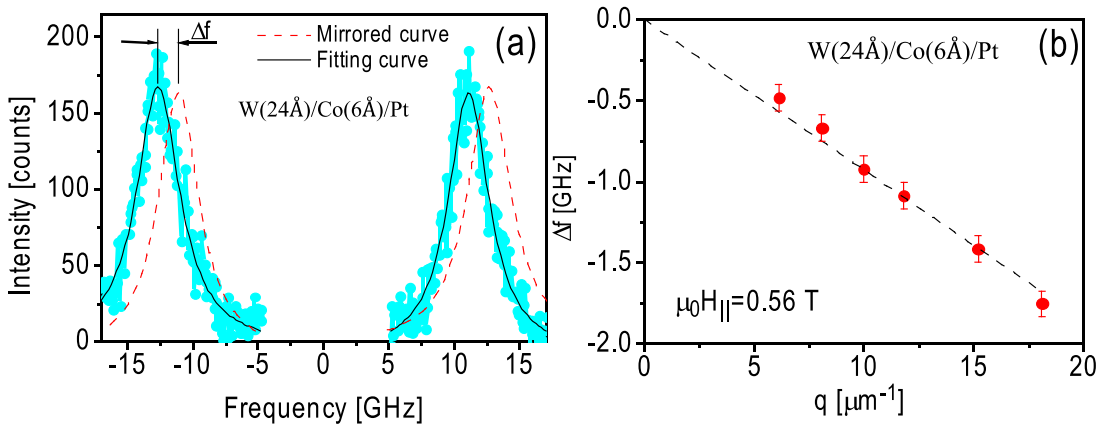

Figure 4.12 (a) : The Stokes and anti-Stokes lines (blue line) registered for the sample Pt/W(24Å)/Co(6Å)/Pt at applied inplane field $\mu 0H_{||}$=0.47 T and the wave vector of 15.2 μm^{-1}. The red dashed line shows the mirror curves of Stokes and anti-Stokes line to highlight and calculate the frequency difference Δf.Figure 4.12 (b): the frequency shift for different magnon wave vectors with external magnetic in-plane field 0.56T. [[8] Journal of Magnetism and Magnetic Materials 558 (2022) 169485].

In conclusion, the magnetic properties of Pt/W (68 Å)/Co(d_{Co})/Pt with Co(3 Å, 9 Å and 18Å) and Pt/W (24 Å)/Co(6 Å)/Pt were investigated by PMOKE, SQUID and BLS to study the dynamics and to calculate the iDMI amplitude due to the presence of neighbouring asymmetric layers to Co. For the ultra-soft magnetic behaviour of Pt/W (24 Å)/Co(6 Å)/Pt with coercivity 0.02mT and the saturation field 1mT the bubble domain structure observed. The evolution of bubbles domains in Pt/W (24 Å)/Co(6 Å)/Pt are very sensitive to the applied external field and the formation of bubble domains is due to presence of strong iDMI amplitude, indicting their topologically protected nature. The observed iDMI strength of 1.12mJ/m^2 is higher than the iDMI amplitude observed in sputtered samples. The detailed study of Co single layer with different W thickness can be found in this paper [[8] Magnetism and Magnetic Materials 558 (2022) 169485].

4.4:-References:

1 M. Kisielewski, A. Maziewski, M. Tekielak, A. Wawro and L. T. Baczewski, *Physical Review Letters*, 2002, **89**, 087203/1-087203/4.

2 J. Kisielewski, A. Maziewski, K. Postava, A. Stupakiewicz, A. Petroutchik, L. T. Baczewski and A. Wawro, *Journal of Magnetism and Magnetic Materials*, 2010, **322**, 1475–1477.

3 A. Wawro, Z. Kurant, M. Tekielak, P. Nawrocki, E. Milińska, A. Pietruczik, M.

Wójcik, P. Mazalski, J. Kanak, K. Ollefs, F. Wilhelm, A. Rogalev and A. Maziewski, *Journal of Physics D: Applied Physics*, , DOI:10.1088/1361-6463/aa6a94.

4 L. Camosi, S. Rohart, O. Fruchart, S. Pizzini, M. Belmeguenai, Y. Roussigné, A. Stashkevich, S. M. Cherif, L. Ranno, M. De Santis and J. Vogel, *Physical Review B*, 2017, **95**, 1–6.

5 M. M. Jakubowski, M. O. Liedke, M. Butterling, E. Dynowska, I. Sveklo, E. Milińska, Z. Kurant, R. Böttger, J. Von Borany, A. Maziewski, A. Wagner and A. Wawro, *Journal of Physics Condensed Matter*, , DOI:10.1088/1361-648X/ab0351.

6 H. Fritzsche, J. Kohlhepp and U. Gradmann, *Physical Review B*, 1995, **51**, 15933–15941.

7 W. Wulfhekel, T. Gutjahr-Löser, F. Zavaliche, D. Sander and J. Kirschner, *Physical Review B - Condensed Matter and Materials Physics*, 2001, **64**, 1–8.

8 Z. Kurant, S. K. Jena, R. Gieniusz, U. Guzowska, M. Kisielewski, P. Mazalski, I. Sveklo, A. Pietruczik, A. Lynnyk, A. Wawro and A. Maziewski, *Journal of Magnetism and Magnetic Materials*, 2022, **558**, 169485.

9 C. Binns and M. J. Maher, *New Journal of Physics*, , DOI:10.1088/1367-2630/4/1/385.

10 Y. M. Lu, Y. Choi, C. M. Ortega, X. M. Cheng, J. W. Cai, S. Y. Huang, L. Sun and C. L. Chien, *Physical Review Letters*, 2013, **110**, 1–5.

11 L. J. Zhu, D. C. Ralph and R. A. Buhrman, *Physical Review B*, 2018, **98**, 1–5.

12 N. Jaouen, G. Van Der Laan, T. K. Johal, F. Wilhelm, A. Rogalev, S. Mylonas and L. Ortega, *Physical Review B - Condensed Matter and Materials Physics*, 2004, **70**, 1–6.

13 A. K. Dhiman, T. Dohi, W. Dobrogowski, Z. Kurant, I. Sveklo, S. Fukami, H. Ohno and A. Maziewski, *Journal of Magnetism and Magnetic Materials*, 2021, **529**, 167699.

14 R. Tolley, S. A. Montoya and E. E. Fullerton, *Physical Review Materials*, 2018, **2**, 1–8.

15 A. Maziewski, J. Fassbender, J. Kisielewski, M. Kisielewski, Z. Kurant, P. Mazalski, F. Stobiecki, A. Stupakiewicz, I. Sveklo, M. Tekielak, A. Wawro and V. Zablotskii, *Physica Status Solidi (A) Applications and Materials Science*, 2014, **211**, 1005–1018.

16 M. Kisielewski, A. Maziewski, T. Polyakova and V. Zablotskii, *Physical Review B - Condensed Matter and Materials Physics*, 2004, **69**, 1–7.

17 I. Lemesh, F. Büttner and G. S. D. Beach, *Physical Review B*, 2017, **95**, 1–16.

18 C. Kooy and U. Eng, *Philips Res. Repts*, 1960, **15**, 7–29.

19 T. Lin, H. Liu, S. Poellath, Y. Zhang, B. Ji, N. Lei, J. J. Yun, L. Xi, D. Z. Yang, T. Xing, Z. L. Wang, L. Sun, Y. Z. Wu, L. F. Yin, W. B. Wang, J. Shen, J. Zweck, C. H. Back, Y. G. Zhang and W. S. Zhao, *Physical Review B*, 2018, **98**, 174425.

20 I. Benguettat-El Mokhtari, A. Mourkas, P. Ntetsika, I. Panagiotopoulos, Y. Roussigné, S. M. Cherif, A. Stashkevich, F. Kail, L. Chahed and M. Belmeguenai, *Journal of Applied Physics*, , DOI:10.1063/1.5119193.

21 I. Benguettat-El Mokhtari, A. Mourkas, P. Ntetsika, I. Panagiotopoulos, Y. Roussigné, S. M. Cherif, A. Stashkevich, F. Kail, L. Chahed and M. Belmeguenai, *Journal of Applied Physics*, 2019, **126**, 133902.

Chapter:-5

W/Co/Pt structures with moderate repetition number

In this chapter, I will present results obtained from the more complex layered structures composed of bigger number of Co layers sandwiched between non-symmetrical non-magnetic films. In addition to DMI interaction also other effects as interlayer coupling or enhanced magnetostatic interactions are expected making the magnetic states of the stack more complicated.

Table of Contents

5.1:-Magnetic properties of the samples containing two Co layers: W/Co/Pt/W/Co/Pt

In natural magnetic materials generally two kinds of magnetic alignments depending on two magnetic moment directions can be found. It can be parallel leading to ferromagnetic and antiparallel forming to antiferromagnetic ordering which has total zero magnetic moment in bulk material (in the case of ferrimagnets a net non-zero moment exists). However, is it possible to engineer the synthetic antiferromagnets by choosing the proper spacer thickness between two ferromagnetic layers. The coupling strength can be tuned by the spacer thickness between two ferromagnetic materials and it is explained successfully in terms of RKKY interaction (discovered by Ruderman, Kittel, Kasuya, and Yosida to explain initially a coupling mechanism between nuclear magnetic moments or localized electron spins through conduction electrons of the material) [1]. Similarly the coupling between magnetic component layers also takes place through the electrons crossing a spacer of non-magnetic material.

In this section, I will discuss the RKKY interaction between two Co layers with perpendicular anisotropy sandwiched between two heavy metals in a presence of iDMI as discussed in the previous chapter. First, two single layers of Co separated by Pt and W films with various thicknesses will be discussed. The investigated structure is the following: Al_2O_3(0001)/Pt(400Å)/W(10Å)/Co(10Å)/Pt(d_{Pt})/W(d_W)/Co(10Å)/Pt(30Å)), where d_{Pt} and d_W are the thicknesses of Pt and W components of double layer spacer ranging between 0-19Å and

0-20Å, respectively. The step-like W and Pt spacers separating Co layers (d_{Co}=10Å) were deposited orthogonally to each other creating a 420-element (cell) matrix sample as shown in figure 5.1. The different thicknesses of the spacer layers W and Pt allowed to switch the coupling between ferromagnetic and antiferromagnetic and tune its strength. The remanence image registered by means of visual MOKE for the stack with varying thicknesses of Pt and W spacers is shown in figure 5.1.

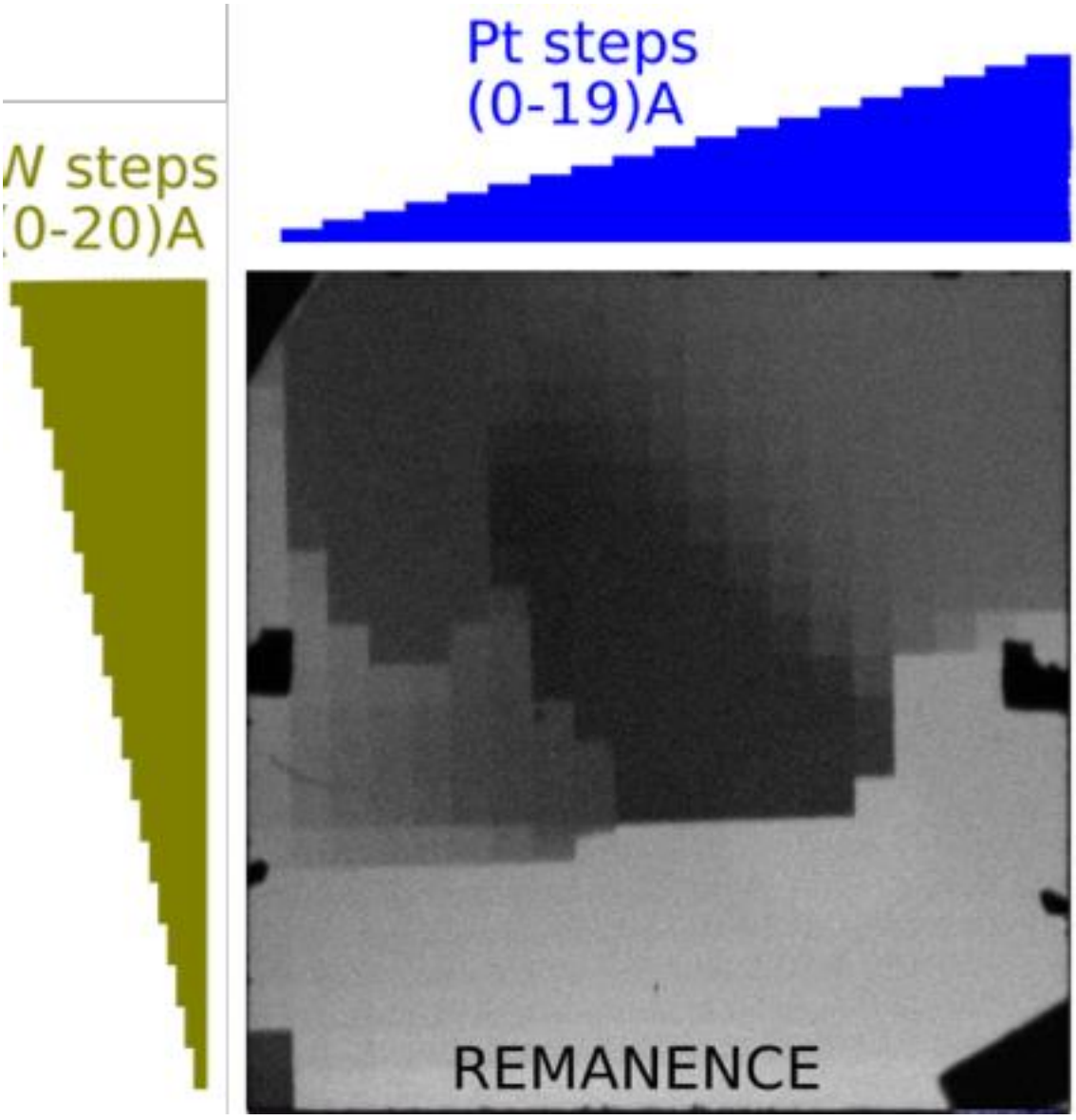

Figure 5.1: The remanence image obtained by means of visual PMOKE of two Co(10 Å) layers separated by Pt and W step-like spacer (thicknesses marked schematically on the image sides). The areas imaged by grey scale correspond to various magnetic alignments of the stack. Detailed explanation is given in the text.

To understand much deeper the coupling nature in the investigated stack, we measured the hysteresis loop by PMOKE in the individual cells of the matrix sample. We found that the complex spacer between two Co layers plays an important role to force the ferromagnetic or antiferromagnetic alignment of the magnetic layers. Its oscillatory behaviour with the spacer thickness can be described according to RKKY theory. The partial map of the hysteresis loops corresponding to magnetization state image shown in figure 5.1is depicted in figure 5.2

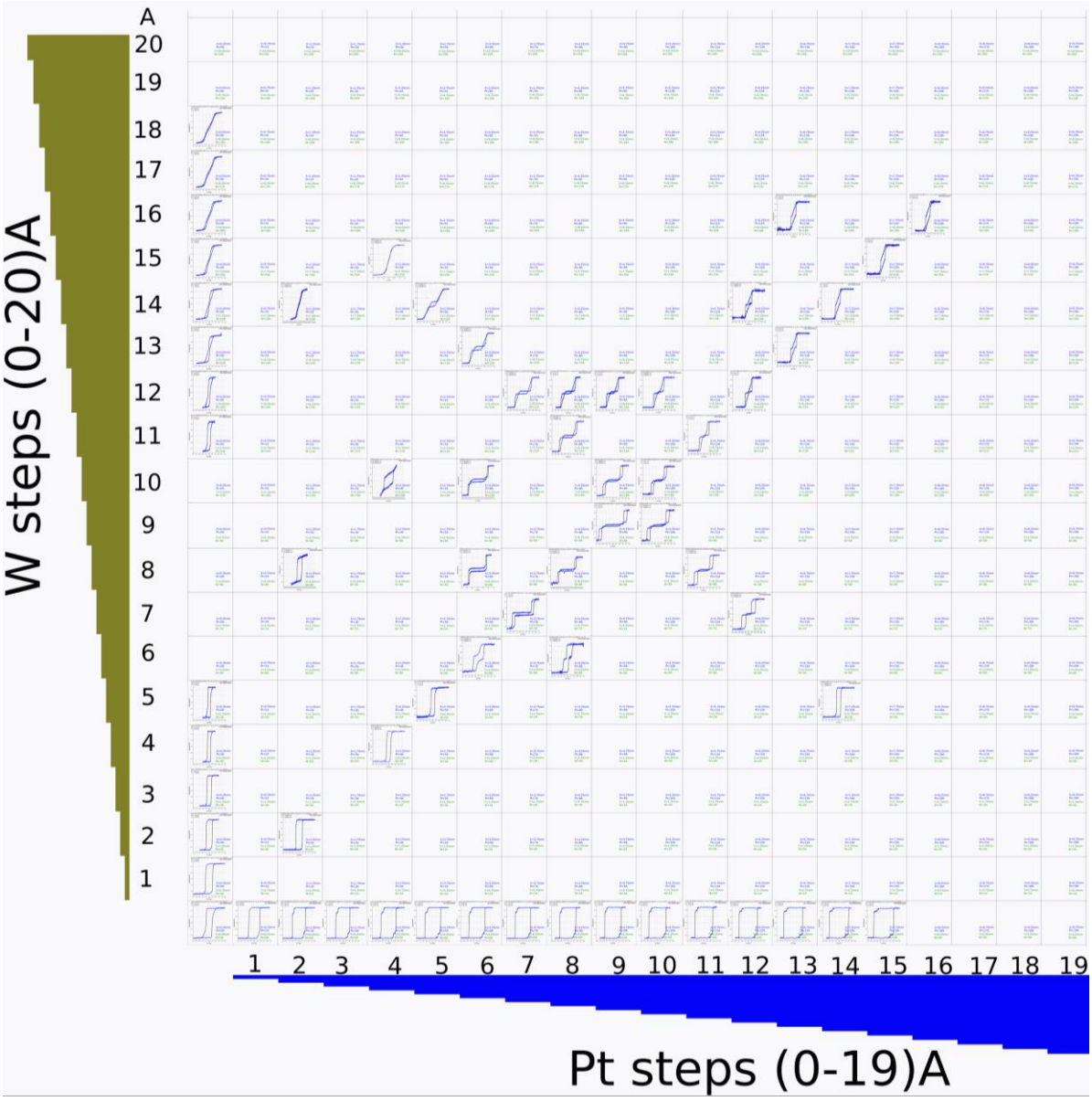

Figure 5.2: Partial map of the hysteresis PMOKE loops registered for Pt(400Å)/W(10Å)/Co(10Å)/Pt(d_{Pt})/W(d_W)/Co(10Å)/Pt(30Å) stack containing two Co layers separated by the double layer Pt/W bilayer with orthogonally oriented steps in the spacer components.

Because of large sample complexity and large number of cells, our attention was focused mainly on the diagonal cells ($d_W = d_{Pt}$) and the single layer spacers (loops along edges of the map). Also some loops in other cells were measured for comparison.

The evolution of the coupling type is directly visible from the hysteresis loop shape. Rectangular loops in the thin spacer range suggest ferromagnetic interlayer coupling. With increasing spacer thickness the change in the loop shape is very clear. For the medium spacer thickness range (central part of the map, Figure 5.2) two step magnetization reversal with switching magnetization direction individual Co layers from parallel to antiparallel and again to parallel alignment is clear. The plateau length in the central part of the loop correspond to antiferromagnetic coupling strength. A strength of the coupling field reaches a value of ca. 0.6 kOe. With further spacer thickness increase the loops evolves toward rectangular shape. From the fragmentary measurements performed for other cells outside the diagonal is evident that the maximum of the coupling strength occurs for the spacer with comparable thickness of the component W and Pt films equal to 9 Å. Further from the diagonal the loops also become more square.

The set of the loops along the edges of the map represent the properties of the reference samples containing single layer spacer: W/Co/Pt/Co/Pt (along the horizontal row) and W/Co/W/Co/Pt (along vertical row). In these stacks one of the Co layer has symmetrical surrounding, whereas the other one asymmetrical. Such difference in surrounding affects both PMA and DMI. Such system is a certain analogy to Au/Co/Mo/Co/Mo one reported in the earlier work [2]. Surprisingly, in the samples with the single layer spacer no antiferromagnetic coupling is observed. The loops with Pt spacer are fully rectangular whereas with W spacer evolve from rectangular to close tilted shape. This difference is clearly visible also for the samples with the single layer spacer thickness equal to the total thickness of the double layer spacer. This loop comparison is shown in figure 5.3. For the spacer layer Pt/W it evidences the presence of antiferromagnetic-type hysteresis loop which can be explained by macrospin model[3]. The magnetization reversal of each Co layer occurs one by one layer with increasing magnetic field in the case of antiferromagnetic coupled layers. In the case of single layer of the spacer Pt or W, the hysteresis loop shows the ferromagnetic-like coupling.

Generally, the RKKY interaction, which is applied to explain the observed coupling depends upon the spacer type and thickness. However, in this complex structure not only RKKY coupling mechanism, but also PMA and DMI are responsible for the interlayer interaction. The structure with W/Co/Pt exhibits significant iDMI strength which was described

in the previous section devoted to Pt/W(28Å)/Co(6Å)/Pt thin films. Various surroundings of the Co layer in the double layer spacer samples and in the reference ones, containing single layer spacer, substantially affects PMA as shown in figure 5.3. The highest PMA appears for Pt/Co/Pt stack, the medium for Pt/Co/W or W/Co/Pt (however they are different) and the lowest for W/Co/W part (exhibiting in-plane magnetization alignment). It should be noticed that in the double layer spacer sample the effective iDMI presence is expected in the both magnetic layers, whereas in the reference ones only in that with asymmetric surrounding.

The estimated value of the effective antiferromagnetic coupling for the double layer spacer samples can be evaluated approximately from the hysteresis loops shown in figure 5.2. The length of the plateau is a measure of its strength J. It can be calculated from the formula:

$$J = \mu_0 M_S H_{IEC} d,$$

where H_{IEC} is the exchange interlayer coupling field, M_S – saturation magnetization and d_{Co} Co layer thickness. It is assumed that H_{IEC} corresponds to the centre of the side hysteresis loops illustrating magnetization switching between parallel and antiparallel alignment. Exact value should be determined from the minor loops. However, in this case the width of the side hysteresis loops is small in comparison plateau length and therefore applied approach gives satisfactory accuracy.

The loop parameters used to determine H_{IEC} are listed in Table 5.1. Figure 5.4 shows the antiferromagnetic coupling strength vs the spacer thickness W/Pt($d_{Pt/W}$). Here, we took the bulk magnetization value of Co layer, Ms=1420 kA/m. The coupling strength decreases with thickness spacer layer increase in the evaluated range. It seems that the value of – 0.083 mJ/m^2 is for $d_{Pt/W}$ = 14Å is maximal as the hysteresis loop registered for $d_{Pt/W}$ = 24Å evolves toward rectangular shape. Therefore, a substantial drop in J value is expected for this thickness.

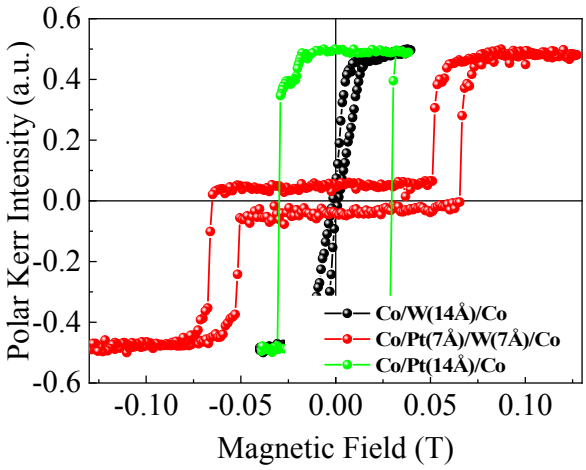

Figure 5.3 :- The selected loops from the map shown in figure 5.2 for the same thickness of the single and double layer spacer. The hysteresis loop marked in red evidences a clear antiferromagnetic coupling in the sample with double layer spacer. The reference samples with single layer spacer (green and black) exhibit ferromagnetic interaction. The rectangular shape of the reference sample with Pt spacer indicates much higher PMA in comparison with that containing W spacer.

Table-5.1 Magnetic parameters used to determine H_{EIC} calculate the coupling strength. $H_{EIC}=(H_{c1}+H_{c2})/2$ where Hc1 and Hc2 are the coercivity of the side loops in M-H curves showing antiferromagnetic coupling. These notation is taken from the literature [2].

Thickness of W(Å)	Thickness of Pt(Å)	Hc1(T)	Hc2(T)	H_{EIC}(kOe)	H_{EIC}(T)	RKKY strength (mJ/m^2)
7	7	0.051	0.066	0.585	0.0585	-0.08307
8	8	0.0493	0.06019	0.54745	0.05475	-0.07774
9	9	0.0336	0.04275	0.38175	0.03818	-0.05421
10	10	0.0170	0.024383	0.20692	0.02069	-0.02938
11	11	0.00949	0.015285	0.12388	0.01239	-0.01759
12	12	0.00635	0.011289	0.08819	0.00882	-0.01252

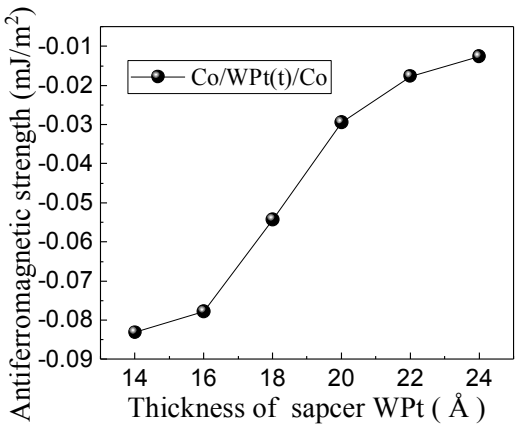

Figure 5.4 The strength of the interlayer coupling as a function of the double layer spacer thickness (equal thickness of the Pt and W component layers) in W/Co/Pt/W/Co/Pt heterostructures.

5.2:- Couplings in W/Co/Pt multilayers

In this section, I discuss the magnetic states and magnetization reversal in W/Co/Pt multilayers with the moderate repetition number of basic trilayer. Presented data shows enhancement of the complex magnetization states at remanence and during reversal process in

comparison to the simpler structure characterised in the previous chapter. Increase in the repetition number of basic trilayer, i.e. increase in the total multilayer thickness introduces enhanced contribution of magnetostatic (dipolar) energy, which participates in the overall energy balance. This additional factor substantially changes behaviour of the multilayers.

I investigated the $[Co(10Å)/Pt(d_{Pt})/W(d_W)/Co(10Å)]_n/Pt(30Å)$ with two thicknesses of the Pt/W spacer $d_W = d_{Pt}$ equal to 5 and 10 Å and two trilayer repetition numbers n = 6 and 7. The layered stack was deposited on the double layer buffer Mo(200Å)/Pt(200Å) and capped with Pt(25Å) layer. The change of the spacer thickness tunes the interlayer coupling whereas different repetition number provides more information on magnetization reversal mechanism (in the case of even number of magnetic component layers the total magnetization is fully compensated antiferromagnetically, whereas for odd number the non-zero magnetization occurs in the remnant state).

Figure 5.5(a) depicts the magnetization reversal of for sample $[W(5Å)/Co(10Å)/Pt(5Å)]_6$, registered by SQUID in the magnetic field applied in perpendicular direction to the film plane. Clearly visible steps and their number equal to 6 suggests that every component Co layer switches its magnetization separately with changing magnetic field. This magnetic state can be characterized by a macrospin model. During the magnetization reversal each layer, ordered ferromagnetically, reverses independently (layer by layer reversal) with changing with lateral spin configuration as described by Hellwig et al.[3]. The same jump of magnetization (height of the step in the hysteresis loop) evidences sequential switching of the individual Co layers. However, it is not possible to assign a specific magnetic layer to the specific jump in the hysteresis loop. In the remnant state magnetization in fully compensated as the magnetization of the same number of Co layer is oriented up and down. Thus, such stack can be considered in terms of fully compensated synthetic antiferromagnet. It should be noted that during the magnetization reversal from positive (negative) saturation to negative (positive) saturation field, the magnetic moments of each layer may reverse not only parallel or antiparallel to each other but also there is a possibility of small tilting in magnetic moment of each layer in the presence of iDMI due to asymmetrical layers W and Pt adjacent to Co layer [4]**.** Recently, it has been reported that the interfacial interlayer DMI can be induced if there is a titled magnetic moment between two magnetic layers with uncompensated magnetic moment separated by spacer. However, the origin of interlayer DMI is still unknown because of deficiency of crystal structure of magnetic material and heavy metal [4, 5].

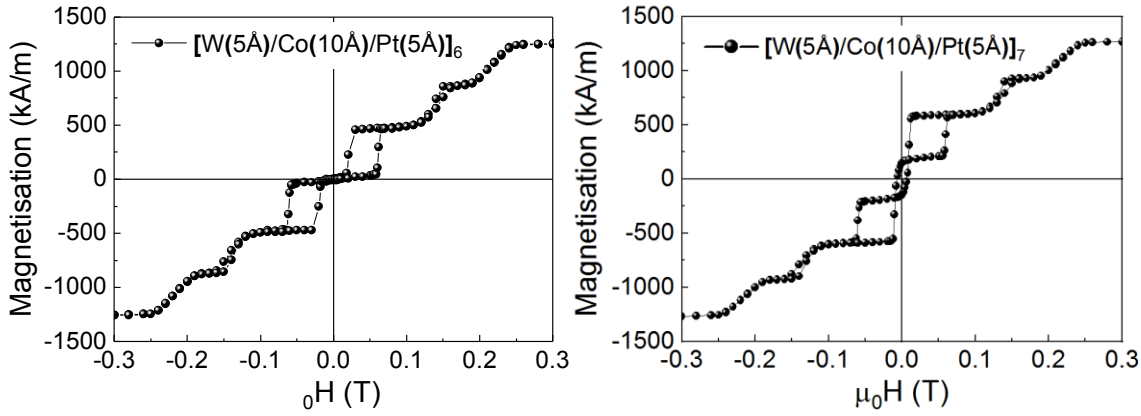

Figure 5.5 (a): The hysteresis loops measured in the field applied in perpendicular direction to the sample plane: (a) for [W(5Å)/Co(10Å)/Pt(5Å)]$_6$ stack with even number of the Co layers and (b): for [W(5Å)/Co(10Å)/Pt(5Å)]$_7$ multilayer with odd number layers of the Co layers.

For bigger and odd repetition numbers of basic trilayer, i.e. for *[W(5Å)/Co(10A)/Pt(5Å)]$_7$*, the magnetization reversal process is a bit more complicated. Again as in the previous case, the step like character of the hysteresis loop evidences the macrospin (ferromagnetic) nature of the individual Co layer. Due to odd number of the Co layer, the magnetic moment of the stack is non-zero at zero magnetic applied field. The hysteresis loop crosses each other near this point from positive saturation to negative saturation and vice versa. It may be a reason of certain coupling strength fluctuation between individual magnetic layers. Also, for small applied fields, the jump of magnetization is twice higher than the others. It is likely that the two component Co layers switch simultaneously in this field leading to entirely antiparallel magnetization alignment. Consequently, the number of magnetization switching between saturated states is reduced by one and is equal to six, like in the previous case. This sample can be treated again as an uncompensated synthetic antiferromagnet.

To learn more details on the stack magnetic state affected by antiferromagnetic exchange coupling and PMA with the presence of asymmetrical heavy W and Pt adjacent layers to Co film, inducing iDMI, the MFM investigations of domain structure were performed. The remanence image after in-plane demagnetization (application of ac-magnetic field with decreasing amplitude from saturation magnetic field to near zero field) shows the existence of magnetic domains even in the system being purely compensated for 6 repetitions as shown in figure 4.17(a). The presence of iDMI creating the tilting of magnetic moment in this W/Co/Pt system might be a main factor responsible for creation of magnetic domains in fully compensated system. In the stack containing the odd number of trilayer repetition, magnetic

domains also appear after the same in-plane demagnetization procedure, as shown in figure 5.6(b). This system is not purely compensated. As a result, the large magnetic domains with non-zero net magnetization (see hysteresis loop in figure 5.5(b)) are induced. Their creation is possible due to local structural imperfections pinning magnetization during demagnetization process and abrupt magnetization switching between up and down global magnetization as shown in figure 5.6(b). However, we cannot again neglect here the iDMI influence on creation of the tilted magnetic moment in each Co layer. In both these systems the domains are large and the contribution of the domain wall energy to the total energy is negligible. In these stack the influence of antiferromagnetic coupling clearly dominates over magnetostatic interactions.

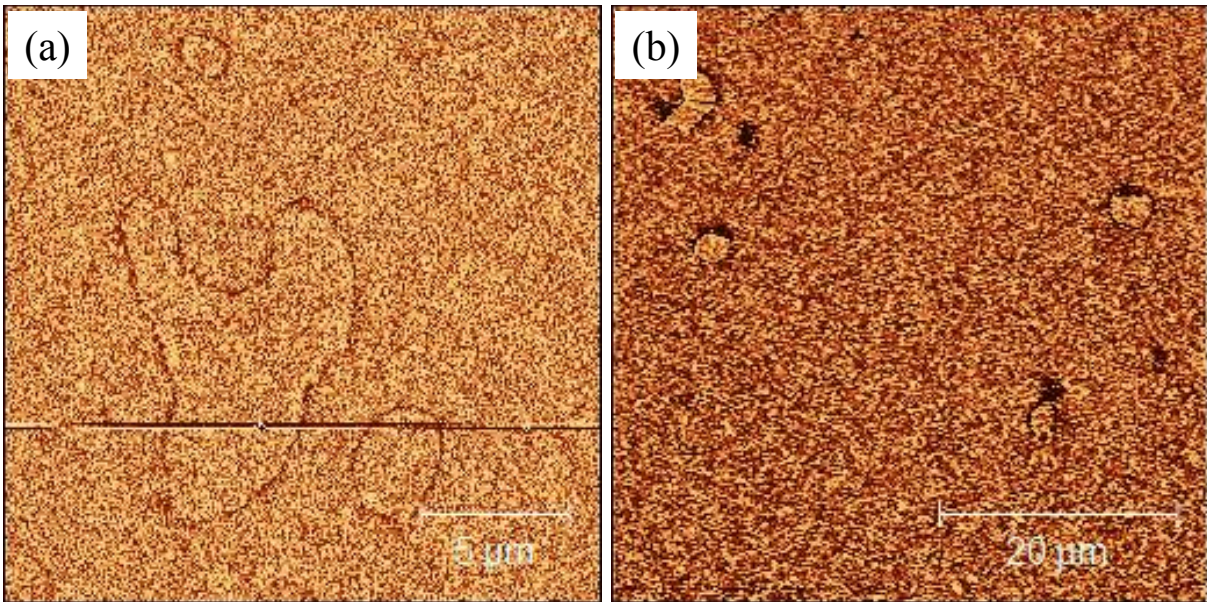

Figure 5.6 The remanence MFM images recorded after in-plane demagnetization for: (a) [W(5Å)/Co(10Å)/Pt(5Å)]$_6$ with area 20x20 µm^2. (b):[W(5Å)/Co(10Å)/Pt(5Å)]$_7$(with area 50x50 µm^2.

To observe the changing competition between exchange coupling strength and the dipolar strength, further we have studied the systems with the larger spacer thickness increasing from 5Å to 10Å for W and Pt individual component layers. According to the dependence shown in figure 5.4 the interlayer coupling strength is expected to be lower for larger spacer thickness.

Figure 5.7(a-b) shows the hysteresis loops measured by SQUID in the magnetic field applied in perpendicular direction to the sample plane for both repetition numbers of 6 and 7 repetitions of [W(10Å)/Co(10Å)/Pt(10Å)] stack. The shape of the hysteresis loops is entirely different from the previous case. The step-like character is not observed any more. Instead, the tilted hysteresis loops with magnetization decrease from saturation well before zero field is very

distinct. Both coercivity and net magnetization at remanence are equal to zero. Such hysteresis loop shape is typical of domain structure formation with perpendicularly up and down oriented magnetization. This interpretation is confirmed by MFM measurements.

Figure 5.8 depicts the MFM images from [W(10Å)/Co(10Å)/Pt(10Å)] stacks with both repetition numbers equal to 6 and 7. They are registered after sample demagnetization following the magnetization saturation in perpendicular direction. The labyrinth-like domain structure is clearly developed. The amount of bright and dark domains is equal. Such distribution confirms the shape of the hysteresis loops shown in figure 5.7.

Increase in the spacer thickness results in the lowering of antiferromagnetic exchange coupling strength and making dipolar interactions dominating. Consequently, uniformly magnetized component Co layers interacting each other by the coupling in the stacks with thinner spacer, switches to locally ferromagnetically coupled ones across the whole stack thickness when the spacer thickness increases (magnetization is vertically correlated within a single magnetic domain area). In the larger lateral scale such volumes with oppositely oriented magnetization (magnetization is laterally anti-correlated) extend periodically creating observed domain structure. Such magnetization evolution gives rise to the domain wall formation which give another energy contribution to the total energy of the system. Therefore, the equilibrium magnetic state of the multilayered structure depends on the balance between interlayer coupling strength, magnetostatic (called also as dipolar or demagnetization) and domain wall (dependent on PMA and DMI) energies. Domain structure formation leads to demagnetization energy lowering. On the other hand, as already mentioned, emerging domain walls additionally contribute to the energy of the system. The domain wall energy depends on PMA strength and in the considered case also on DMI. Increase in iDMI strength lowers domain wall energy. Formation of the domain structure means that the cost of the increasing domain wall energy is lower that decrease of magnetostatic energy placing the system in the total energy minimum. In this condition the domain structure becomes stable.

In the discussed here case increasing role of dipolar interaction, leading to magnetic state modification from macrospin-like behaviour to domain structure, was obtained by the spacer layer increase with the fixed repetition number of the basic building block. However, it is also possible to convert antiferromagnetic exchange coupled systems to purely dipolar coupled systems not only by increasing in spacer thickness between Co layers but also by increasing in a repetition number as described in Ref [3]. Therefore, there are two main factors i.e. spacer thickness and increasing the repetition numbers in multilayers which play main role

for transition from strong interlayer exchange coupling to strong dipolar coupling in a specified systems.

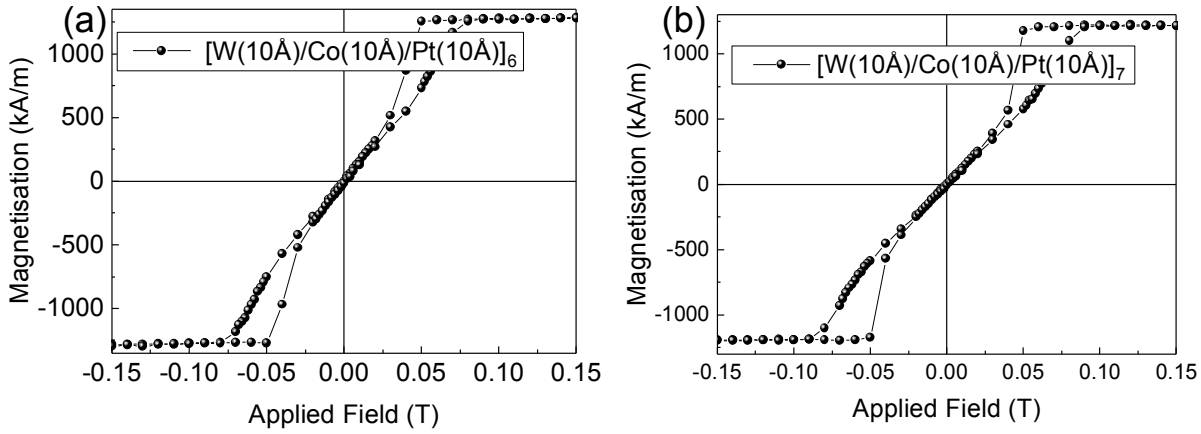

Figure 5.7:- The SQUID hysteresis loops measured in the perpendicular magnetic field for: (a) [W(10A)/Co(10A)/Pt(10A)]$_6$, and (b) [W(10Å)/Co(10Å)/Pt(10Å)]$_7$ stacks.

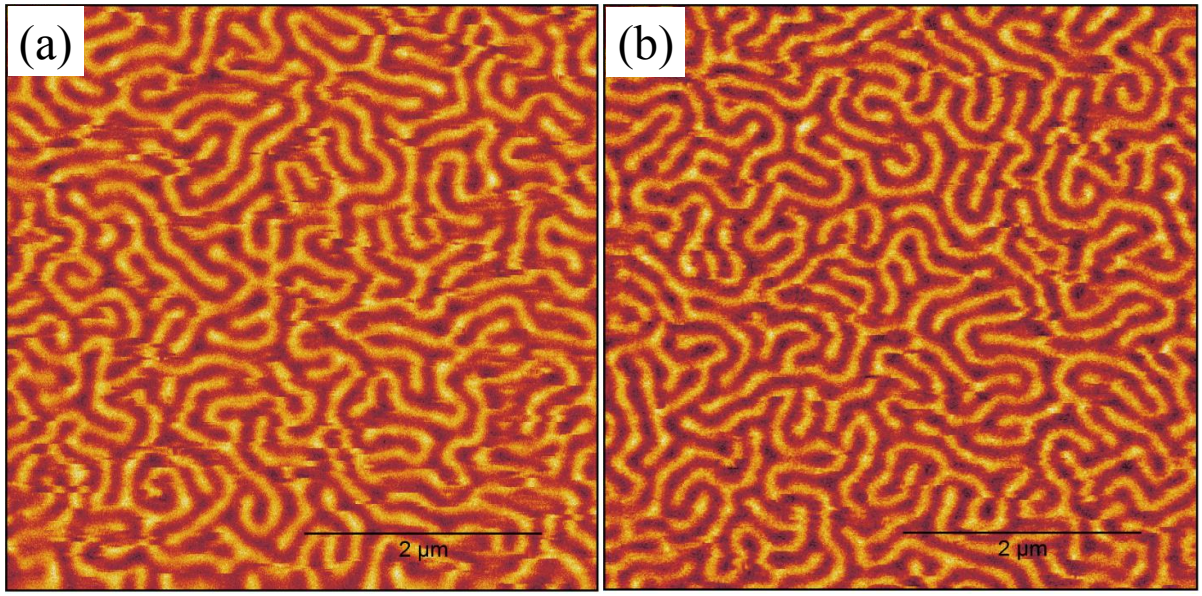

Figure 5.8 The MFM images after demagnetization following sample saturation in perpendicularly oriented magnetic field: (a) for [W(10Å)/Co(10Å)/Pt(10Å)]$_6$, and (b) W(10A)/Co(10A)/Pt(10A)]$_7$ stacks. The scan area is 5x5um^2 for both images (a) and (b).

5.3:-References

1. Parkin, S. S. P. & Mauri, D. Spin engineering: Direct determination of the Ruderman-Kittel-Kasuya-Yosida far-field range function in ruthenium. *Physical Review B* **44**, 7131–7134 (1991).

2. Kurant, Z., Tekielak, M., Sveklo, I., Wawro, A. & Maziewski, A. Interlayer coupling-driven magnetic ordering and magnetization processes in ultrathin Au/Co/Mo/Co/Au film. *Journal of Magnetism and Magnetic Materials* **475**, 683–694 (2019).

3. Hellwig, O., Kirk, T. L., Kortright, J. B., Berger, A. & Fullerton, E. E. A new phase diagram for layered antiferromagnetic films. *Nature Materials* **2**, 112–116 (2003).

4. Fernández-Pacheco, A. *et al.* Symmetry-breaking interlayer Dzyaloshinskii–Moriya interactions in synthetic antiferromagnets. *Nature Materials* **18**, 679–684 (2019).

5. Han, D. S. *et al.* Long-range chiral exchange interaction in synthetic antiferromagnets. *Nature Materials* **18**, 703–708 (2019).

Chapter:-6

Interfacial Dzyaloshinskii-Moriya interaction in the epitaxial W/Co/Pt multilayers

Table of Contents

In the previous section, I described the stacks containing single or double Co layer with W and Pt adjusting layers. The double Co layer structure o separated by spacer W/Pt with different thicknesses allows engineering the antiferromagnetic and ferromagnetic coupling state depending upon the spacer thickness. Here, I will describe the structural and magnetic properties of $[W(10Å)/Co(6Å)/Pt(10Å)]_N$ multilayers, where N=10 and 20, in which a presence of strong dipolar and iDMI coupling may create the chiral particles i.e. skyrmions by applying magnetic field at room temperature. Further, to support the experimentally obtained iDMI strength, the density functional theory calculations were done to determine the interfacial DMI at the interface of W/Co and Co/Pt for the idealized crystalline fcc structure of of W, Co and Pt component layers. The domain structure modelled by micromagnetic simulation supports both iDMI strength values determined from DFT calculation and the experiment using Keff method. This chapter is based mainly on the work already published in our paper [1]. My contribution to this work is the following: sample design, fabrication and initial characterization, magnetic force microscopy (MFM) measurements and data interpretation, SQUID data analysis, determination of DMI strength from the K_{eff} method, preparation of the paper draft, and contribution in preparation of its final version.

6.1:- Structural Characterisation

The multilayers were fabricated by molecular beam epitaxy (MBE) technique to create the layered epitaxial structure. All three materials Pt, W and Co were evaporated by e-beam at

the rates of 0.2Å/s with base and operating pressure 1*10E-9 and 1*10E-7 mbar respectively. The rate of material growth was measured by quartz crystal monitor and XBS cross-beam mass spectrometer. The substrate $Al_2O_3(0001)$ was heated at 850°C for one hour and after that cooled down to 750°C to deposit the seed layer of Pt(100Å). At higher temperature, Pt grows in the fcc(111) plane as confirmed by in-situ RHEED and XRD (PANalytical Empyrean X-ray diffractometer with Cu Kα1, analyzed using Maud [2] software) measurements as shown in the figures 6.1 and 6.2, respectively. After the seed layer of Pt deposition, the multilayer W/Co/Pt layer deposition was performed at room temperature to reduce possible intermixing. To examine the epitaxy of W and Co, a separate reference trilayer sample W(10 Å)/Co(30 Å)/Pt(30 Å) with the same deposition condition as multilayers was grown.

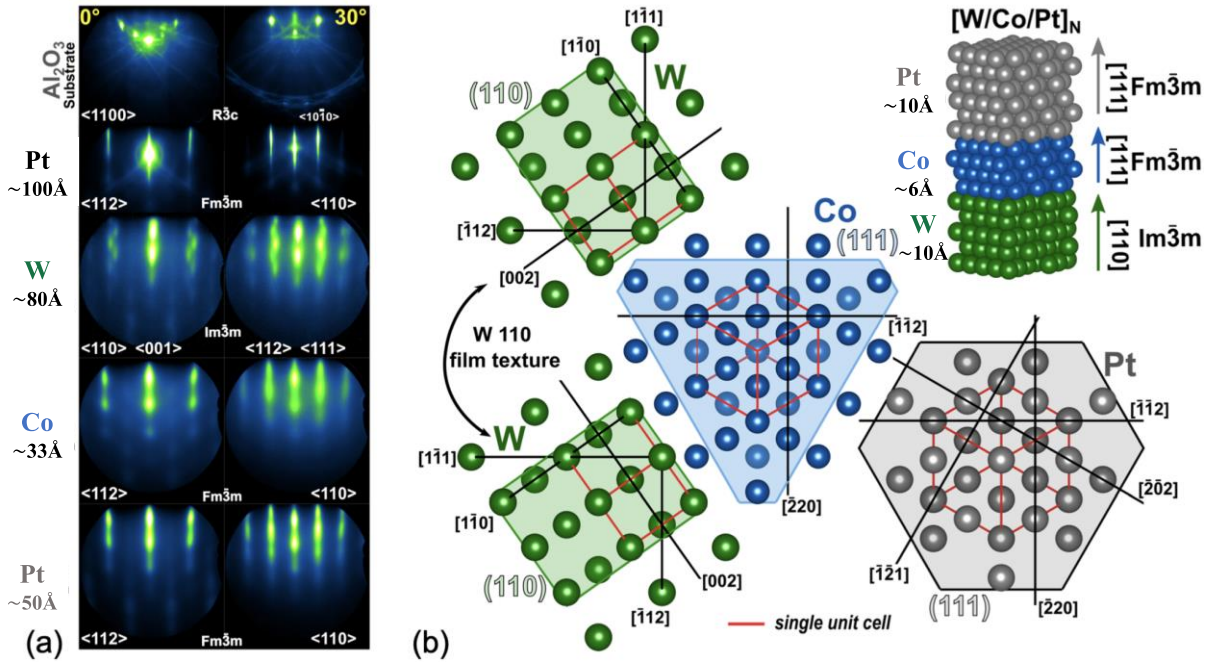

6.1 (a) The RHEED patterns obtained for the sapphire substrate, Pt buffer, W, Co, and Pt cap layers. (b) the epitaxial relations between the component W, Co and Pt layers in $[W/Co/Pt]_N$ multilayer stack deduced from RHERD X-ray diffraction investigations. The planes of atoms of each W, Co and Pt layers are represented by different coloring and the single unit cell of each layer is marked by red lines. Mutual azimuthal directions are indicated by the black lines in the same reference axis. The direction of W crystallites are rotated by 30°when deposited on the Pt layer; however, only rotation by 90° forms the constructively RHEED patterns shown in figure 6.1 (a). This image has been taken from the literature [1].

The evolution of the RHEED pattern was recorded for the reference tri-layer W(100 Å)/Co(30 Å)/Pt(30 Å) at different angles of grown material with respect to the electron beam

as shown in the figure 6.1(a). From the specific sample plane, the streaks were observed along the <110> and <112> azimuths of the Pt buffer layer which indicates the Pt layer was grown in good quality of epitaxial films. Similarly, the same procedure has been done to take the different azimuths of the W and Co layer. From the interatomic distances, it is possible to deduce the atomic relation and construct the atomic model (figure 6.1(b)) which was used in density functional theory to calculate the interfacial DMI energy. It should be noted that the thin layer atomic arrangement or atomic distance may differ from the system with the higher thickness of constituent layers.

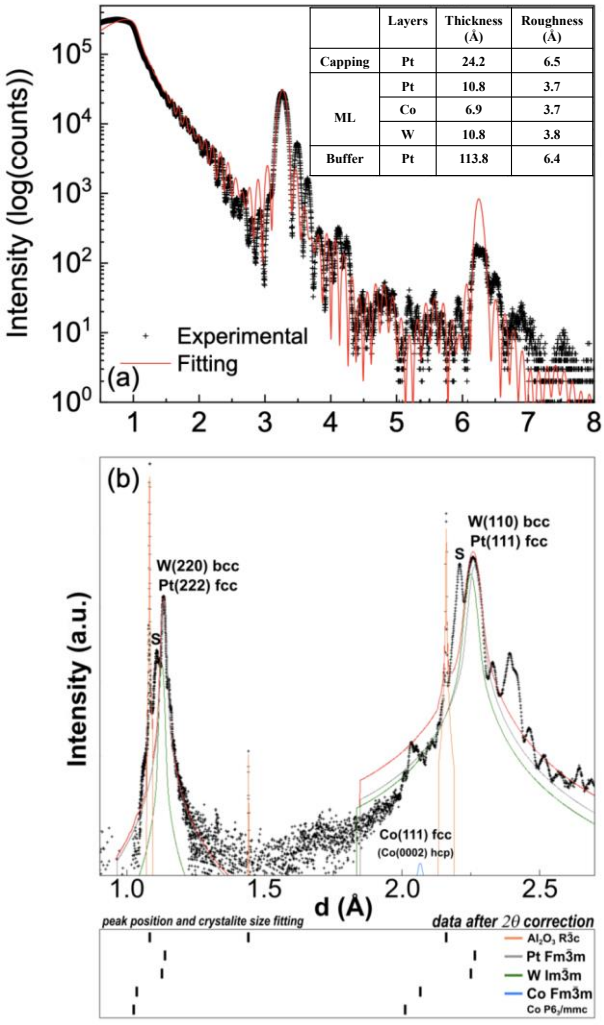

Figure 6.2 (a) Experimental X ray reflectivity signal (black crosses) and fitting (red line) for the W/Co/Pt multilayer heterostructure. The calculated thickness and roughness of W/Co/Pt layers are given in the inserted table. (b) The measured XRD spectrum for the W/Co/Pt multilayer. The XRD pattern contains mainly signal from W bcc(110) and Co fcc(111) planes and W/Co/Pt superlattice peaks (S), diffuse scattering, and Kato thickness fringes. The color

lines illustrate fitting for different materials W, Co, Pt and Al_2O_3 substrate. The fitting positions are indicated in the bottom panel for every individual material [1].

Figure 6.2(a) shows X-ray reflectivity measurements of the multilayered sample W/Co/Pt with N=20, from which the interfacial roughness and the thickness of the constituent layer of the multilayered stacks can be deduced. There are clearly visible two Bragg peaks with numerous Kiessig fringes which indicates the total number of tri-layer repetition in the whole heterostructures. The fitting parameters of the component layer thickness and the roughness at the interfaces is given in the inserted table in figure 6.2(a). Figure 6.2(b) shows the XRD pattern from the W/Co/Pt multilayer. The structural parameters and the lattice constants determined from XRD, XRR and RHEED measurements, used in the DFT calculation are listed table-6.1.

	Crystalline structure	a (Å)	c (Å)	γ (°)
Al2O3 substrate	$R\bar{3}c$ Trigonal	4.754	12.982	
Pt	$Fm\bar{3}m$ fcc	3.9237		
Co	$Fm\bar{3}m$ fcc	3.5212		
W	$Im\bar{3}m$ bcc	3.1875		
[W/Co/Pt] Model M1Co	$P1$	2.489		
[W/Co/Pt] Model M2wt	$P1$	2.694		120
[W/Co/Pt] Model M3s	$P1$	2.707	33.149	
[W/Co/Pt] Model M4Pt	$P1$	2.774		
[W/Co/Pt] Model M5d	$P1$	2.707		120.197

Table-6.1 Structural parameters used to construct the crystal structure for multilayer W/Co/Pt stack applied in DFT calculation to determine the iDMI strength. First four lines contain the lattice parameters determined from the experiment (RHEED and XRD). In the five bottom rows the parameters used to construct the different crystalline models of W/Co/Pt multilayers which are discussed in the further part of this chapter.

6.2:- Magnetic Properties

The multilayers W/Co/Pt with N=10 and 20 were measured by SQUID to estimate the saturation magnetization value and magnetic anisotropy H_K value (the anisotropy field is equal to saturation field applied in the sample plane direction). The process of magnetization reversal can be described from the M-H loops registered in both directions of the applied field: perpendicular and parallel to the sample plane (figure 6.3). With the perpendicular field decrease from saturation the magnetization suddenly decreases and takes a value of zero at zero field. Beginning of magnetization decrease is associated with nucleation of the domain structure

which still preserves perpendicular magnetization. Further, increasing the field towards the negative saturation field, the magnetization oriented with the applied field increases slowly and saturates at the negative saturation field. Similar procedure done for reversed magnetic field sweep from negative saturation field to positive saturation field evidences symmetrical nature of the loop. At zero magnetic field the net magnetization value is zero which suggests that the total number of magnetic moments in the upward direction is equal to the total magnetic moments in the downward direction. So, the remanence state is the multidomain state with vertical antiparallel domains. Below the saturation filed the loops are slightly open indicating that the domain configuration depends not only on the applied field but also on a magnetic history of the sample. The closed loop registered with the parallel field to the sample plane indicates that the magnetization reversal in this direction has a reversible nature and spins rotates toward the sample plane following the applied field. From the hysteresis loops, one can estimate the M_S and $\mu_0 H_k$ value, Ms=1420 kA/m and 1433 kA/m, and the magnetic anisotropy field $\mu_0 H_k$=0.959 T and 0.606 T for N=10 and N=20 respectively. Table 6.2 collects the all magnetic parameters determined from the discussed hysteresis loops for both repetition numbers N = 10 and 20.

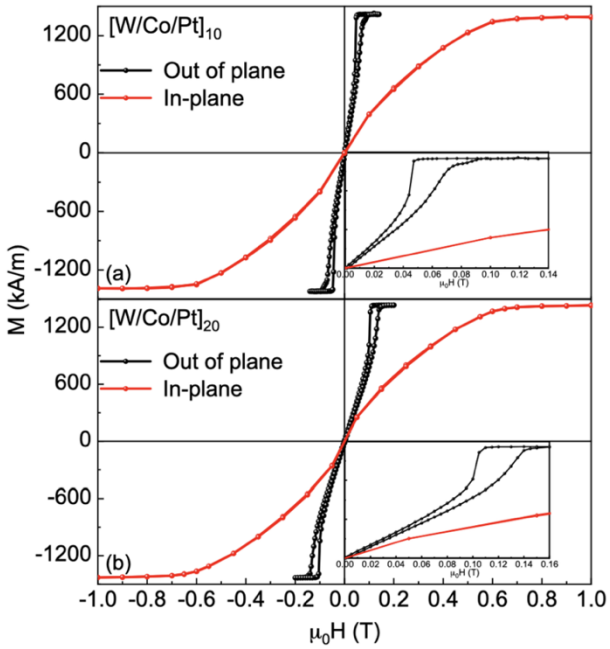

*Figure 6.3 The M-H loops for registered by SQUID for (a) [W/Co/Pt]*10 and (b) [W/Co/Pt]*20 multilayers. The black and the red colors represent the loops measured in in-plane and out of plane oriented external field* [1].

N	M_s (kA/m)	$\mu_0 H_k$ (T)	W (Å)	Δ (Å)	σ_{dw} (mJ/m^2)	K_u (MJ/m^3)	K_{eff} (MJ/m^3)	D (mJ/m^2)	D_s (pJ/m^2)	D_{thr} (mJ/m^2)
10	1420	0.595	1080	43.7	3.56	1.68	0.442	2.65	1.83	0.39
20	1433	0.606	930	39.7	5.25	1.72	0.434	2.49	1.72	0.63

Table-6.2 Determined magnetic parameters for W/Co/Pt multilayer samples with repetition number N = 10 and 20:Saturation magnetization ($\boldsymbol{M_s}$), anisotropy field ($\mu_0 H_k$), domain width($\boldsymbol{W}$), domain wall width(Δ), domain wall energy ($\boldsymbol{\sigma_{dw}}$), uniaxial anisotropy constant($\boldsymbol{K_u}$), effective anisotropy constant ($\boldsymbol{K_{eff}}$), iDMI strength($\boldsymbol{D}$), surface iDMI constant($\boldsymbol{D_{su}}$) and threshold iDMI($\boldsymbol{D_{thr}}$).

To observe the magnetic domain structure of the multilayer thin-films, the MFM measurements were performed in the remnant state. Before observation the samples were demagnetized in the alternating perpendicular field with decreasing amplitude down to zero. The measurements were carried out with low moment magnetic probe to avoid modification of the domain structure by the stray field emitted by the MFM tip. The MFM images of the domain structure in demagnetized multilayers are shown in figure 6.4(a) and (c). The multilayers exhibit the labyrinth domain structure with equal contribution of domains with perpendicular magnetization oriented up and down. This images entirely confirms our conclusions on magnetic state at remanence drawn from the hysteresis loop shapes. Figures 6. 4(b) and (d) show the parallel strip domains formed after demagnetization in the alternative magnetic field higher than the saturation field with decreasing amplitude applied in the plane of the multilayers. We show that the labyrinth-like domains can be easily converted to parallel strip domains. The parallel domains can be considered as 1D magnonic crystals which are very interesting [3] in the presence of iDMI interactions from application point view.

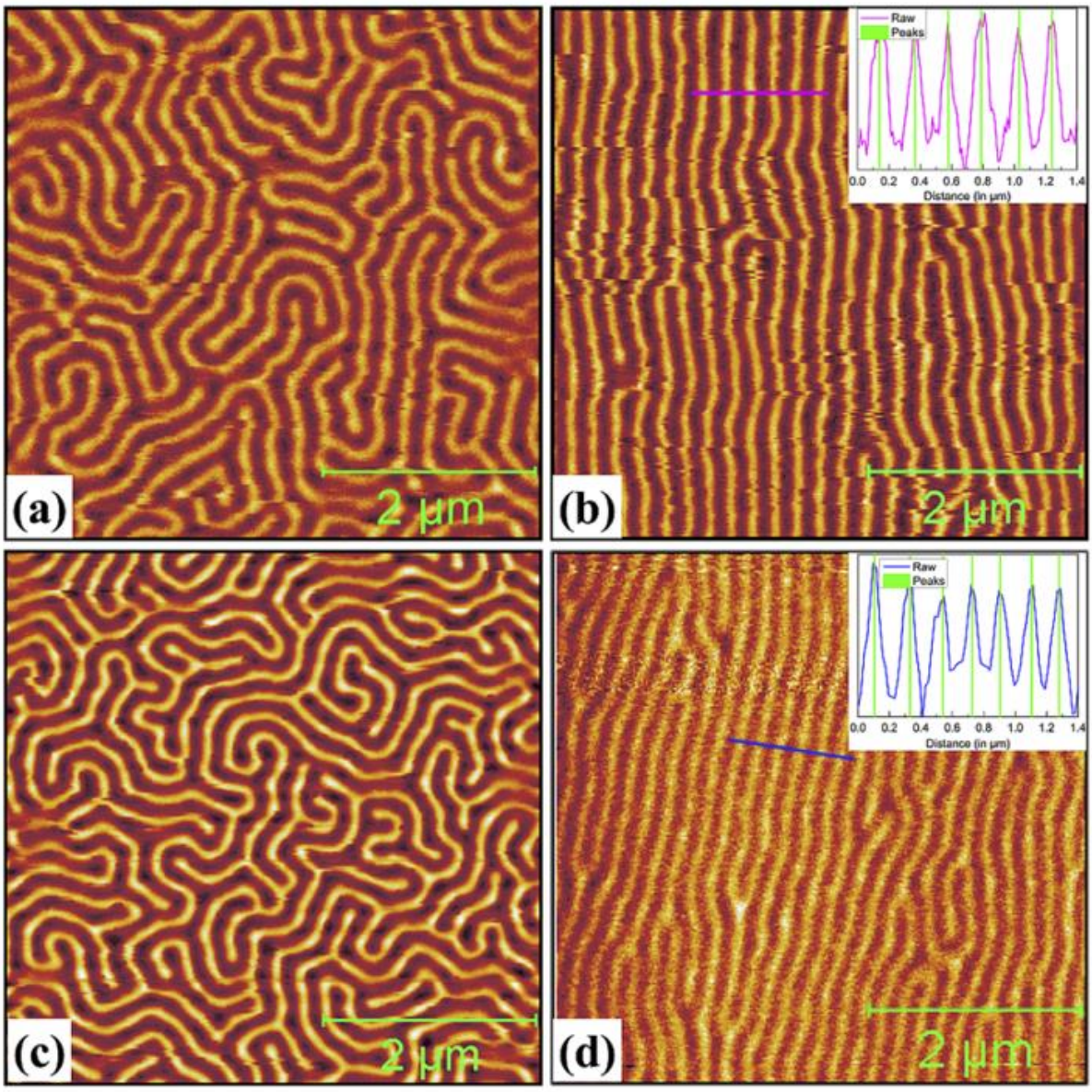

Figure 6.4 Remanence MFM images: (a) and (b) demagnetized state after applying ac magnetic field perpendicular to the sample plane for sample $[W/Co/Pt]_{10}$ *and* $[W/Co/Pt]_{20}$*,respectively. (b) and (d) stripe-like alignment of domains after applying ac demagnetizing field parallel to the sample plane for samples* $[W/Co/Pt]_{10}$ *and* $[W/Co/Pt]_{20}$*,respectively* [1].

6.3:- Interfacial DM interaction:-

There are many methods to calculate the DMI strength in single and multilayer thin films. One of the most reliable methods is Brilloiun light scattering (BLS) technique [4,5] in which one can estimate the DMI strength from the frequency difference of the Stokes and anti-Stokes peaks. However, this method is only reliably applicable for single layer thin films. In multilayer thins films under some conditions other modes of magnonic spectra may appear which are

related to skyrmion resonance or chiral resonance in the case of sufficient iDMI strength [6]. Therefore, it is not a good approach to measure iDMI by BLS or optical methods i.e. bubble expansion. Also, bubble expansion is valid for single layer thin films. However, for multilayers the iDMI strength is overestimated where, it increases with increasing the multilayer repetition [7]. In the ideal structures the iDMI strength should be the same for single or multilayer. For determination of iDMI in our W/Co/Pt multilayers, we adopted the novel procedure described by Legrand *et al.* [6] to estimate the iDMI value from the parallel strip domains which are expected to form in the minimum energy state of the investigated system. The domain wall energy can be calculated by putting the magnetic parameters and the iDMI energy strength can be estimated. This method is called K_{eff} method applied for effective medium, in which the whole layered film is considered as an magnetically homogeneous effective medium starting from bottom magnetic layer to top magnetic layer. The total thickness starting from the bottom magnetic layer to the top magnetic layer is considered as effective diluted magnetic moments. All magnetic parameters have be scaled by scaling factor f, where f is the ratio of magnetic layer thickness to the total basic trilayer thickness in the multilayer thin films. The scaling enables the effective medium to imitate the static and dynamic behaviour of the multilayer stack. This K_{eff}model is applicable only when: $\Delta \ll W$, $P \ll W$ and $P \ll 2\pi\Delta$, where: Δ is the domain wall width, P is periodicity of the multilayer stacks and W is the domain width [8]. The $K_{eff}$is effective anisotropy energy and H_K is the anisotropy magnetic field. The relation between K_{eff} and $H_K$can be written as

$$K_{eff} = 0.5\mu_0 M_S H_K$$

Different anisotropy coefficients are mutually related taking into account demagnetization energy:

$$K_{eff} = K_u - {}^1/_2\,\mu_0 M_s^2 \qquad (6.1)$$

where K_{eff} is effective anisotropy coefficient, M_s -magnetization at saturation applied field, and K_u– uniaxial anisotropy coefficient.

According this model, all magnetic parameter can be scaled in our multilayers by the factor f [8].

$f = \frac{t_m}{t_{stack}} =$ 0.24 (=0.69/2.87):

The scaling procedure covers the following magnetic parameters, which values are listed in the table 6.2:

$$f = \frac{M_S'}{M_S} = \frac{A'}{A} = \frac{D'}{D} = \frac{K_u'}{K_u} = \frac{K_{eff}'}{K_{eff}} \qquad (6.2)$$

where A is an magnetic exchange stiffness constant of Co, D is interfacial DMI strength, t_m is Co layer thickness and t_{stack} is total thickness of the basic trilayer stack W/Co/Pt. Symbols with an apostrophe correspond to the scaled values after scaling with f.

In the K_{eff} method, the magnetic domain wall is considered as a monodomain magnetic body expanding through the entire multi-layered stack. The domain wall is considered to have a shape of elliptical cylinder as a good approximation to estimate the demagnetising fields [9, 10]. The domain wall width is given by equation 6.3.

$$\Delta = \sqrt{\frac{A'}{K_u' + \frac{\mu_0 M_S'^2 (t'-2\Delta)}{2 \quad (t'+2\Delta)}}} \tag{6.3}$$

where, $t' = (T * f)$ and T is the total thickness of the magnetic multilayer including the HM layers inside the multilayers (however excluding top and bottom HM) starting from bottom ferromagnetic layer to top ferromagnetic layer.

The domain wall energy (σ_{dw}) including the all energy contributions can be expressed by:

$$\sigma_{dw} = {2A'}/{\Delta} + 2K_u'\Delta - \pi D' + \frac{\mu_0 M_S'^2}{2} 2\Delta \left(\frac{t'-2\Delta}{t'+2\Delta}\right) \tag{6.4}$$

On the other hand , the domain wall energy in effective medium after scaling the all magnetic parameters can be also estimated from the domain structure periodicity (=$2W$) where the parallel stripes are assumed to be in the minimum energy state:

$$\sigma_{dw} = \mu_0 M_S'^2 \frac{(2W)^2}{t'} \frac{1}{\pi^3} \sum_{n\geq 1, odd}^{\infty} \frac{1}{n^3} \left(1 - e^{-\pi n t'/W} - \frac{\pi n t'}{W} e^{-\pi n t'/W}\right) \tag{6.5}$$

Comparing equations (6.4) and (6.5) and putting the domain wall width Δ from equation (6.3), the parameter scaled D' can be estimated. Then D can be calculated as $D = D'/f$.

The estimated the iDMI strengths are equal to: D = 2.65 mJ/m^2 and 2.49 mJ/m^2, and D_s= 1.83 pJ/m and 1.72pJ/m (where Ds = D * tCo) for multilayers with repetition number N=10 and N=20, respectively under assumption of the magnetic stiffness exchange constant A=13 pJ/m. The high iDMI is observed due to presence of additive iDMI at both Co/Pt and W/Co interfaces and the strength value is higher than that reported in literature [11, 12]. A critical threshold value of iDMI strength D_{thr} above which a pure Néel type domain walls are formed is defined by the following equation [8].

$$D_{thr} = \frac{2 * \mu_0 M_S'^2}{\frac{\pi}{t'+log2} + \pi \sqrt{\frac{K_u' + \frac{\mu_0 * M_S'^2}{2}}{A'}}} \tag{6.6}$$

The estimated threshold value of iDMI is equal to D_{thr} =0.69 mJ/m^2 and 0.83 mJ/m^2 for multilayers with N= 10 and N = 20, respectively. Therefore, it seems that the domain walls appearing in the W/Co/Pt multi-layered structures might be of purely Neel type walls. . However, it is not possible to estimate on the experimental way from the MFM images whether visible domain walls are of Néel or Bloch type. To prove it, it is necessary to perform XMCD or circular dichroism in x-ray resonant magnetic scattering investigations [6].

6.4:- Micromagnetic simulations

To support the experimental estimation of iDMI strength, the micromagnetic simulations for the influence of iDMI energy on the magnetic domain pattern in multi-layered systems were performed using the mumax3 software [13]. The total thickness 600 Å of the W/Co/Pt multilayer was taken into consideration. The total area of the simulated structure was set to 5120 A × 5120 Å in x-y direction and the cell size was taken 20 Å × 20 Å in x-y direction and 6Å in z-direction so that it is lower than the Co exchange length. The input magnetic parameters for the simulations were taken from the experiment as given in the table-6.2. At the initial state the magnetization direction of the cells was randomly oriented around perpendicular to sample plane z-axis. The DMI strength coefficient was used a variable parameter. The simulations were performed for the wide range of D from 0.5 mJ/m^2 to 6 mJ/m^2. Figure 6.5 shows that the simulated magnetic domain size and pattern with different iDMI energy for N = 20. The labyrinth and parallel domains are observed after minimizing energy.

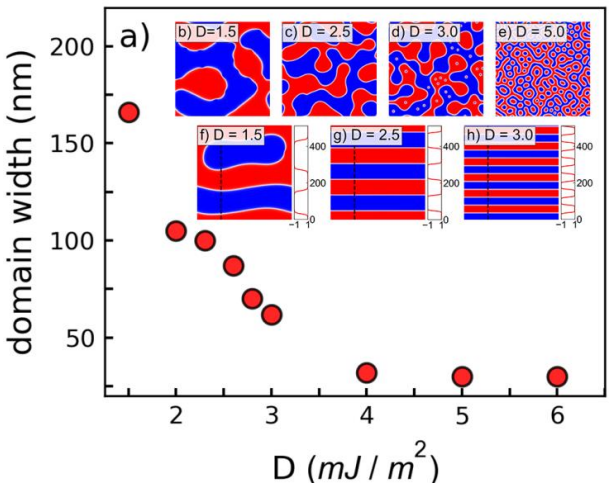

Figure 6.5. Domain patterns for various DMI strengths D for [W/Co/Pt]$_{20}$ multilayer obtained from micromagnetic simulations. (a) The variation of domain widths for different strengths of iDMI. (b-e) out of plane magnetised simulated domains showing labyrinth type. (red and blue colours stand for the up and down domains, respectively) for different values of D_{eff}= 1.5, 2.5, 3.0, 5.0 mJ/m^2. (f-h) domain alignment after application of the in-plane field

with different iDMI strengths: D = 1.5, 2.5, and 3.0 mJ/m^2. The magnetic profiles visible on the right side of the maps measured along the black dashed lines were used to determine the domain width plotted in (a).

The domain size evidently decreased with reinforcement of iDMI. Figure 6.5 (b-e) depicts the equilibrium position of static labyrinth domains in the multi-layered thin films as after application of the perpendicular field. The strip parallel domains were obtained by applying alternating in-plane field H=0.65T with decreasing the amplitude to zero. Figures 6.5(f-h) show the aligned parallel stripe domains for the D=1.5, 2.5, and 3.0 mJ/m^2. Both the modelled labyrinth domain pattern and stripe-shaped domain pattern reproduce the experimental MFM data very precisely. By using first inverse-Fourier transformation analysis, the domain width of labyrinth and parallel domains was calculated. The best agreement between the experimentally observed domains and the simulated domains is found for the D in the range between 2 mJ/m^2 – 2.5 mJ/m^2, where the domain width changes from 110 Å to 90 Å which agrees well with the experimental one. These values of DMI strength reproduce very well those estimated from the experiment.

6.5:- Density functional theory calculations

The iDMI strength determined from the experiment was also compared to the iDMI values obtained from density functional theory (DFT) calculations using VASP which based upon the plane wave basis set and projector augmented wave method [14]. The calculation is fully relativistic with the presence of spin orbit coupling and by considering a plane wave with energy cut-off of 350 eV since the iDMI strength is purely dependent upon the SOC. The GGA approximation [15] is assumed for the exchange correlation function because it gives better results for the magnetic metallic multilayers simulation [16].

As the multilayer stack repetition increases, it doesn't substantially affect the values of iDMI amplitude [17]. Therefore, the first principle calculation was performed for a single basic W/Co/Pt trilayer. The crystallographic structures taken for DFT calculations were designed based on the results from structural analysis performed by RHEED and XRD.

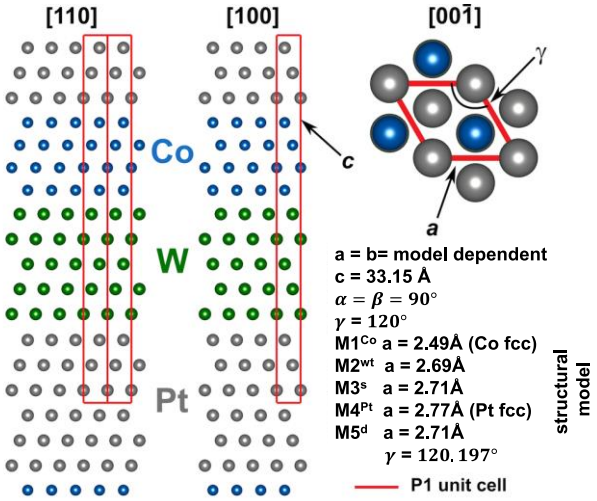

Figure 6.6 Different structures of the basic tri-layer [W/Co/Pt] stack (models M1-M5, see their description in the text) taken for the DFT calculations. The red lines mark the considered unit cell P1 [1].

In DFT calculations five different crystalline models of W/Co/Pt stack were considered. Figure 6.6 shows the primitive P1 space group crystalline structure which was used to construct the supercell of W/Co/Pt stack. The aim of consideration of the all these models was estimation of possible DMI strength variation for different idealized models used in DFT calculations. A structure of the real superlattice is a mixture of these well-defined crystalline orderings. The total number of atomic layers is equal to 15 being a sum of 5, 4 and 6 corresponding to W, Co and Pt component layer thickness, respectively. The in-plane lattice constant a was varied for each crystalline model. The details are presented in table-6.1. The unit cell parameter c=33.15 Å was extracted from fitting of XRD superlattice (111) peak position ($d^{S}_{(111)}$ = 2.21 Å). Each atomic layer has fcc like structure in DFT calculation, whereas W layer has bcc structure as determined from the experiment. However, the considered unit cell should be described as a one space group call and cannot be applied as more than one space group in DFT calculation. This forces, therefore, the crystal structure of W for changing structure from bcc to fcc crystal symmetry. In all 5 models described below the c parameter is fixed, whereas the a parameter varies for each model and gives main differences between them.

In the first and fourth model, the lattice constant values of Co (Co - M1^{Co} model, $a^{Co}_{(110)}$ = 2.49 A) and Pt (Pt - M4^{Pt} model, $a^{Pt}_{(110)}$ = 2.77 Å) between in-plane atoms measured in the experiment were assumed, respectively. In the second model M2^{wt} the phase-weighted mean spacing $a^{wtMean}_{(110)}$ = 2.69 Å of each individual element (W, Co, Pt) in the multi-layered structure,

determined also from the experiment, was considered. In the third model, $M3^S$, $a^S_{(110)}$ = 2.71 Å parameter is considered which is evaluated from the superlattice XRD peak $d^S_{(111)}$. Finally in the last model 5, $M5^d$, the lattice constant from the model $M3^S$ ($a^S_{(110)}$ = 2.71 Å) was taken with the the angle γ = 120.197° making in the P1 unit cell slightly distorted. As mentioned earlier, all the parameters for all models are given in table-6.1.

To corroborate the experiment to theoretical calculation, first-principle or DFT calculation has been performed by using

The procedures and notations similar to ours were used in literature [18]**.** *The* 4 in-plane translated unit cells are inside the supercells in the x direction and the 3×12×1 k-points centred in Γ have been used for calculation. The iDMI effect basically arises at the interface between FM and HM in the multilayers and the strength of the iDMI does not change beyond the 4-monolayers of the heavy metal at the interface to ferromagnetic layers [19]. The clockwise (CW) and anticlockwise (ACW) spin orientation was taken according to Ref. [18]. *The difference in the total energies of opposite spin chirality E_{CW} and E_{ACW} gives total energy of iDMI strength for specified value of cycloid wavelength.*

$$d^{tot} = -(E_{ACW} - E_{CW})/m \tag{6.7}$$

where E_{ACW} and E_{CW} are the total energies of the ACW and CW spin orientation, respectively. The value of of $m = 12\sqrt{3}$ was taken, which depends upon the wavelength of the cycloid, because the magnetic cycloid with the wavelength 4 has been simulated as described by [18]. The total energy of iDMI can be expressed as micromagnetic energy per unit volume in multilayers [20, 21]. The DMI coefficient D can be written in terms of total iDMI energy d^{tot} and is given by the following expression:

$$D = 3\sqrt{2}d^{tot}/(N_F a^2) \tag{6.8}$$

where a and N_F represent the in-plane lattice constant and the total number of ferromagnetic atomic layers, respectively.

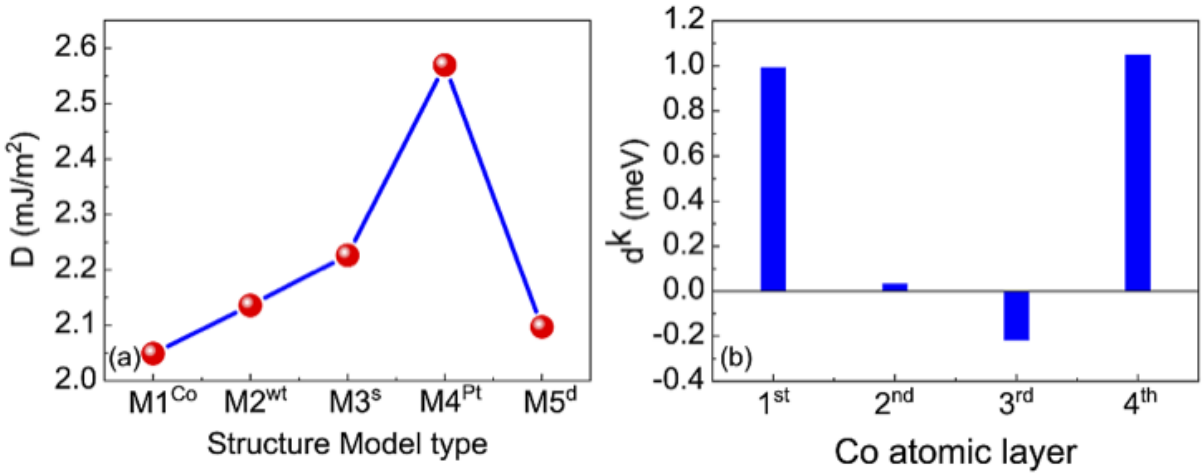

Figure-6.7 (a) iDMI amplitude determined by DFT calculation for different models of W/Co/Pt stacks described in the text. (b)the layer resolved iDMI for each Co atomic layers in the W/Co/Pt stack for M5^d model [1].

Figure 6.7(a) shows the results of the DFT calculations of iDMI strength D for five different structural models of the W/Co/Pt stack, described above. The amplitude of D was estimated to vary in the range 2.04 - 2.57 mJ/m^2 for ACW chirality. It should be noted that all results give a good agreement to the observed experimental value of iDMI strength. Furthermore, the layered resolved DMI energy d^k for each atomic layer strength was investigated for the crystal structure M5^d (Figure 6.7(b)). This model has the highest degree of freedom and seems to be the best fitted to the real structure investigated in the experiment. The four atomic layers of the Co film are named as Co1, Co2, Co3 and Co4, where Co1 and Co4 are the 1st and the 4th Co layer near to the interface W and Pt heavy metal layer, respectively. Co2 and Co3 layers are the inner layers which do not form the interface. From the layer resolved iDMI, one may conclude that the iDMI is interfacial in nature. At the W/Co and Co/Pt interfaces, the iDMI amplitude is substantially higher than that in the inner atomic Co layers. The spin chiralities at the W/Co and Pt/Co interfaces are opposite in nature. However, in the W/Co/Pt heterostructure due to reversed symmetry, the iDMI vectors at the interfaces are oriented in the same direction which make additive iDMI strength contributions to the whole heterostructure. Therefore, the individual iDMI strength is lower than the net iDMI strength. The figure 6.7(b) shows the distribution of the d^k for crystal structure M5^d. However the remaining considered crystal structures give the same qualitative behaviour. The total sum of iDMI strengths from individual atomic Co layers is 1.85 meV which is closely equal to the total iDMI strength of structural model M5^d. The chirality of 1st, 2nd and the 4th Co atomic layer is ACW whereas the chirality is CW for 3rd layer of Co atom as shown in figure 6.7(b).

6.6:- Discussions

The iDMI coefficient, D, in epitaxial W/Co/Pt heterostructures was determined by three independent methods: K_{eff} effective method based on the experimental parameters and by micromagnetic simulations with experimental parameters, and the first principle calculations considering a set of five ideal lattice structures with parameters extracted from XRD and RHEED analysis. All these three methods reveal a similar iDMI amplitude substantially exceeding 2 mJ/m^2.

The obtained value of D in this studied W/Co/Pt system is higher than for similar systems investigated by other groups. The value of D is reported to be from the range from 0.2 to 1.5 mJ/m [11, 12, 17, 22]. All these layered systems were prepared by sputtering and had a reversed layer sequence i.e. Pt/Co/W. It should be noted that the iDMI strength is very sensitive to the FM/HM interface quality. It depends on a chemical type of the interface. The interface sharpness and epitaxial quality depend. upon the fabrication technique. The sharp interface and the good quality of epitaxial nature is expected to give the higher iDMI magnitude. This property was also found in the Re/Co/Pt multilayers which are discussed in the next section of this thesis. Fabrication of layered structures by a sputtering technique gives lower quality of layer crystallinity and interfaces in grown heterostructures. We believe that good quality with well-defined epitaxial nature of multilayer samples is obtained in MBE method. This technology offers better possibility to create a well-defined specific crystalline structure of the component layers and separating them interfaces. In such epitaxial systems, the non-negligible interfacial DMI effect was obtained in the epitaxial symmetric system Pt/Co/Pt [23]. This work shows that iDMI strength is very sensitive to structural aspects of the interfaces related to epitaxial details although they are of the same chemical type. In our studied W/Co/Pt system, Pt and Co have the same epitaxial relations for the closed packed atomic layers forming this interface. However, there is a lattice mismatch at the W/Co interface. As a result, such W/Co/Pt configuration exhibits the lower PMA than Pt/Co/W opposite sequence [11, 12].

The high amplitude of iDMI strength in our samples is compared to similar systems reported in the literature, however grown by sputtering. It arises from the high quality interface and the crystalline structure. The interfacial quality and the crystalline structure were proved by RHEED pattern, satellite peaks in XRD measurement and observation of the Bragg peaks in the XRR measurement. Experimentally determined value of D well agrees with the numerical calculations performed with use of density functional theory for different five models with ideal crystalline structures and very sharp interfaces. In the literature, it is reported that the iDMI

strength can be reduced by half if the intermixing at the interface between FM/HM is at the level of 25% [24]. In this point view, an unexpected results obtained by K_{eff} method and simulation assuming the experimental values were reported for the Co/Pd multilayers [7], where the iDMI strength increased with increasing repetition layers being related to increase in the interfacial roughness.

5.7:- Stabilization of skyrmion lattices in W/Co/Pt multilayers by magnetic field

Above discussed domain structure was registered by MFM at the remnant state. As visible from the hysteresis loop shape (figure 6.3), it should change with the magnetic field applied in the perpendicular direction to the sample plane. To observe this expected magnetic domain evolution, the magnetic field dependent MFM measurements were also performed for the W/Co/Pt multilayers with the repetition number N=20. It is illustrated in a sequence of the MFM images shown in figure 6.9. At low field of 0.004T the remnant labyrinth-like configuration disappears and a coexistence of both stripes and bubbles is present. With further increase in the magnetic field, the pure bubble lattice is visible (H = 0.020 T, figure 6.9 (d)), reaching a density of 500/25μ^2(around). While approaching the saturation field this bubble lattice disappears and at the field of 0.102 T no magnetic contrast is visible, evidencing that the sample reached a saturated state (figure 6.9(f)). With magnetic field decreasing towards zero the magnetic bubbles again become visible as shown in figures 6.9 (g-h).

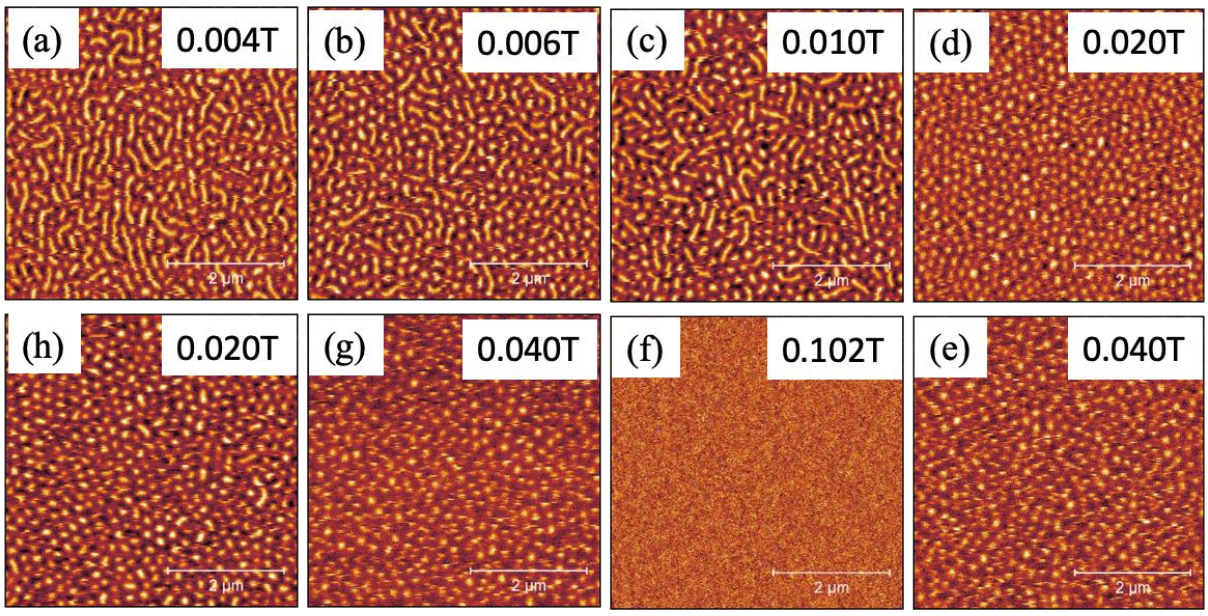

*Figure 6.9. Evolution of the magnetic domain structure in [W(10Å)/Co(6Å)/Pt(10Å)]*20 multilayers.*

6.8:- References

1. Jena, S. K. *et al.* Interfacial Dzyaloshinskii-Moriya interaction in the epitaxial W/Co/Pt multilayers. *Nanoscale* **13**, 7685–7693 (2021).
2. Lutterotti, L. Total pattern fitting for the combined size-strain-stress-texture determination in thin film diffraction. *Nuclear Instruments and Methods in Physics Research, Section B: Beam Interactions with Materials and Atoms* **268**, 334–340 (2010).
3. Banerjee, C. *et al.* Magnonic band structure in a Co/Pd stripe domain system investigated by Brillouin light scattering and micromagnetic simulations. *Physical Review B* **96**, 3–10 (2017).
4. Nembach, H. T., Shaw, J. M., Weiler, M., Jué, E. & Silva, T. J. Linear relation between Heisenberg exchange and interfacial Dzyaloshinskii-Moriya interaction in metal films. *Nature Physics* **11**, 825–829 (2015).
5. Belmeguenai, M. *et al.* Interfacial Dzyaloshinskii-Moriya interaction in perpendicularly magnetized Pt/Co/AlOx ultrathin films measured by Brillouin light spectroscopy. *Physical Review B - Condensed Matter and Materials Physics* **91**, 1–4 (2015).
6. Legrand, W. *et al.* Hybrid chiral domain walls and skyrmions in magnetic multilayers. *Science Advances* **4**, eaat0415 (2018).
7. Davydenko, A. V. *et al.* Dzyaloshinskii-Moriya interaction in symmetric epitaxial [Co/Pd(111)]N superlattices with different numbers of Co/Pd bilayers. *Physical Review B* **99**, 1–12 (2019).
8. Lemesh, I., Büttner, F. & Beach, G. S. D. Accurate model of the stripe domain phase of perpendicularly magnetized multilayers. *Physical Review B* **95**, 174423 (2017).
9. Osborn, J. A. Demagnetizing Factors of the General Ellipsoid. *Physical Review* **67**, 351–357 (1945).
10. Mougin, A., Cormier, M., Adam, J. P., Metaxas, P. J. & Ferré, J. Domain wall mobility, stability and Walker breakdown in magnetic nanowires. *Europhysics Letters (EPL)* **78**, 57007 (2007).
11. Jiang, W. *et al.* Quantifying chiral exchange interaction for Néel-type skyrmions via Lorentz transmission electron microscopy. *Physical Review B* **99**, 104402 (2019).

12. Lin, T. *et al.* Observation of room-temperature magnetic skyrmions in Pt/Co/W structures with a large spin-orbit coupling. *Physical Review B* **98**, 174425 (2018).
13. Vansteenkiste, A. *et al.* The design and verification of MuMax3. *AIP Advances* **4**, 107133 (2014).
14. Kresse, G. & Furthmüller, J. Efficient iterative schemes for ab initio total-energy calculations using a plane-wave basis set. *Physical Review B* **54**, 11169–11186 (1996).
15. Perdew, J. P., Burke, K. & Ernzerhof, M. Generalized gradient approximation made simple. *Physical Review Letters* **77**, 3865–3868 (1996).
16. Autieri, C. & Sanyal, B. A systematic study of 4d and 5d transition metal mediated exchange coupling between Fe and Gd nanolaminates. *Journal of Physics: Condensed Matter* **29**, 465802 (2017).
17. Benguettat-El Mokhtari, I. *et al.* Interfacial Dzyaloshinskii-Moriya interaction, interface-induced damping and perpendicular magnetic anisotropy in Pt/Co/W based multilayers. *Journal of Applied Physics* **126**, 133902 (2019).
18. Yang, H., Thiaville, A., Rohart, S., Fert, A. & Chshiev, M. Erratum: Anatomy of Dzyaloshinskii-Moriya Interaction at Co/Pt Interfaces [Phys. Rev. Lett. 115, 267210 (2015)]. *Physical Review Letters* **118**, 219901 (2017).
19. Hajr, A., Hariri, A., Manchon, G., Ghosh, S. & Manchon, A. Semirealistic tight-binding model for Dzyaloshinskii-Moriya interaction. *Physical Review B* **102**, 224427 (2020).
20. Sampaio, J., Cros, V., Rohart, S., Thiaville, A. & Fert, A. Nucleation, stability and current-induced motion of isolated magnetic skyrmions in nanostructures. *Nature Nanotechnology* **8**, 839–844 (2013).
21. Fert, A., Cros, V. & Sampaio, J. Skyrmions on the track. *Nature Nanotechnology* **8**, 152–156 (2013).
22. Kim, D. Y. *et al.* Quantitative accordance of Dzyaloshinskii-Moriya interaction between domain-wall and spin-wave dynamics. *Physical Review B* **100**, 1–9 (2019).
23. Shahbazi, K. *et al.* Domain-wall motion and interfacial Dzyaloshinskii-Moriya interactions in Pt/Co/Ir(tIr)/Ta multilayers. *Physical Review B* **99**, 094409 (2019).
24. Yang, H., Thiaville, A., Rohart, S., Fert, A. & Chshiev, M. Anatomy of Dzyaloshinskii-Moriya Interaction at Co/Pt Interfaces. *Physical Review Letters* **115**, 267210 (2015).

Summary

The investigations of layered structures, displaying complex magnetic properties, are the subject of my thesis. My attention was focused on W/Co/Pt stacks with perpendicular to the sample plane magnetization. Their ultrathin film structure and asymmetrical sandwiching of the ferromagnetic layer with heavy metal films induces numerous specific properties such as: perpendicular magnetic anisotropy (PMA), Dzyaloshinskii-Moriya interaction (DMI) and interlayer exchange coupling (IEC). They can be tuned by thickness of the component layers and repetition number of the basic trilayer stack in the multilayered structure in the wide range. Increase in the trilayer repetition number: from 1 via moderate value up to 20, introduces an additional contribution from ICE and magnetostatic interactions to initially occurring PMA and DMI. As a consequence evolution of numerous magnetic states, magnetization reversal processes as well domain structures, including topologically protected magnetic vortexes, called skyrmions, is observed. Observed magnetic properties are correlated with structural features of the stacks.

Initially we expected that from the epitaxy point of view the properties of the W/Co/Pt system should be very similar to earlier investigated in detail Mo/Co/Au stack as Mo and W have the same bcc crystalline structure and almost identical lattice parameter, whereas Au and Pt are the noble metals neighbouring in the table of elements. However, fine difference in electron structure of Mo vs W and Au vs Pt makes these systems quite different.

In Pt/W/Co/Pt system, the Co layer thickness, d_{Co}, range with PMA shifts toward higher values with d_W increase. This finding is associated with the W/Co interface properties where a dead layer is formed. The Pt/W/Co/Pt system exhibits various magnetic states being a function of d_W and d_{Co} evolving from non-magnetic phase via superparamagnetic with tendency to perpendicular magnetization, ferromagnetic ultra-soft and normal with PMA up to ferromagnetic with in-plane anisotropy. Influence of the bottom W layer is very strong. Even atomic submonolayer coverage drastically suppress anisotropy from perpendicular to in plane. The specific PMA (d_W, d_{Co}) spatial dependence makes that spin reorientation transition (SRT) from perpendicular to in-plane oriented magnetization can be induces both by d_{Co} increase for fixed d_W as well by d_W decrease for fixed d_{Co}. Additionally in the ultra-soft phase a bubble (skyrmion) domain lattice is observed being easily modified by the applied magnetic field. BLS measurement shows appearance of DMI in this structure.

In the double Co layer system Pt/W/Co/Pt/W/Co/Pt containing two Co layers magnetized in the perpendicular direction, we observed interlayer coupling across double layer

spacer Pt/W with varying thicknesses d_{Pt} and d_W. For the case $d_W=d_{Pt}$ a crossover from ferromagnetic via antiferromagnetic and back to ferromagnetic coupling was observed. For $d_W \neq d_{Pt}$ configuration, antiferromagnetic coupling seems to evolve more rapidly to ferromagnetic one. Surprisingly for the analogue thickness of the single layer spacer Pt or W, the antiferromagnetic coupling does not occur. It evidences that not only thickness but also composition of the spacer plays a crucial role. Resultant magnetic configurations are the effect of balance interplay between iDMI and PMA in individual Co layers as well ICE between them. Increase in the repetition number results in enhancing contribution from the magnetostatic interaction. The magnetic states and magnetization reversal processes are the effect of interplay between this contribution and antiferromagnetic coupling competition. The tuning of this balance was demonstrated in the $(W/Co/Pt)_n$ (n = 6 or 7) multilayers with perpendicular magnetization by the change of thickness of the double layer spacer. Smaller thickness favours coupling role whereas the bigger one magnetostatic interaction. It is clearly evidenced that in the prevailing role of the coupling the individual Co layers are ordered ferromagnetically in the whole their volume and their magnetization reversal undergoes by step-like (layer by layer) mode and can characterised in terms of macrospin model. For larger spacer thickness demagnetization effect prevails. Locally neighbouring Co layers are coupled ferromagnetically with periodic antiparallel alignment in the lateral direction. In consequence such sample exhibits a labyrinth domain structure in the remnant state.

In the W/Co/Pt multilayers with the highest repetition number (n=20), my attention was focused on the domain structure and estimation of iDMI strength. As the magnetostatic interactions are dominating the labyrinth domain structure is well developed in the remnant state. It can be converted to stripe-like domain structure by appropriate magnetic field treatment. Using a model of effective magnetic medium and anisotropy effective approach a DMI strength exceeding 2 mJ/m^2 was determined from the domain size. Experimental results were confirmed in two independent theoretical modelling based on micromagnetic simulations and density functional theory (DFT). The high value of iDMI strength was ascribed to additive contributions from both types of interfaces and the higher crystalline quality of the component layers and sharper interfaces (grown by molecular beam epitaxy) in comparison to similar structures grown commonly by sputtering methods.

My thesis describes the possibility to tune intentionally the complex properties (PMA, DMI, IEC and magnetostatic interactions) in the asymmetrical heavy metal / ferromagnet layered structures. I show how they evolve with change of the structural parameters such as: component layer thickness and repetition number of the basic trilayer stack. As consequence

numerous magnetic states and magnetic domain structures including stripe- like alignment and bubble (skyrmion) lattice formation were obtained. Reported here results contribute in general to fundamental knowledge progress in the field and nanomagnetism and chiral spin structures. However, discussed here domain structures are potentially promising in novel practical applications such as: one-dimensional magnonic crystals (stripe-like structure) for spin wave propagation and carriers for magnetic storage information (skyrmions).

The End.